Lakehead University

Reliability Analysis of Slopes with Truncated Quantile Functions from Small, Truncated/Censored Samples

By

Reza Zaeri

1200635

A thesis submitted in partial fulfillment for the degree of Master of Science in:

Civil Engineering

Department of Civil Engineering

August 2024

Author's Declaration

I hereby certify that I am the sole author of this thesis and that no part of this thesis has been published or submitted for publication.

I certify that, to the best of my knowledge, my thesis does not infringe upon anyone's copyright nor violate any proprietary rights and that any ideas, techniques, quotations, or any other material from the work of other people included in my thesis, published or otherwise, are fully acknowledged in accordance with the standard referencing practices. Furthermore, to the extent that I have included copyrighted material that surpasses the bounds of fair dealing within the meaning of the Canada Copyright Act, I certify that I have obtained a written permission from the copyright owner(s) to include such material(s) in my thesis and have included copies of such copyright clearances to my appendix.

I declare that this is a true copy of my thesis, including any final revisions, as approved by my thesis committee and the Graduate Studies office, and that this thesis has not been submitted for a higher degree to any other University or Institution.

Abstract

Truncated and censored samples encountered in geotechnical engineering arise from various factors such as equipment limitations, formation characteristics, sample disturbance, unsuitable sampling methods, environmental conditions, human error, budget constraints, and geological complexities. In addition to this, unprecedented events like the COVID-19 pandemic can impede soil and rock sampling efforts, necessitating engineers and designers to work with truncated samples. The primary objective of the research is to explore novel approaches for probabilistic slope stability analysis and design under small, truncated/censored samples.

Landslides represent a prevalent and impactful geo hazard in Canada, particularly in relation to human lives and infrastructure sustainability. Thousands of landslides occur across Canada annually, resulting in direct and indirect damage estimated to range between $200 and $400 million per year. Reliability analysis, specifically utilizing the reliability index, serves as a valuable tool for evaluating engineering uncertainties, especially within the realm of slope stability. This study assesses the challenges posed by probability distribution limitations, emphasizing the relevance of truncated random variables in engineering contexts. The application of maximum entropy principles (MEPs) to estimating quantile functions (QFs) from truncated samples is discussed in the research. By employing MEPs along with partial probability weighted moments (PPWMs), the study demonstrates the effective estimation of truncated quantile functions. The optimization of these functions, determined by the Akaike information criterion (AIC), prevents the use of excessively complex models, thereby ensuring flexibility in model selection. In the next step, a modified first order reliability method (FORM) based on quantile functions for truncated samples is proposed. The efficacy of the proposed algorithm is verified through illustrative examples, including a rock slope stability analysis using the optimal order of maximum entropy quantile functions with varying degrees of truncation. This algorithm can present a viable a solution for conducting reliability analyses with truncated samples.

A comprehensive reliability analysis of slopes in the Nipigon River Landslide incident of 1990 near Nipigon, Ontario, Canada, is also presented. The application of truncated

maximum entropy quantile functions for reliability analysis, involving the incorporation of undrained shear strength values obtained from previous laboratory tests. The study concludes with a comparative analysis of outcomes utilizing various quantile functions, affirming the agreement between the parent normal distribution and maximum entropy quantile functions. The findings contribute to a better understanding of the Nipigon River Landslide, revealing hazardous and unsatisfactory performance levels while emphasizing the effectiveness of the maximum entropy quantile function-based FORM in evaluating slope stability with truncated samples. Finally, several possible remedial measures are discussed, accompanied by recommendations for future considerations.

Keywords: slope stability, landslide, uncertainties, reliability analysis, truncated samples, censored samples, maximum entropy distribution, first order reliability method, Nipigon River Landslide.

Acknowledgements

I would like to express my sincere gratitude to my supervisor, Dr. Jian Deng, for his invaluable guidance, professional support, and insightful feedback throughout the entire process of researching and writing this master thesis.

I am also deeply thankful to my co-supervisor, Dr. Eltayeb Mohamedelhassan and the members of the thesis committee, Dr. Liang Cui, and Dr. Deli Li, for their constructive comments and suggestions to ensure the academic achievement of my research. I am also thankful to Dr. Mahdi Shadabfar for his valuable comments and the complete review of the thesis.

I would like to underscore the profound impact of the financial support that I have received. The Natural Sciences and Engineering Research Council of Canada (NSERC) [RGPIN 2019 06069] and the Government of Canada's New Frontiers in Research Fund (NFRF) [NFRFR-2021-00262] have played a pivotal role, and I am deeply appreciative. I extend my appreciation to the Civil Engineering Department at Lakehead University for providing a productive academic environment and access to resources that greatly contributed to the success of this study.

Lastly, special thanks go to my family and friends for their understanding, encouragement, and patience during the challenging periods of this academic journey.

Dedicated to my soulmate,

AZIN

who has profoundly changed my life with her love and inspiration

Contents

List of Figures

List of Tables

Abbreviations

AIC	Akaike information criterion
CDF	Cumulative distribution function
FDM	Finite difference method
FEM	Finite element method
FORM	First order reliability method
FOS	Factor of safety
FOSM	First order second moment
FPPWM	Fractional partial probability weighted moment
ICDF	Inverse cumulative distribution function
IPPWM	Integer partial probability weighted moments
KL	Kullback-Leibler
LEM	Limit equilibrium method
MCS	Monte Carlo simulation
MEP	Maximum entropy principles
PDF	Probability density function
PWM	Probability weighted moment
PPWM	Partial probability weighted moment
QF	Quantile function
SWCC	Soil-water characteristics curve
β	Reliability index
Φ	Friction angle
c_u	Undrained shear strength
$g_{(X)}$	Limit state function
P_f	Probability of failure

1. Introduction

Landslides have been identified as one of the most common types of disaster in across Canada (Strouth and McDougall, 2021). Hunger (2004) used advice from experts engaged in the study and management of landslides and estimated that landslides cause an average of three fatalities annually, with associated financial costs ranging from $54 to $135 million per year. Notable landslides in Canada (e.g., Figure 1.1) have led to the loss of 580 lives and caused nearly $9.5 billion in financial damage between 1841 and 2012 (Couture et al. 2013). According to a report by Natural Resources Canada (2019), landslides contribute to a direct and indirect financial burden of approximately $200 to $400 million in Canada. Based on the assessment by industrial and governmental Canadian landslide practitioners, the financial impacts of prairie landslides are estimated to exceed $281 to $450 million per year, including damages to the oil and gas sector, public and private transportation systems, and local communities (Porter et al. 2019).

Figure 1.1. Cecil Lake road landslide, Peace River (Couture et al. 2013)

1.1. Motivations

The considerable financial burdens associated with slope disasters in Canada underline the urgent need for reliable strategies to mitigate these risks. The presence of uncertainties within material properties in geotechnical engineering further emphasizes the necessity of

accurately assessing slope stability and associated risks. Additionally, limitations in conducting laboratory and field tests in civil engineering projects, particularly when dealing with small or truncated/censored samples, necessitate innovative approaches for data analysis and interpretation. With a growing demand for more efficient and reliable design approaches, addressing these challenges aligns with industry expectations for improved engineering practices. Moreover, identifying a gap in the existing literature highlights the imperative for further research in this area, positioning the study within the broader context of knowledge advancement. Ultimately, the overarching goal of the research is to develop methods that can effectively prevent or minimize future slope disasters, thereby enhancing safety and reducing risks in infrastructure projects.

1.2. Research objectives

Reliability analysis often involves situations where data may be truncated due to censoring or limitations in measurement. This research proposes a novel method for reliability assessment that addresses truncated data by leveraging truncated quantile functions. The key objectives of this research are:

- Derive quantile functions (QF) for truncated samples using the MEPs and PPWMs. This step establishes a framework for analyzing truncated data using quantile functions.
- Develop a new approach that integrates FORM with the derived truncated quantile functions. This builds upon previous research by Deng and Pandey (2023) and Melchers et al. (2003) to create a more robust reliability assessment tool specifically suited for reliability analysis with truncated data.
- Verify the proposed method through real-world case studies. Applying the method to practical scenarios demonstrates its effectiveness and validates its usefulness for real-world applications.

1.3. Thesis outline

The remainder of this thesis is organized as follows,

Chapter 2: defines the significance of reliability analysis within the context of slope stability and discusses challenges encountered in reliability analysis when dealing with truncated random variables. Furthermore, Chapter 2 reviews the concept of reliability analysis using quantile functions.

Chapter 3: explains the MEPs and the application in probability distributions and reviews the concept of PPWMs. In addition, this chapter details the methodology for deriving truncated quantile functions using the MEPs. It concludes by presenting two illustrative examples that showcase the application of the MEPs in obtaining quantile functions from truncated samples, comparing the results with normal and lognormal distributions.

Chapter 4: introduces the concepts of FORM and subsequently proposes a modified method for conducting reliability analysis through FORM with truncated quantile functions. Practical examples are provided in this chapter to demonstrate the application of the proposed reliability method and demonstrate how the methodology can be employed in different scenarios.

Chapter 5: presents an overview of the Nipigon River Landslide in 1990. It then follows by applying the proposed methodology for the FORM with truncated quantile functions to conduct reliability analysis on the slope within in the Nipigon River Landslide region. Finally, this chapter presents findings and discusses how the approach performs in a real-world scenario.

Chapter 6: summarizes the findings and conclusions obtained from the research and provides recommendations for further research in the future.

2. Literature review

Slope stability assessments are regularly conducted to evaluate the stability of natural and artificial slopes. The selection of an analysis method depends on the conditions of the case study and the possible failure mode. It involves an accurate examination of the different strengths, weaknesses, and limitations associated with each methodology (DeWolfe et al. 2011). In traditional slope stability analysis, the task involves determining the critical slip surface's position for a given slope and calculating the safety factor at that particular location (Reale et al. 2015). Various approaches have been developed to address slope stability analysis, including the limit equilibrium method (LEM), the finite difference method (FDM), and the finite element method (FEM). In deterministic analysis, stability is assessed using a factor of safety (FOS), which relies on fixed parameter values. In contrast, probabilistic analysis assigns statistical distributions to every random variable and evaluates stability based on a reliability index (β), or probability of failure (P_f) (Reale et al. 2015).

2.1. Main factor contributing to causing landslides

The main reasons contributing to causing landslides can be divided into two main groups including natural and human-related factors. Regarding natural mechanisms, water, seismic activity, and volcanic activity are the three main factors in stimulating landslides (Highland and Bobrowsky, 2008).

Water: Saturation in slopes is a result of various procedures such as intense rainfall, snowmelt, fluctuation of ground water levels, and changes in water surface level along coastlines, earth dams, lakes, reservoirs, canals, and rivers. One example of landslides triggered by a tropical storm and extremely heavy rainfall is the Mameyes, Puerto Rico landslide which happened in 1985 (Figure 2.1). As a result of this fatal landslide, 129 people lost their lives and 120 houses were destroyed. (Highland and Bobrowsky, 2008).

Seismic activity: A considerable proportion of landslides in mountainous areas are related to earthquake activities. Earthquakes can lead to the rapid infiltration of water resulting from shaking-caused dilation of soil materials and increase the likelihood of landslides in steep landslide-prone areas (Highland and Bobrowsky, 2008). In comparison with other phenomena (e.g., meteorological events), landslides induced by earthquakes pose more

severe problems from the disaster-management perspective (Del Gaudio et al. 2003). The 1964 Great Alaska earthquake in the United States led to widespread landslides and ground failures (Highland and Bobrowsky, 2008).

Figure 2.1. The Mameyes, Puerto Rico, landslide, 1985 (Photograph by Randall Jibson, U.S. Geological Survey)

Volcanic activities: Landslides triggered by volcanic activities are among some of the most devastating landslide records. Rapidly melted snow by volcanic lava can form a deluge of rock, soil, ash, and water that rapidly moves and has a devastating power. One of the most famous volcanic-induced landslides is the failure of the side of Casita Volcano in Nicaragua, Central America, which happened on October 30, 1998 (Highland and Bobrowsky, 2008).

Human activities: The expansion of the human population and the construction of new residential areas, towns and cities can lead to landslides. These activities can negatively influence drainage patterns, the stabilization of slopes, and vegetation, all of which are common factors in causing human-induced landslides. In addition to the previously mentioned causes, landslides can also happen in areas that were previously stable as a result of other human activities like irrigation, the construction and draining of reservoirs, pipe leaks, and poorly executed excavation or grading on slopes (Highland and Bobrowsky, 2008).

2.2. Methods for slope stability analysis

In the past, slope stability analysis relied on simplified, hand-performed calculations. However, as computer technology has advanced and become more accessible, engineers have devised more complicated but more accurate methods. Generally, slope stability analysis (Table 2.1) aims to calculate a FOS against potential failure or landslides (Pourkhosravani and Kalantari, 2011). The FOS in evaluating the stability of slopes can be defined as a ratio of the resisting force to the driving force. The FOS higher than 1 represents a stable slope, while the FOS for unstable slopes is less than 1 (Jahanfar, 2014).

The earliest method for slope stability analysis is commonly referred to as the LEM. This approach involves analyzing the stresses and strengths over a hypothetical sliding surface in the soil slope and then calculating a FOS with respect to these two main quantities. A number of potential failure surfaces are examined to identify the most critical surface, which has the minimum value for the FOS (Pourkhosravani and Kalantari, 2011). The mass procedure and the method of slices are the two main limit equilibrium approaches used in the slope stability analysis. Various researchers have suggested different methods for evaluating the stability of slopes using the mass procedure method. Solutions were offered by Fellenius (1927) and Taylor (1937) to determine critical circles. Koppula (1984) analyzed the stability of saturated soil sloped Michalowski (2002) used a kinematic approach to conduct the slope stability analysis.

In order to conduct the slope stability analysis using the method of slices, the soil above the sliding interface is divided into some vertical parallel slices. Then, the stability of each slice needs to be calculated separately in order to obtain the FOS for the slope. This method is recommended when the soil is nonhomogeneous. (Das, 2002). Different researchers suggested the method of slices for calculating the FOS in slopes among which Bishop (1955), Janbu (1955), and Spencer (1967) are the most commonly used.

Numerical analysis methods provide more precise estimates of the exact mathematical solution for the mechanics of slope stability's controlling equations. These methods are significantly more advanced and sophisticated in comparison with LEM s as they consider

deformations (strains) in addition to forces (stresses), which are the focus of traditional LEMs (Pourkhosravani and Kalantari, 2011).

The widespread use of numerical techniques over the past few decades can be attributed to the progress made in computer science. Generally, numerical methods used in slope stability analysis can be categorized into three groups: the FDM, the FEM, and the Distinct Element Method (DEM) (Pourkhosravani and Kalantari, 2011).

Table 2.1. Different methods of slope stability analysis

LEM	Mass Procedure: Fellenius (1927), Taylor (1937), Koppula (1984), and Michalowski (2002).
	Method of Slices: Bishop (1955), Janbu (1955), and Spencer (1967).
Numerical Methods	Finite Difference Method (FDM)
	Finite Element Method (FEM)
	Distinct Element Method (DEM)

2.3. Uncertainties in geotechnical engineering

One of the main characteristics of geotechnical engineering is working with natural materials, which can impose considerable levels of uncertainty on engineering decision making. Soil is a type of geological material that is formed through different procedures including weathering, erosion, and sedimentation. Soils are exposed to a wide range of stresses, and pore fluids, as well as physical and chemical processes. Therefore, the physical and mechanical properties of soils can differ significantly across various sections of the deposits (Huber, 2013). Generally, the uncertainties in geotechnical engineering can be categorized into three main groups.

2.3.1. Aleatoric uncertainty

This type of uncertainty is also referred to as inherent or intrinsic uncertainty, involving the inherent randomness of a parameter, such as the variation in soil strength parameters throughout a soil mass. This type of uncertainty is a natural characteristic of soil that cannot be avoided (Huber, 2013).

2.3.2. Epistemic uncertainty

This uncertainty mainly stems from three varied factors: errors in data collection, processing, and design analysis. Epistemic uncertainty can be identified and reduced, as it is mostly related to incorrectness rather than a lack of required knowledge. Epistemic uncertainty is categorized into four groups, including engineering decision bias, structural uncertainty, measurement error, and simulation error (Abdulai and Sharifzadeh, 2019).

2.3.3. Design Parameter-Selection Uncertainty

The selection of parameters in order to use in the design process needs to satisfy all values within the range over which they vary. The uncertainties related to the selection of design parameters can be caused by numerous factors such as limitations in the measurement. Some parameters used in slope stability like cohesion or friction angle can take on any possible value within a specified range. Moreover, these parameters must satisfy all values within the range over which they vary. These types of uncertainties include design variable uncertainties, model-parameter uncertainties, model uncertainties and geometric uncertainties (Abdulai and Sharifzadeh, 2019).

2.4. Reliability in slope stability analysis

Deterministic slope stability includes calculating the FOS which is determined by comparing the resisting forces to the driving forces on a possible sliding surface. Then, the slope is considered safe if the FOS is greater than one (Malkawi et al. 2000). The concept of the FOS is not a comprehensive measure of the relative reliability of geotechnical structures for different performance modes. One of its main limitations is that it requires assigning a single, precise value to various design parameters such as material shear parameters and loads while the appropriate values may actually be uncertain (Kamien, 1997). However, in a probabilistic analysis, the FOS is expressed as a mean value and variance. In order to evaluate uncertainties in engineering variables like slope stability, reliability analysis is used. The reliability index (β) is defined to measure the degree of uncertainty in the calculated FOS (Malkawi et al. 2000). Christian et al. (1994) also stated that probability theory can be applied to analyze slope stability, and the most effective way to express uncertainties is by

using a reliability index. The reliability index is defined as a measure of the probability of failure in slope stability analysis (Eq. 2.1).

$$\beta = \frac{E[F] - 1.0}{\sigma[F]}, \tag{2.1}$$

where β is the reliability index and $E[F]$ and $\sigma[F]$ are the mean and standard deviation of the calculated FOS, respectively.

The reliability index quantifies the safety of slope stability by measuring the number of standard deviations between the estimated FOS and the defined failure value of 1.0. In addition to this, it can be interpreted as a normalization of the FOS with respect to its standard deviation (Christian et al. 1994).

The reliability index offers a relative measure of the current condition of a structure and provides a qualitative estimate of the performance that can be expected from the structure (Table 2.1). Slopes with higher reliability indexes are expected to have acceptable function, while those with lower reliability indexes are more likely to perform poorly and present significant rehabilitation issues. Based on this scale, slopes with a low reliability index can be considered a hazard with a higher probability of failure (Christian et al. 1994). The application of reliability analysis has attracted the attention of researchers during the last two decades. Many researchers developed more effective methods in order to incorporate reliability analysis into slope stability analysis. For example, Christian et al. (1994) applied the reliability analysis to the slope stability analysis and stated that probabilistic methods are most valuable when applied to situations that include assessing the relative likelihoods of failure or providing insights into the influence of uncertainties in the parameters. Malkawi et al. (2000) used various reliability methods, such as the first order second moment (FOSM) method and Monte Carlo simulation (MCS), in the slope stability analysis. They also concluded that the application of FOSM requires a smaller number of calculations in comparison with MCS. However, MCS has demonstrated its effectiveness and capability in conducting through the reliability analysis for slope stability. Wang et al. (2011) introduced a novel approach for reliability analysis of slope stability problems by utilizing MCS. To enhance efficiency and accuracy, an advanced MCS technique known as "subset simulation" was employed, particularly effective in handling small probability levels. Chiu et al. (2012)

investigated and analyzed the reliability of the soil-water characteristics curve (SWCC) and its impact on slope stability. In this research, the reliability of the SWCC was demonstrated through an engineering example of probabilistic slope stability analysis, highlighting its practical application. Jiang et al. (2015) suggested a new method that enables the explicit modeling of spatial variability in soil properties during a reliability analysis of slope stability. It simplifies the analysis by considering representative slip surfaces, which are the primary modes of slope failure, along with multiple stochastic response surfaces. Deng (2022) proposed a method that offers an objective approach to estimate probability distributions of soil properties. This estimation is accomplished using the maximum entropy method, which utilizes fractional moments derived from observed data. The probability distribution used in this study relies on the principle of maximum entropy and does not rely on the assumptions of traditional distributions.

Table 2.2. Relationship between reliability index (β) and probability of failure (P_f) (Christian et al. 1994)

β	P_f	Expected performance level
1	0.16	Hazardous
1.5	0.07	Unsatisfactory
2	0.023	Poor
2.5	0.006	Below average
3	0.001	Above average
4	0.00003	Good
5	0.0000003	High

2.5. Steps in modeling uncertainties

There are series of steps that need to be taken in order to evaluate uncertainties in reliability analysis. For example, the level of uncertainty associated with the yearly rainfall or maximum wind speed in a specific city needs to be assessed. It is evident that we can gather the necessary information by collecting all the existing recorded data related to rainfall or wind speed. There could be records of data for the past decades that can create a sample of data, including 50, 75, or 100 records. The required statistical parameters can be calculated from this sample of data, and a graphical representation such as a histogram or

frequency diagram can be used to show the randomness of the data (Haldar and Mahadevan, 2000).

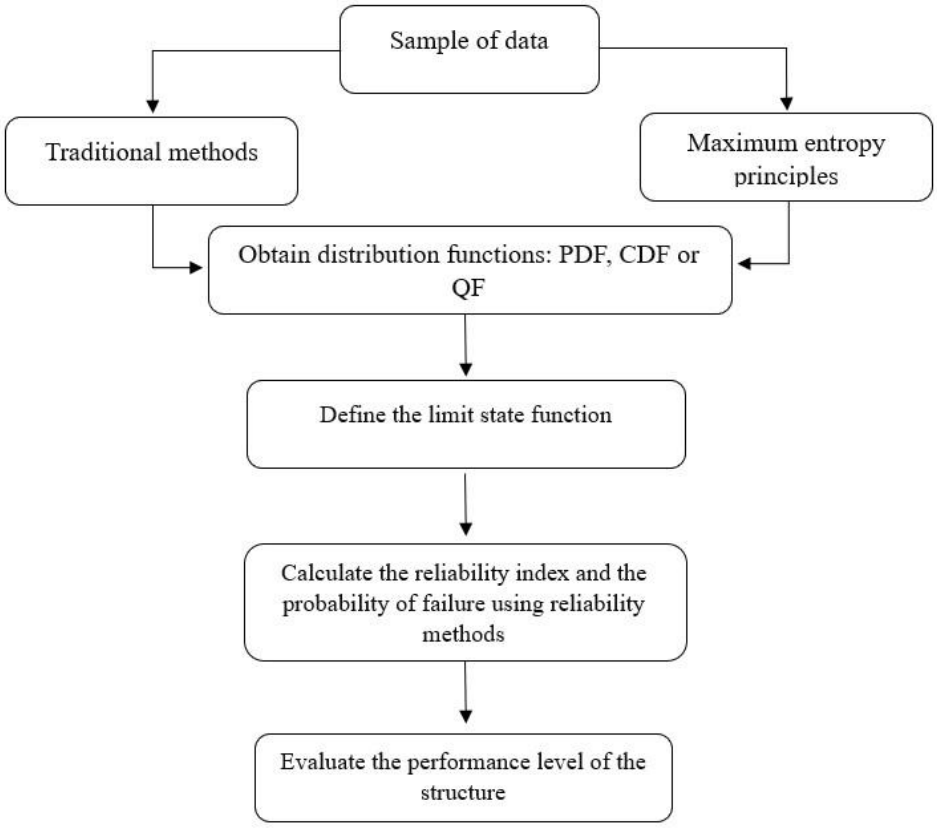

Figure 2.2. General steps in a reliability analysis

Providing a broader representation of randomness is possible with the frequency diagram obtained using a known theoretical probability density function (PDF), cumulative density function (CDF) or quantile function (QF) using traditional methods or the MEPs (Figure 2.2). However, it is necessary to estimate specific parameters associated with the distribution in order to accurately describe the density functions. The estimation of these parameters is known as statistics, which is one of the main steps in reliability analysis. The level of randomness present in both the load and resistance parameters can be measured by utilizing these statistical measures (Haldar and Mahadevan, 2000). Finally, the associated risk in the design can be evaluated for a particular performance criterion using the reliability index or the probability of failure.

2.6. Reliability analysis with truncated random variables

Reliability analysis with truncated random variables involves assessing the probability of system failure or success when data samples are limited by certain constraints or thresholds. This scenario commonly arises in engineering, finance, and other fields where data collection may be constrained by practical limitations or defined boundaries. One approach to analyzing reliability with truncated random variables involves understanding the probability distributions of the truncated variables. These distributions are derived from the original distributions but are confined within the specified bounds. Analytical techniques such as moment matching, or maximum likelihood estimation can be used to characterize these truncated distributions (Johnson et al. 1995).

In reliability analysis, truncated random variables are often incorporated into probabilistic models to account for incomplete or censored data. For example, in reliability engineering, when failure times are only observed up to a certain point, truncated distributions can be used to model the remaining lifetime of the system (Nelson, 2009).

Truncated samples are used when the range of a random variable is limited either from below or above due to certain reasons which is a common condition in conducting reliability analysis (Zhang and Xie, 2011). Truncated samples, which are also the focus of this study, refer to samples that exclude certain values from the entire population. A more precise way to describe this is that truncation affects populations, and samples described as truncated are actually samples taken from truncated populations. Censored samples are characterized by specimen measurements that fall within the limits of the sample space. While these specimens are identified and counted, they are not measured in any other way (Cohen, 1991).

Truncated samples are categorized based on the availability of information regarding the truncation points, also known as terminals. When these points are unknown, they become additional parameters that need to be estimated using the data from the sample. Cohen (1991) summarized truncated samples with known terminals as follows:

- *Left singly truncated samples*: For each of n observations, $x \geq T$, where T is a fixed (known) point of truncation.

- *Right singly truncated samples*: For each of n observations, $x \leq T$, where T is a fixed (known) point of truncation.
- *Doubly truncated samples*: For each of n observations, $T_1 \leq x \leq T_2$ where T_1 and T_2 are fixed (known) points of truncation.

In practice, truncated samples are the case in various experimental situations where sample selection is limited to only a partial range of the variable. For example, Johari et al, (2013) investigated the application of the jointly distributed random variables method in the reliability assessment of rock slope stability by considering a truncated normal probability distribution function for the friction angle of the sliding surface and apparent cohesion. They also used a truncated exponential probability distribution function to represent the depth of water in tension cracks and the earthquake acceleration ratio. In another study, Guo et al, (2018) conducted a reliability analysis of embankment dam sliding stability using sparse polynomial chaos expansion. They concluded that the raw data can be represented with both a beta distribution and a truncated normal distribution and result in reasonable outcomes for the studied dam. However, the findings suggested that utilizing beta distributions may result in a slightly increased probability of failure compared to truncated normal distributions.

A truncated distribution (Eq. 2.2) also refers to a specific segment of an untruncated distribution that is either higher or lower than a designated threshold (Greene, 2008). If a continuous random variable x has pdf $f(x)$ and a is a constant, then

$$f(x|\, x > a) = \frac{f(x)}{\text{Prob}\,(x > a)}. \tag{2.2}$$

The proof relies on the definition of conditional probability and essentially involves adjusting the density of the distribution to ensure that it integrates to one within the range above a. It is important to note that the truncated distribution is a type of conditional distribution (Greene, 2008). An example of the truncated standard normal distribution, with $\mu = 0$ and $\sigma = 1$, is shown for $a = -0.5, 0$ and 0.5 in Figure 2.3.

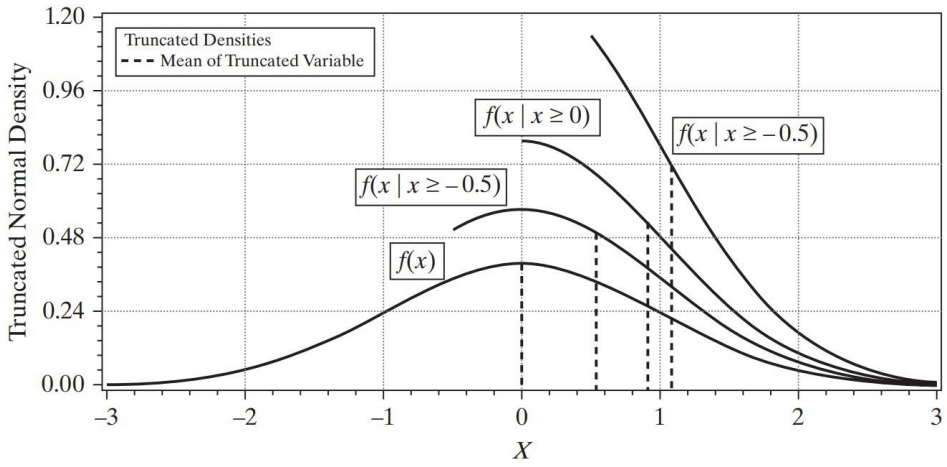

Figure 2.3. Example of truncated standard normal distribution (Greene, 2008)

2.7. Truncated samples in geotechnical engineering

Truncated samples in geotechnical engineering can occur due to several reasons, and understanding these reasons is crucial for interpreting soil behavior accurately. Some of the most common reasons for truncated samples of data in geotechnical engineering are presented in the following.

2.7.1. Budgetary Constraints

In some cases, budget limitations may prevent the drilling or sampling process from continuing to the desired depth, especially in projects located in remote areas. resulting in the truncation of samples (Das, 2002).

2.7.2. Sample Disturbance

During the sampling process, disturbances to the soil structure can occur, resulting in a partial or truncated sample. This can happen due to vibrations, rotation, or lateral movement of the sampling tool, especially in loose or poorly compacted soils (Das, 2002).

2.7.3. Geological complexity

This can significantly influence the occurrence of truncated samples in geotechnical engineering. Geological complexity can be related to numerous factors including variability

in soil composition, the presence of geological structures, layered soil strata, heterogeneity of soil properties and depth of investigation (Das, 2002).

2.7.4. Equipment Limitations

Truncation may happen due to limitations in the equipment used for soil sampling. For instance, the drilling or sampling equipment may not penetrate the soil to the desired depth due to physical constraints such as hard layers, boulders, or equipment malfunction (Das, 2002).

2.7.5. Sampling Technique

Improper sampling techniques or inadequate quality control measures can also result in truncated samples. For example, if the sampling tool is not properly aligned or stabilized during the sampling process, it may not recover a full-length sample (Das, 2002).

2.8. Reliability analysis with quantile functions

Distribution functions, including PDFs, cumulative distribution functions (CDF), and quantile functions (QF), provide a complete description of random variables (Deng and Pandey, 2023). While all forms of distribution functions convey the same information regarding the distribution, PDFs are commonly utilized in various statistical theories and practices, employing distinct interpretations and methodologies. Quantile-based studies were primarily conducted in situations where the traditional approach proved challenging or unsuccessful in yielding the desired outcomes (Nair et al. 2013).

In the field of probabilistic analysis, it is crucial to accurately determine the density functions of random variables in order to minimize errors. Mathematics and statistics employ various distribution types, but in geotechnical engineering, only a limited number of distributions, such as normal, lognormal, and gamma, are commonly used. The task of choosing and fitting a probability distribution that closely matches a given dataset can be achieved through a range of approaches and techniques. The quantile function can be understood as the inverse of the CDF. When the quantile function of a random variable is clearly defined, probability weighted moments (PWM) have the potential to be useful in determining explicit

expressions for the distribution parameters of these random variables (Deng and Pandey, 2023).

In many instances, estimating quantiles consists of empirically selecting a common probability distribution, like normal or lognormal, followed by assessing distribution parameters using statistical techniques such as the method of moments or maximum likelihood estimation. Another compelling approach to distribution fitting stems from the MEPs. This principle uses PWMs as a constraint in order to directly obtain quantile functions from a sample of data. This method offers an unbiased distribution, independent of any specific distribution assumption, based on observed data and sample moments (Pandey 2000).

2.9. Advantages of the quantile-based reliability analysis

An important challenge in the reliability analysis of engineering systems is accurately estimating the tail of a probability distribution. Traditionally, this involves assuming a common distribution type based on the available data sample, like normal or lognormal, and then estimating distribution parameters using methods like maximum likelihood or the method of moments. However, this approach risks introducing bias and error due to the inherent assumptions about the distribution type prior to estimation (Deng and Pandey, 2009).

The advantages of quantile functions directly obtained by using PWMs can be described in several ways. Firstly, the benefit of PWMs over ordinary statistical moments in limited sample sizes lies in their ability to provide more accurate estimates of higher-order moments. In situations where the available data is limited, traditional statistical moments may not yield reliable estimates of moments beyond the first order (mean). However, PWMs are specifically designed to address this limitation by incorporating probability weights, allowing for more precise estimation of higher-order moments with small sample sizes.

Furthermore, PWMs exhibit resistance to the influence of outliers or extreme observations within the dataset. This resilience is a consequence of their formulation as linear combinations of observed data values. Unlike ordinary moments, which subject the data to operations like squaring, cubing, etc., PWMs maintain a more stable response to outliers.

Therefore, PWMs offer a more reliable framework for statistical modeling, as they are less prone to distortions caused by extreme data points.

2.10. Summary

The assessment of slope stability is a critical aspect of engineering endeavors, frequently involving the evaluation of both natural and artificial slopes. Traditionally, slope stability analysis revolves around identifying the critical slip surface within a slope and calculating the safety factor at that location.

In deterministic analysis, stability is typically assessed using a FOS, which relies on deterministic parameter values. However, probabilistic analysis introduces statistical distributions to account for uncertainties, evaluating stability based on parameters such as reliability index (β) or probability of failure (P_f). Landslides, a significant concern in slope stability, can be triggered by natural factors like water saturation, seismic activity, and volcanic eruptions, as well as human activities such as urbanization and construction. Uncertainties inherent in geotechnical engineering, categorized as aleatoric and epistemic, pose challenges to reliability analysis.

Truncated random variables, frequently encountered in reliability analysis, arise when data samples are limited by certain constraints. Understanding the probability distributions of truncated variables and incorporating them into probabilistic models are crucial steps in analyzing reliability. Truncated samples, common in geotechnical engineering, may occur due to budget constraints, sample disturbance, geological complexity, equipment limitations, or sampling techniques. Employing quantile-based reliability analysis offers advantages in accurately estimating tail probabilities without relying on distribution assumptions, providing more reliable estimates especially with limited sample sizes and in the presence of outliers.

3. Truncated quantile functions from truncated samples

The fundamental importance of engineering analysis, design, and planning is widely recognized, along with probability, reliability, and statistics (Alfredo and Wilson, 1975). It is essential to consider most engineering variables as random variables, meaning their potential values depend on the results of specific random events (Deng and Pandey, 2023).

Random variables can be effectively described using distribution functions, which include PDFs, CDFs, and quantile functions (QFs). These functions offer a complete understanding of the characteristics of random variables. Furthermore, descriptive statistics, specifically the first four moments, are commonly employed to provide some aspects of the characteristics of random variables. The first moment is the mean value of a random variable. The second central moment is the variance, which shows the degree of spread (dispersion) (Deng and Pandey, 2023). In practical applications, the third and fourth central moments play a significant role in capturing important characteristics of the probability distribution. Skewness, the third central moment, serves as a measure of the distribution's asymmetry. On the other hand, kurtosis, the fourth central moment, quantifies the degree of peakedness in the central region around the mean within the probability distribution (Baecher and Christian, 2005).

The moments of a random variable can be derived from its distribution functions. However, it is important to note that determining the distribution functions uniquely from sample moments poses a challenge as it is an indeterminate inverse problem. Various methods are available in order to recover probability distribution functions from the moments of random variables including the saddle point approximation, the Pearson family of distributions, the Gram-Charlier and Edgeworth expansions, and the Hermite model (Winterstein, 1988). The MEPs is another method for calculating probability distribution functions from the moments of a random variable. The MEPs method is attractive because it allows for the creation of a probability distribution that is minimally biased, maximizing entropy while incorporating constraints provided by the available information (Rao and Hsieh, 1987).

3.1. Maximum entropy principles

Entropy quantifies the level of uncertainty (Chen and Dai, 2011). In MEPs modeling, a PDF is chosen in a way that maximizes entropy while considering the available information in the form of moments (Deng, 2022). The central claim of the MEPs states that the probability distribution with the highest degree of unbiasedness is the one that maximizes entropy while meeting the imposed constraints (Kesavan and Kapur, 1989). Additionally, it is a logical approach for choosing the probability distribution with the least amount of bias, minimizing the presence of misleading information while remaining compatible with the available sample data (Jaynes, 2003; Shore and Johnson, 1980).

Maximum entropy distribution defined by Shannon is a highly unbiased distribution with moments as constraints and an optimization algorithm. The entropy of a random variable X can be written as

$$H = -\int_{-\infty}^{+\infty} f(x) \ln f(x) \mathrm{d}x, \tag{3.1}$$

where $f(x)$ is the PDF and H is the entropy of random variable X with $f(x)$. The probability distribution that best represents the current state of knowledge may be obtained by maximizing Eq. (3.1).

$$H = -\int_{-\infty}^{+\infty} f(x) \ln f(x) \, \mathrm{d}x = \text{maximum}. \tag{3.2}$$

Subjected to some known moment constraints

$$\int_{-\infty}^{+\infty} x^i f(x) \mathrm{d}x = \mu_i, \ \ (i = 0, 1, 2, \dots, N), \tag{3.3}$$

where N is the number of moments to be used and μ_i is the i-th moment of the origin which can be determined originally from the sample of data.

In order to solve the maximum problem, the Lagrange multiplier method can be used,

$$L = H - (\lambda_0 - 1) \int_{-\infty}^{+\infty} f(x) \, \mathrm{d}x + \sum_{i=1}^{N} \lambda_i \left[\mu_i - \int_{-\infty}^{+\infty} x^i f(x) \, \mathrm{d}x \right]. \tag{3.4}$$

Setting the derivative $\frac{\delta L}{\delta f(x)} = 0$ gives

$$-\int_{-\infty}^{+\infty}[\ln f(x)+1]\mathrm{d}x-(\lambda_0-1)\int_{-\infty}^{+\infty}\mathrm{d}x-\sum_{i=1}^{N}\lambda_i\left[\int_{-\infty}^{+\infty}x^i\mathrm{d}x\right]=0, \tag{3.5}$$

or

$$f(x)=\exp\left[-\sum_{i=0}^{N}\lambda_i\,x^i\right], \tag{3.6}$$

where $\lambda=(\lambda_0,\lambda_1,\ldots,\lambda_N)$ are unknown parameters. These unknown parameters can be calculated from the following nonlinear equations

$$\int_{-\infty}^{+\infty}x^i\exp\left[-\sum_{j=0}^{N}\lambda_j\,x^j\right]\mathrm{d}x=\mu_i\,,\quad i=0,1,\ldots,N. \tag{3.7}$$

The distribution $f(x)=\exp[-\sum_{i=0}^{N}\lambda_i\,x^i]$ from or approximate a number of known distributions that are obtained by choosing an appropriate N.

3.2. Probability weighted moments (PWMs)

In conventional practice, the MEP is commonly employed to estimate the PDF by imposing specific moment constraints. The density function is subsequently integrated to calculate the CDF, which, in turn, requires inversion to determine the quantile associated with a particular probability value (Pandey, 2000). However, when dealing with small sample sizes, the estimation of higher-order moments (order > 2) often suffers from significant sampling errors. Consequently, utilizing the maximum entropy distribution derived from these imprecise moment estimates can result in inaccurate quantile values (Deng and Pandey, 2008). The primary challenge in employing the MEPs for quantile estimation has been the difficulty of obtaining precise moment estimates from small samples. This obstacle has negatively influenced the widespread application of the maximum entropy approach (Pandey, 2000).

Pandey (2000) introduced a method in order to directly calculate quantile functions using the MEPs. He suggested using PWMs in order to directly estimate the quantile function. Unlike ordinary statistical moments, the notable advantage of utilizing PWMs is that their

higher order values can be accurately estimated even with small sample sizes (Pandey, 2000).

The definition of a PWM for a random variable X was introduced by Greenwood et al. (1979) as follows

$$M_{r,s,t} = E[X^r F^s (1-F)^t] = \int_0^1 [x(F)]^r F^s (1-F)^t \mathrm{d}F, \tag{3.8}$$

where $M_{r,s,t}$ is the integral PWM with integral order r, s and t, E is the mathematical expectation and F is the probability of non-exceedance. The following two forms of PWMs are particularly simple and useful,

Type 1:

$$\alpha_t = M_{1,0,t} = \int_0^1 x(F)(1-F)^t \mathrm{d}F = \int_0^1 x(q) q^t \, \mathrm{d}q, \tag{3.9}$$

and Type 2:

$$\beta_s = M_{1,s,0} = \int_0^1 x(F) F^s \mathrm{d}F, \tag{3.10}$$

where $q = 1 - F$.

Unbiased estimates, denoted as b_s and a_t, of β_s and α_t, respectively, can be obtained from an ordered random sample of size n, as stated in (Hosking (1997),

$$b_s = \frac{1}{n} \sum_{i=1}^{n} \binom{i-1}{s} x_i / \binom{n-1}{s}, \tag{3.11}$$

$$a_t = \frac{1}{n} \sum_{i=1}^{n} \binom{n-1}{t} x_i / \binom{n-1}{t}, \tag{3.12}$$

where $s, t = 0, 1, \ldots, (n-1)$ are non-negative integers.

3.3. Maximum entropy quantile functions with PWMs as constraints

Pandey (2000) proposed a distribution-free procedure for calculating the quantile function of a non-negative random variable. The MEPs method is constrained by conditions defined in relation to PWMs derived from observed data. The entropy of a quantile function can be written as

$$H[x(F)] = -\int_0^1 [x(F)\ln x(F)]\,\mathrm{d}F, \tag{3.13}$$

where $H[x(F)]$ is the entropy, $x(F)$ is the quantile function and F is the probability of non-exceedance.

The available information is also presented as PMWs

$$\int_0^1 x(F)\,F^s\,\mathrm{d}F = b_s\,,\ \ (s = 0, 1, \dots, K), \tag{3.14}$$

where b_s is a sample estimate of population PWM, β_s, and K is the highest order of PWM considered in the analysis. To maximize the entropy in Eq. (3.13) the method of Lagrange multipliers is used, and the Lagrangian function $\bar{H}$ can be given by

$$\begin{aligned}\bar{H} = &-\int_0^1 [x(F)\ln x(F)]\,\mathrm{d}F - (\lambda_0 - 1)\left[\int_0^1 x(F)\mathrm{d}F - 1\right] \\ &-\sum_{s=1}^{K}\lambda_s\left[\int_0^1 x(F)F^s\mathrm{d}F - b_s\right],\end{aligned} \tag{3.15}$$

where λ_s represents an unknown Lagrangian multiplier. In order to derive the quantile function, the entropy can be maximized using the usual condition

$$\frac{\partial\bar{H}}{\partial x(F)} = 0. \tag{3.16}$$

Substituting Eq. (3.15) into Eq. (3.16) and then simplifying further yields the subsequent solution as presented in Eq. (3.17).

$$x(F) = \exp\left[-\sum_{s=0}^{K}\lambda_s\,F^s\right]. \tag{3.17}$$

The Lagrangian multipliers can then be calculated by solving a system of $K+1$ nonlinear equations

$$\int_0^1 F^s \exp\left[-\sum_{i=0}^{K} \lambda_i F^i\right] \mathrm{d}F = b_s, s = 0, 1, \ldots, K. \tag{3.18}$$

3.4. Partial probability weighted moments (PPWMs) from Truncated samples

PPWMs can be defined as (Wang, 1990)

$$M_{r,s,t}^{P} = \int_{F_0}^{1} [x(F)]^r F^s (1-F)^t \mathrm{d}F, \tag{3.19}$$

where $M_{r,s,t}^{P}$ is the integral PPWM with integral order r, s and t. In this context, the notation P denotes the partial, $F_0 = F(x_0)$ represents the cumulative probability lower bound within a restricted ascending sample affected by truncation, x_0 refers to the threshold where truncation occurs, and $x(F)$ signifies the inverse of the CDF. If $F_0 = 0$, it reduces to the ordinary PWMs (Greenwood et al. 1979).

When considering nonnegative real numbers r, s, and t, the fractional form of the fractional partial probability weighted moments (FPPWMs) is denoted as $M_{r,s,t}^{P}$, while integer partial probability weighted moments (IPPWMs) represent the integer order PPWMs. In the case of a particular truncated value, x_0, an estimate of the empirical frequency for F_0 can be derived

$$\hat{F}_0 = \frac{n_0}{n}. \tag{3.20}$$

The order number of x_0 in the complete ascending sample is represented by n_0. There are two definitions for PPWMs that are particularly useful,

$$\beta_s^P = M_{1,s,0}^P, \tag{3.21}$$

and

$$\alpha_t^P = M_{1,0,t}^P. \tag{3.22}$$

Unbiased estimations for these two dual forms of PPWMs can be obtained when considering a left truncated sample (Wang, 1990)

$$b_s^P = \frac{1}{n}\sum_{i=1}^{n}\binom{i-1}{s} x_i^P \,/\, \binom{n-1}{s}\ , x_i^P = \begin{cases} x_i, & x_i > x_{0,} \\ 0, & x_i \le x_{0,} \end{cases}, \tag{3.23}$$

and

$$a_t^P = \frac{1}{n}\sum_{i=1}^{n}\binom{n-i}{t} x_i^P \,/\, \binom{n-1}{t}\ , x_i^P = \begin{cases} x_i, & x_i > x_{0,} \\ 0, & x_i \le x_{0,} \end{cases}, \tag{3.24}$$

where $t, s = 0, 1, \ldots, n-1$ are nonnegative integers.

In the case of right-truncated samples PPWMs can be obtained as

$$b_s^P = \frac{1}{n}\sum_{i=1}^{n}\binom{i-1}{s} x_i^P \,/\, \binom{n-1}{s}\ , x_i^P = \begin{cases} x_i, & x_i < x_{0,} \\ 0, & x_i \ge x_{0,} \end{cases}, \tag{3.25}$$

and

$$a_t^P = \frac{1}{n}\sum_{i=1}^{n}\binom{n-i}{t} x_i^P \,/\, \binom{n-1}{t}\ , x_i^P = \begin{cases} x_i, & x_i < x_{0,} \\ 0, & x_i \ge x_{0,} \end{cases}. \tag{3.26}$$

3.5. Extended maximum entropy quantile functions from truncated samples

An extended maximum entropy method (EMEM) is formulated as Eq. (3.27) with a cut-off x_0 (Lee and Lee, 2002)

$$H[f, x_0] = -\int_{x_0}^{+\infty} f(x) \ln f(x)\, \mathrm{d}x. \tag{3.27}$$

By denoting $x(F)$ as the unknown true quantile function of the random variable X, the partial entropy of a quantile function ($H^P[x(F)]$) within a finite interval $[F_0, 1]$ can be defined in the following manner (Deng et al. 2012)

$$H^P[x(F)] = -\int_{F_0}^{1} x(F) \ln x(F) \mathrm{d}F. \tag{3.28}$$

Furthermore, the information is derived from a truncated data set

$$\int_{F_0}^{1} x(F)\, F^k \mathrm{d}F = b_k^P, \quad k = 0,1, \ldots, M. \tag{3.29}$$

The lower bound F_0 represents a point of left truncation, which is known and fixed, in terms of quantiles. b_k^P denotes the k-th PPWMs obtained from Eq. (3.23), and M represents the highest order of PPWM. When F_0 is equal to 0, the model simplifies to Pandey's model

(Pandey, 2000). To maximize the entropy in Eq. (3.28) the method of Lagrange multipliers is used, and the Lagrangian function $\bar{H}$ can be given by

$$\begin{aligned}\bar{H} = &-\int_{F_0}^{1}[x(F)\ln x(F)]\,\mathrm{d}F - (\lambda_0 - 1)\left[\int_{F_0}^{1} x(F)\mathrm{d}F - 1\right] \\ &-\sum_{k=1}^{M}\lambda_k\left[\int_{F_0}^{1} x(F)F^k\mathrm{d}F - b_k^P\right],\end{aligned} \tag{3.30}$$

where λ_k represents an unknown Lagrangian multiplier. In order to derive the extended quantile function for left truncated samples, the entropy can be maximized using the usual condition

$$\frac{\partial \bar{H}}{\partial x(F)} = 0. \tag{3.31}$$

Substituting Eq. (3.30) into Eq. (3.31) and then simplifying further yields the subsequent solution as presented in Eq. (3.32) provides the extended quantile function from a left-truncated sample

$$x_M(F) = \exp\left[-1 - \sum_{k=0}^{M}\lambda_k\, F^k\right], \quad F_0 \le F \le 1. \tag{3.32}$$

The Lagrangian parameters are obtained numerically by solving the following set of M+1 nonlinear simultaneous equations using any mathematical software, such as MATLAB

$$\int_{F_0}^{1} F^k \exp\left[-1 - \sum_{i=0}^{M}\lambda_i\, F^i\right]\mathrm{d}F = b_k^P \quad k = 0, 1, \ldots, M. \tag{3.33}$$

In the case of right-truncated samples, the partial entropy of a quantile function ($H^P[x(F)]$) within a finite interval $[0, F_0]$ can be written as

$$H^P[x(F)] = -\int_{0}^{F_0} x(F)\ln x(F)\mathrm{d}F. \tag{3.34}$$

In addition to this, the information is derived from a truncated data set

$$\int_{0}^{F_0} x(F)\, F^k\mathrm{d}F = b_k^P, \quad k = 0,1, \ldots, M. \tag{3.35}$$

The upper bound F_0 represents a point of right truncation, which is known and fixed, in terms of quantiles. b_k^P denotes the k-th PPWMs obtained from Eq. (3.25), and M represents the highest order of PPWM. To maximize the entropy in Eq. (3.34), the method of Lagrange multipliers is used, and the Lagrangian function $\overline{H}$ can be given by

$$\begin{aligned}\overline{H} = &-\int_0^{F_0} [x(F)\ln x(F)]\,\mathrm{d}F - (\lambda_0 - 1)\left[\int_0^{F_0} x(F)\mathrm{d}F - 1\right] \\ &-\sum_{k=1}^{M} \lambda_k \left[\int_0^{F_0} x(F)F^k \mathrm{d}F - b_k^P\right],\end{aligned} \tag{3.36}$$

where λ_k represents an unknown Lagrangian multiplier. In order to derive the extended quantile function for right truncated samples, the entropy can be maximized using the usual condition

$$\frac{\partial \overline{H}}{\partial x(F)} = 0. \tag{3.37}$$

Substituting Eq. (3.36) into Eq. (3.37) and then simplifying further yields the subsequent solution as presented in Eq. (3.38) provides the extended quantile function from a right truncated sample

$$x_M(F) = \exp\left[-1 - \sum_{k=0}^{M} \lambda_k\, F^k\right], \quad 0 \le F \le F_0. \tag{3.38}$$

Once again, the Lagrangian parameters are obtained numerically by solving the following set of M+1 nonlinear simultaneous equations

$$\int_0^{F_0} F^k \exp\left[-1 - \sum_{i=0}^{M} \lambda_i\, F^i\right] \mathrm{d}F = b_k^P \quad k = 0, 1, \ldots, M. \tag{3.39}$$

3.6. Optimal order

This section aims to introduce a procedure for identifying the most suitable order for the extended maximum entropy quantile functions using a particular dataset. This approach relies on the utilization of the AIC, which serves as a tool for selecting the appropriate model (Burnham and Anderson, 2002).

Let $x(F)$ represent the actual yet unknown quantile function (QF) for the random variable X, and $x_K(F)$ denote the extended quantile function estimation derived from a K-order PPWMs as described in Eq. (3.32).

In this situation, Kullback-Leibler (KL) entropy can provide a degree of the closeness among $x(F)$ and $x_K(F)$

$$\mathrm{KL}[x(F), x_K(F)] = \int_{F_0}^{1} x(F) \ln \frac{x(F)}{x_K(F)} \, \mathrm{d}F = C - L(\lambda, K), \tag{3.40}$$

where

$$C = \int_{F_0}^{1} x(F) \ln x(F) \, \mathrm{d}F \,, \tag{3.41}$$

and

$$L(\lambda, K) = \int_{F_0}^{1} x(F) \ln x_K(F) \, \mathrm{d}F. \tag{3.42}$$

The KL entropy acts as a measurement for gauging the difference between the actual QF and the estimated extended QF. When $\mathrm{KL}[x(F), x_K(F)]$ is smaller, it indicates a closer alignment of $x_K(F)$ with $x(F)$, signifying a higher quality fit for the model $x_K(F)$. In the most extreme scenario, $\mathrm{KL}[x(F), x_K(F)]$ equals zero when $x_K(F)$ perfectly matches $x(F)$. As a result, when choosing parameters for $x_K(F)$, the aim is to minimize the KL entropy.

The variable C in Eq. (3.41) remains unaffected by $x_K(F)$. Therefore, when we strive to minimize the KL entropy by adjusting K and λ, we can treat C as a constant. Meanwhile, by evaluating Eq. (3.42), it becomes evident that the expression $L(\lambda, K)$ represents the expected value of $\ln x_K(F)$. Consequently, from a set of N measurements, we can derive a "natural estimate," denoted as $\hat{L}(\lambda, K)$, for $L(\lambda, K)$

$$\hat{L}(\lambda, K) = \frac{1}{n} \sum_{i=1}^{n} [x_i \ln x_k(F_i | \lambda, K)], \tag{3.43}$$

$$\widehat{\mathrm{KL}}(\lambda, K) = C - \hat{L}(\lambda, K), \tag{3.44}$$

where $x_i : i = 1, 2, \dots, N$ represents the N measured sample values. When K is a known quantity, optimizing $\widehat{\mathrm{KL}}(\lambda, K)$ will yield the most suitable value for λ. This process is equivalent to solving the system of nonlinear equations presented in Eq. (3.33).

The expression $\hat{L}(\lambda, K)$ represents the log-likelihood function. Therefore, the values of λ and K that minimize the KL entropy estimate $\widehat{\mathrm{KL}}(\lambda, K)$ correspond to maximum likelihood estimates. It is also important to recognize that, in the case of a finite sample size (denoted as N), these maximum likelihood estimates are frequently subject to bias and may deviate from the true parameters.

Akaike (1973) introduced an impartial estimation for $\hat{\mathrm{L}}(\lambda, K)$, subsequently recognized as the AIC. One of these unbiased estimates for $-\hat{L}(\lambda, K)$ is provided by

$$\hat{\Gamma}(\lambda, K) = -\hat{L}(\lambda, K) + \frac{K}{N}, \tag{3.45}$$

where $\hat{\Gamma}(\lambda, K)$, called differential entropy, are the unbiased estimates of $-\hat{L}(\lambda, K)$. Considering Eq. (3.45) it can be expanded as

$$\hat{\Gamma}(\lambda, K) = \sum_{s=0}^{K} \lambda_s \left\{ \frac{1}{n} \sum_{i=1}^{n} [x_i (F_i)^s] \right\} + \frac{K}{N}, \tag{3.46}$$

which is equal to

$$\hat{\Gamma}(\lambda, K) = \sum_{S=0}^{K} (\lambda_s b_s^P) + \frac{K}{N}, \tag{3.47}$$

where b_s^P is the sample estimate of the type 2 PPWMs for left truncated samples obtained from Eq. (3.23).

In the case of right truncation, KL entropy can be written as

$$\mathrm{KL}[x(F), x_K(F)] = \int_0^{F_0} x(F) \ln \frac{x(F)}{x_K(F)} \, \mathrm{d}F = C - L(\lambda, K), \tag{3.48}$$

where

$$C = \int_0^{F_0} x(F) \ln x(F) \, \mathrm{d}F, \tag{3.49}$$

and

$$L(\lambda, K) = \int_0^{F_0} x(F) \ln x_K(F) \, \mathrm{d}F. \tag{3.50}$$

Similar to left truncated samples, the differential entropy for right truncated samples can be obtained using Eq. (3.47) while using type 2 PPWMs for right truncated samples obtained from Eq. (3.25).

Akaike's method of estimation can be summarized as follows:

- Calculate the corresponding Lagrangian multipliers (λ_s) for different K-order using Eq. (3.33) for left truncated samples or Eq. (3.39) for right truncated samples and establish the extended quantile functions.
- Determine the differential entropy ($\hat{\Gamma}(\lambda, K)$) for different orders of the extended quantile function using Eq. (3.47).
- Obtain the relation between $\hat{\Gamma}(\lambda, K)$ and K.
- Find the best order of approximation that minimizes the value of $\hat{\Gamma}(\lambda, K)$ as a function of K.

3.7. Illustrative example of maximum entropy quantile function from a truncated sample (cohesion of rock discontinuities)

Rock slopes are a common occurrence in global open pit mining and civil engineering endeavors. Designs that are overly cautious or prone to instability can result in significant adverse economic consequences. Therefore, incorporating reliability analysis is a crucial stage in achieving optimized designs (Deng and Pandey, 2023). In order to illustrate the application of maximum entropy in estimating quantile functions from truncated samples, an example is provided in this section. The result of this example will be used to conduct quantile-based FORM for a truncated sample in Chapter 4.

A data set including 50 samples (Table 3.1) was created using MCS to evaluate the ability of the quantile function to represent truncated samples. This data represents the cohesion of rock discontinuities on the Sau Mau Ping rock slope in Hong Kong, as suggested by Hoek (2006). The mean and standard deviation are 100 kPa and 20 kPa, respectively. This sample also follows a normal distribution.

The first step in evaluating the effect of truncated samples on the quantile functions calculated by the MEPs is to calculate the quantile functions for the original sample while considering different orders of PWMs. Using the data provided in Table (3.1), it is possible to derive PWMs (Table 3.3) by using Eq. (3.11). Subsequently, solving Eq. (3.17) with corresponding PWMs allows for the determination of the maximum entropy quantile function for the original data set.

Table 3.1. Illustrative sample (cohesion of rock discontinuities)

No.	Value (kPa)	No.	Value (kPa)	No.	Value (kPa)	No.	Value (kPa)
1	62.86	14	92.84	27	101.27	40	119.94
2	64.07	15	92.88	28	101.34	41	122.68
3	65.58	16	93.53	29	102.35	42	123.44
4	65.72	17	93.68	30	103.15	43	124.32
5	68.67	18	94.33	31	104.13	44	126.95
6	77.90	19	95.19	32	105.05	45	129.34
7	80.61	20	95.68	33	106.35	46	130.84
8	80.95	21	96.44	34	106.48	47	131.80
9	81.72	22	96.93	35	106.95	48	135.39
10	83.43	23	97.18	36	107.60	49	135.48
11	87.80	24	98.03	37	108.03	50	136.00
12	89.67	25	98.62	38	110.69		
13	90.16	26	99.70	39	117.96		

In the next step the effects of different truncation percentages on maximum entropy quantile functions are evaluated. Using the data provided in Table 3.1 and considering different amounts for truncation including 4, 6, 8, and 10 percent for both left and right sides (Table 3.2), it is possible to derive PPWMs (Table 3.3) through using Eqs. (3.23) and (3.25). Subsequently, solving Eqs. (3.32) and (3.38) with corresponding PPWMs allow for the determination of extended maximum entropy quantile functions for left and right truncated samples, respectively. Calculated Lagrangian multipliers (λ_s) for all the mentioned conditions are provided in Appendix A (Tables A.1 to A.9).

Table 3.2. Removed sample elements for different truncation conditions

Truncation	10% left	8% left	6% left	4% left	4% right	6% right	8% right	10% right
Removed elements	62.86	62.86	62.86	62.86	135.48	135.39	131.80	130.84
	64.07	64.07	64.07	64.07	136.00	135.48	135.39	131.80
	65.58	65.58	65.58			136.00	135.48	135.39
	65.72	65.72					136.00	135.48
	68.67							136.00

Table 3.3. PWMs and PPWMs for the original and truncated samples

Truncation		10% left	8% left	6% left	4% left	original	4% right	6% right	8% right	10% right
PWM and PPWM Order (K)	1	94.30	95.67	96.98	98.30	100.00	95.40	92.70	90.06	87.44
	2	55.69	55.80	55.88	55.94	55.96	54.48	53.67	52.87	52.04
	3	39.17	39.18	39.18	39.18	39.18	38.16	37.61	37.10	36.58
	4	30.31	30.31	30.31	30.31	30.31	29.50	29.06	28.66	28.24
	5	24.79	24.79	24.79	24.79	24.79	24.12	23.75	23.41	23.05
	6	21.00	21.00	21.00	21.00	21.00	20.44	20.11	19.82	19.51
	7	18.23	18.23	18.23	18.23	18.23	17.75	17.46	17.21	16.93
	8	16.11	16.11	16.11	16.11	16.11	15.69	15.44	15.21	14.97
	9	14.44	14.44	14.44	14.44	14.44	14.07	13.84	13.64	13.42
	10	13.08	13.08	13.08	13.08	13.08	12.76	12.54	12.37	12.17

In the next step, differential entropy is calculated using Eq. (3.47) to find the optimum order of the quantile functions (Appendix A, Figures A.1 to A.9). For a fixed constant N, the term $\frac{K}{N}$ in Eq. (3.47) increases with respect to K. As a result, there must be a minimum value for differential entropy $\hat{\Gamma}(\lambda, K)$ at a specific K. In other words, when considering a range of K values, there exists a particular K that minimizes the differential entropy $\hat{\Gamma}(\lambda, K)$ in Eq. (3.47). This specific K is the optimal order for the maximum entropy quantile functions.

The term $\frac{K}{N}$ in the AIC serves as a penalty component, aiming to restrict the creation of extra complex models that cannot be justified by the available data sample. When working with limited data, the combination of MEPs and AIC is employed to find the most suitable order

of PWMs or PPWMs for estimating a quantile function (Deng, 2022). This approach helps prevent the adoption of models that are excessively detailed, possess an excessive number of adjustable parameters that cannot effectively capture the sample information, or are excessively simplistic. Using Appendix A, the optimal order of the maximum entropy quantile function and the optimal order of the extended maximum entropy quantile functions are obtained from the original and truncated samples, which are provided in Eqs. (3.51) to (3.59).

$$x(F)_{(\text{original})} = \exp(4.009260594 + 3.857893962\,F - 10.27669061\,F^2 + 12.22220741\,F^3 - 4.874544052\,F^4). \tag{3.51}$$

$$x(F)_{(4\%\text{left})} = \exp(4.087696758 + 3.682881587\,F - 10.65013437\,F^2 + 13.42996566\,F^3 - 5.623491466\,F^4). \tag{3.52}$$

$$x(F)_{(6\%\text{left})} = \exp(4.140115757 + 3.404298302\,F - 10.14307342\,F^2 + 13.10719504\,F^3 - 5.58459012\,F^4). \tag{3.53}$$

$$x(F)_{(8\%\text{left})} = \exp(4.21600081 + 2.803174627\,F - 8.459002782\,F^2 + 11.1917928\,F^3 - 4.825658216\,F^4). \tag{3.54}$$

$$x(F)_{(10\%\text{left})} = \exp(4.356473778 + 0.944717749\,F - 1.297395076\,F^2 + 0.974380173\,F^3). \tag{3.55}$$

$$x(F)_{(4\%\text{right})} = \exp(4.0787458 + 2.4335708\,F - 3.9678913\,F^2 + 2.4301120\,F^3). \tag{3.56}$$

$$x(F)_{(6\%\text{right})} = \exp(4.0728289 + 2.4622539\,F - 4.0279858\,F^2 + 2.4485860\,F^3). \tag{3.57}$$

$$x(F)_{(8\%\text{right})} = \exp(4.0653499 + 2.5098953\,F - 4.1398364\,F^2 + 2.5054175\,F^3). \tag{3.58}$$

$$x(F)_{(10\%\text{right})} = \exp(4.0591499 + 2.5385064\,F - 4.1964208\,F^2 + 2.5210470\,F^3). \tag{3.59}$$

The distribution of a random variable can also be determined by conventional methods from a sample of data (Table 3.1). First, assume a normal or lognormal distribution, then use the method of maximum likelihood to calculate the parameters. The normal and lognormal distributions can be obtained as follows

$$f_{(X)}(x) = \frac{1}{\sigma_X\sqrt{2\pi}}\ \exp\left[-\frac{1}{2}\left(\frac{x-\mu_X}{\sigma_X}\right)^2\right], -\infty < x < +\infty, \tag{3.60}$$

$$f_{(X)}(x) = \frac{1}{\zeta_X x\sqrt{2\pi}}\ \exp\left[-\frac{1}{2}\left(\frac{\ln x - \lambda_X}{\zeta_X}\right)^2\right],\ \ x \geq 0, \tag{3.61}$$

where σ_X is the standard deviation, μ_X is the mean, ζ_X and λ_X are also the parameters of the lognormal distribution which can be calculated using Eqs. (3.62) and (3.63).

$$\zeta_X^2 = \ln\left[1 + \left(\frac{\sigma_X}{\mu_X}\right)^2\right], \tag{3.62}$$

$$\lambda_X = \ln \mu_X - \frac{1}{2}\zeta_X^2. \tag{3.63}$$

Cohen (1959) offered a method to calculate the mean and the standard deviation of truncated samples

$$\sigma_X^{P\,2} = \sigma_X{}^2 + \lambda(h,\alpha)(\mu - T)^2, \tag{3.64}$$

$$\mu_X^P = \mu_X - \lambda(h,\alpha)(\mu - T)^2, \tag{3.65}$$

where σ_X^P is the standard deviation, μ_X^P is the mean of a truncated sample, σ_X and μ_X are the standard deviation and the mean directly obtained from the sample and T is the value of the data at the truncation point. Furthermore, λ is a function of h (Eq. 3.66) and α (Eq. 3.67) that can be obtained from the chart in Appendix D.

$$h = \frac{c}{N}, \tag{3.66}$$

$$a = \frac{\sigma^2}{(\mu_X - T)^2}, \tag{3.67}$$

where c is the number of missing data and N is the number of the original sample of data. Based on the method suggested by Cohen (1959) the parameters of the normal and lognormal distributions are calculated (Table 3.4).

After calculating the parameters for normal and lognormal distributions from truncated samples, the value of the random variable for various quantile amounts can be calculated using the *NORM.INV* and *LOGNORM.INV* functions in Microsoft Excel. These calculated values from normal and lognormal distributions are then compared with those obtained from maximum entropy quantile functions (Eq. (3.51) to Eq. (3.59)) in the next section.

Table 3.4. Parameters for normal and lognormal distributions

Distribution	Normal		Lognormal	
	μ_X^P	σ_X^P	λ_X^P	ζ_X^P
10% left	103.8342	16.8941	4.6297	0.1616
8% left	102.7189	18.3229	4.6163	0.1770
6% left	102.1970	18.4429	4.6109	0.1790
4% left	101.7800	18.2483	4.6070	0.1779
original	100	20	4.5856	0.1980
4% right	99.9573	18.3626	4.5881	0.1822
6% right	99.3185	18.0783	4.5820	0.1805
8% right	98.9506	18.2737	4.5779	0.1831
10% right	98.5550	18.4071	4.5735	0.1852

3.7.1. Comparison between fit lines obtained from different methods

For left truncated samples (Figures 3.2 to 3.5), from the truncation point to a probability of 0.3, all quantile functions yield comparable fit lines. Within the range of 0.3 to 0.65, the optimal order of the maximum entropy quantile function exhibits a better fit compared to normal and lognormal quantile functions. Between 0.65 and 0.75, fit lines from various methods converge, presenting nearly identical results. Ultimately, from 0.75 to the end, the maximum entropy quantile function is more effective in producing the best fit line for the given dataset.

Furthermore, for the right truncated samples (Figures 3.6 to 3.9), between 0 and 0.15, the optimal order of quantile functions results in a better fit line than that of normal and lognormal quantile functions. In the interval from 0.15 to 0.22, all quantile functions generate similar fit lines. Following this, from 0.22 to 0.75, the most advantageous fit is achieved with the optimal order of the maximum entropy quantile function. Lastly, from 0.75 to the truncation point, the lines derived from different methods nearly overlap.

In addition to this, the residual sum of squares (RSS) method is employed in order to compare fit lines obtained from different methods. The formula for RSS with n data points is (Archdeacon, 1994)

$$\mathrm{RSS} = \sum_{i=1}^{n} (y_i - \bar{y}_i)^2, \tag{3.68}$$

where y_i is the actual observed value for the data point i, and $\bar{y}_i$ is the predicted value for the data point i.

The fit line that minimizes the sum of squared differences between observed and predicted values can be considered the best fit for the sample of data. A lower RSS indicates a better fit because it means that the model's predictions are closer to the actual observed values. The results of calculating RSS for normal, lognormal, and optimal maximum entropy are provided in Table 3.5, which shows that the optimal order of maximum entropy is more capable of minimizing RSS in all conditions including the original and different truncated samples.

Table 3.5. Comparison for the residual sum of squares (RSS)

Distribution	Normal	Lognormal	Optimal order maximum entropy
10% left	1502.13	1828.63	729.42
8% left	1442.58	1938.54	855.51
6% left	1375.48	2087.28	773.83
4% left	1256.27	2188.82	543.66
original	1049.43	2414.66	195.63
4% right	547.98	726.44	358.67
6% right	697.81	930.33	531.21
8% right	859.83	1146.25	739.72
10% right	1013.93	1352.88	939.00

In conclusion, the examination of both left and right truncated samples consistently reveals that the optimal order of the maximum entropy quantile function consistently outperforms normal and lognormal quantile functions in providing a best fit line for different truncations conditions. This is based on the notion that the optimum maximum entropy quantile function involves four or five PPWMs, guaranteeing a higher level of information compared to only two ordinary moments present in a normal distribution. Another benefit of the suggested model lies in the fact that maximum entropy quantile functions are not limited to traditional

probability distributions like the normal and lognormal functions. The selection of a maximum entropy quantile function solely relies on the sample information, making it an objective choice rather than a subjective one.

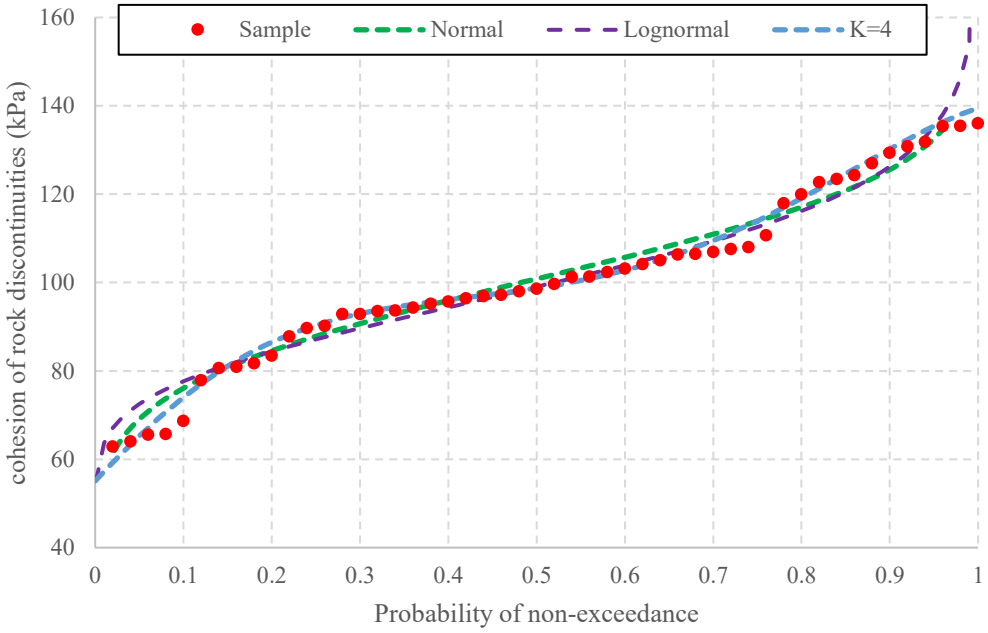

Figure 3.1. Maximum entropy quantile function for the original data set

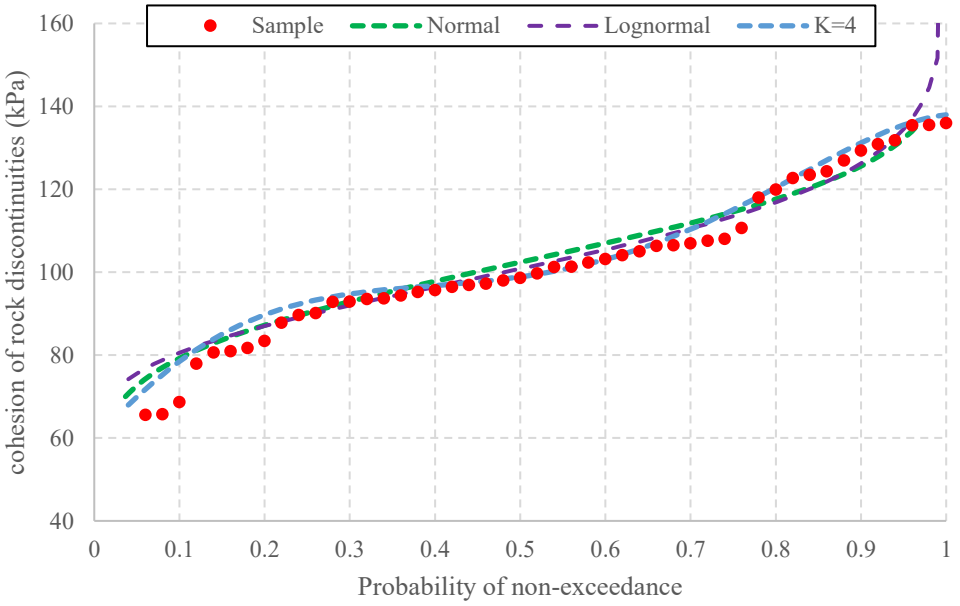

Figure 3.2. Maximum entropy quantile function for 4% left truncated data set

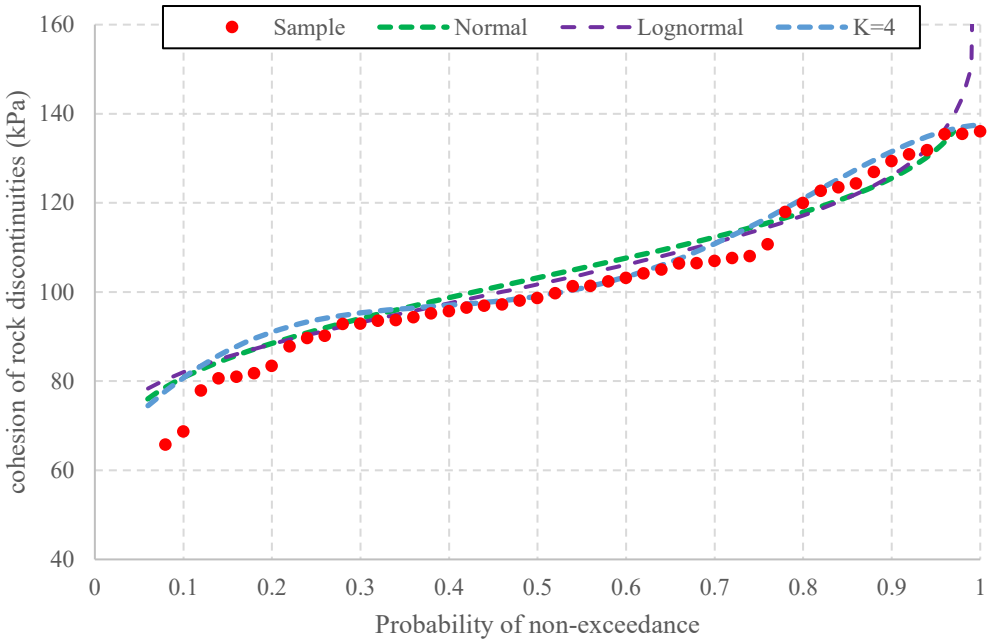

Figure 3.3. Maximum entropy quantile function for 6% left truncated data set

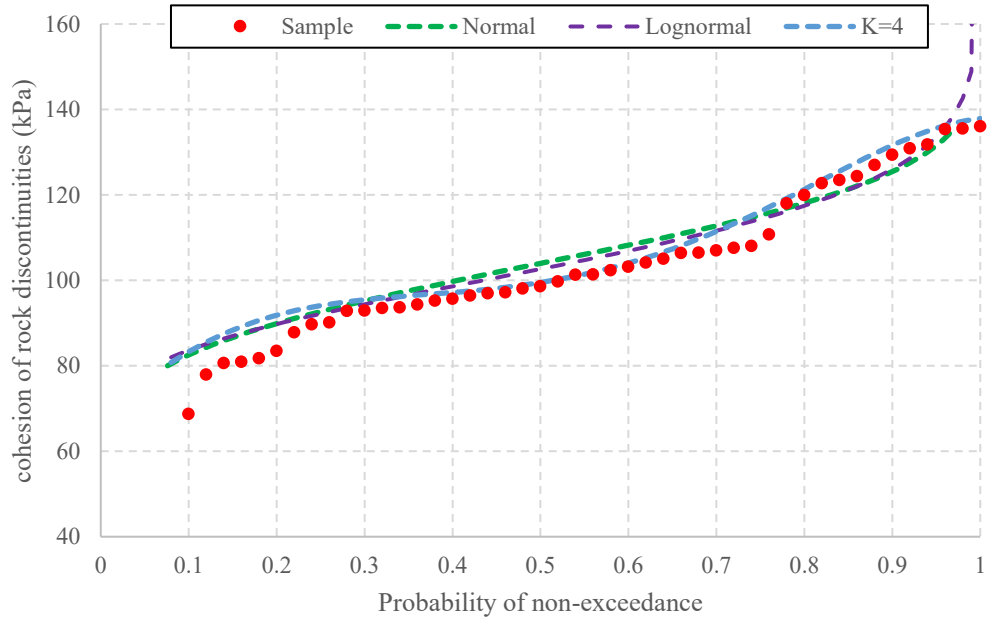

Figure 3.4. Maximum entropy quantile function for 8% left truncated data set

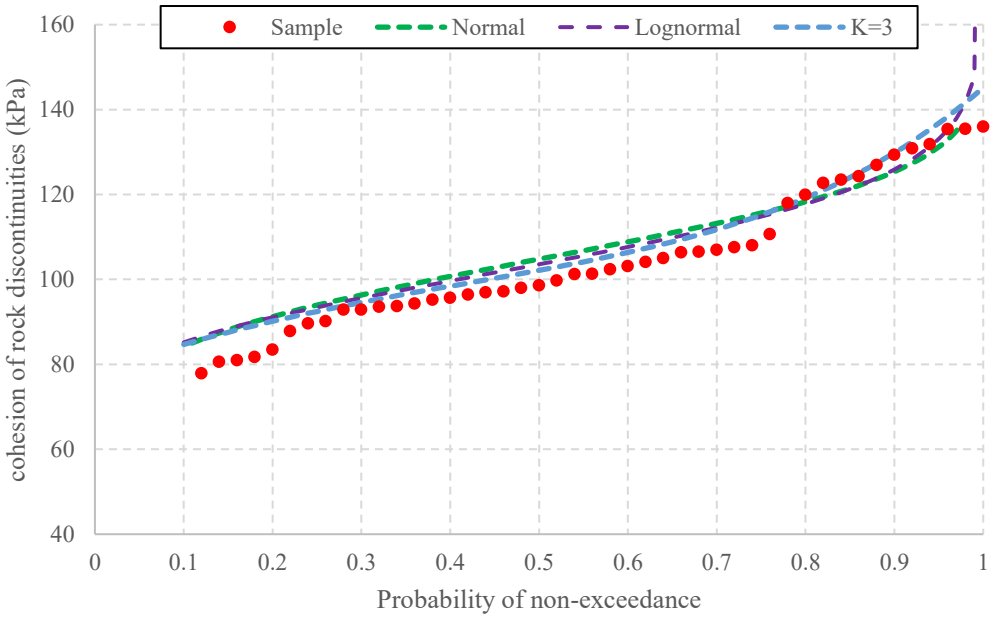

Figure 3.5. Maximum entropy quantile function for 10% left truncated data set

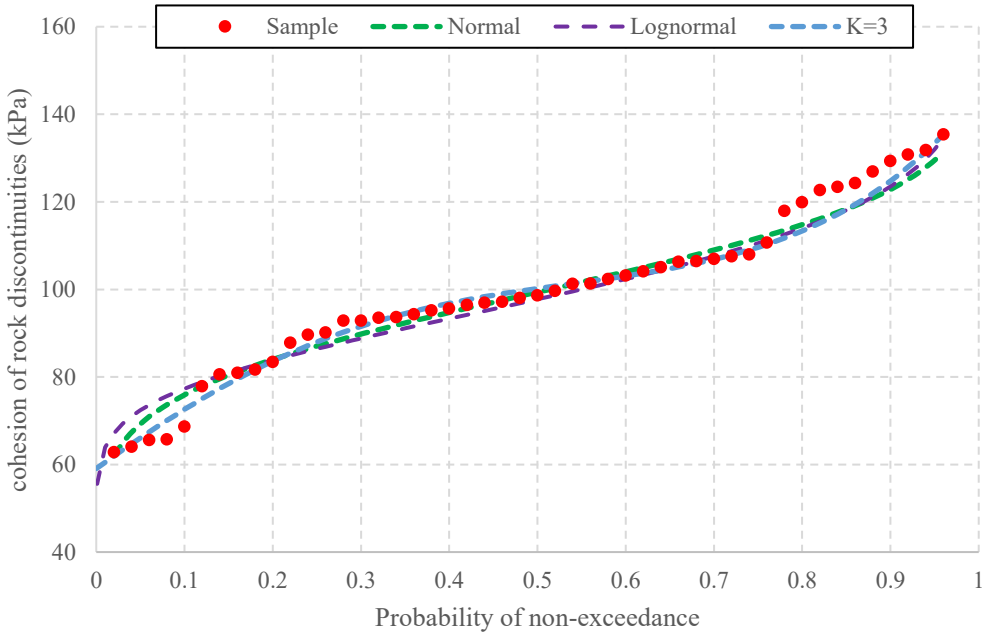

Figure 3.6. Maximum entropy quantile function for 4% right truncated data set

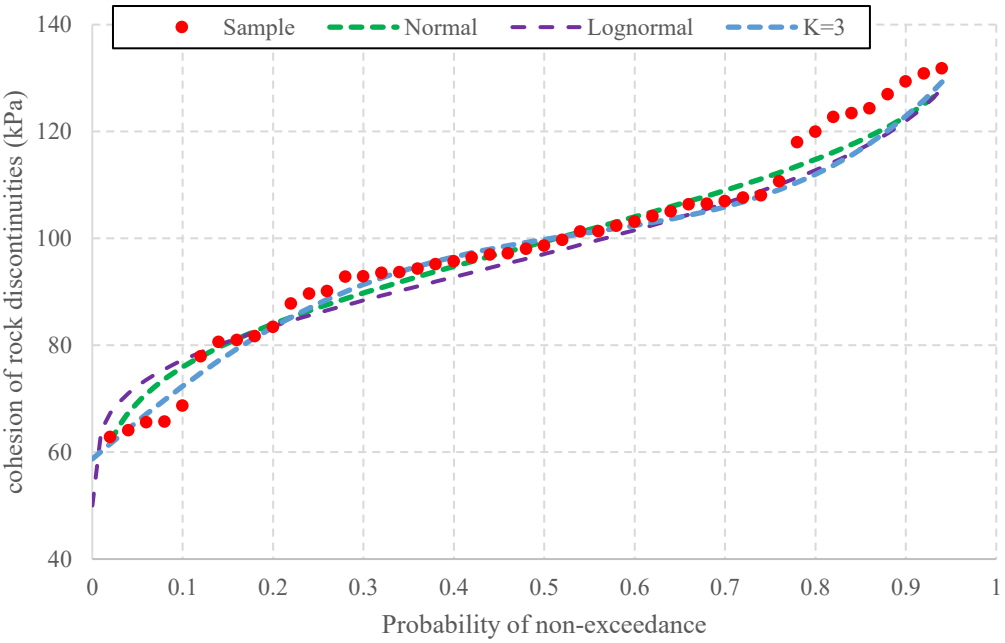

Figure 3.7. Maximum entropy quantile function for 6% right truncated data set

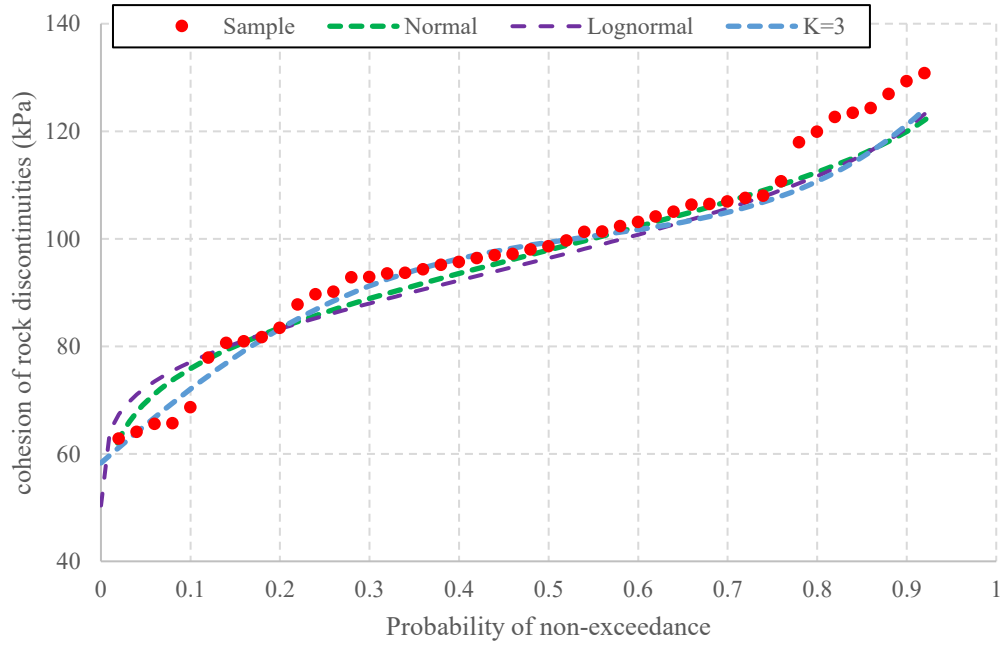

Figure 3.8. Maximum entropy quantile function for 8% right truncated data set

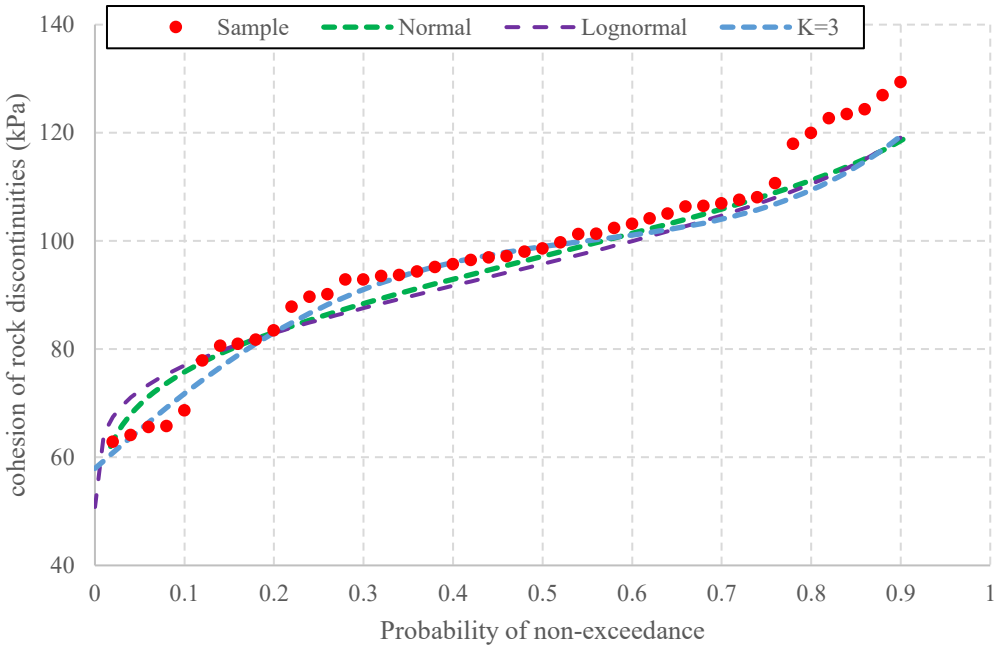

Figure 3.9. Maximum entropy quantile function for 10% right truncated data set

3.8. Illustrative example of maximum entropy quantile function from a truncated sample (rock uniaxial compression strength)

The variability in natural rock consistently results in uncertainty regarding the parameters obtained from compressive testing data obtained from a limited number of specimens. Estimating the rock mass parameters is one of the most important and challenging parts of engineering designs in civil engineering projects. Uniaxial compression strength is also considered one of the most useful types of information regarding rock mass classification and the calculation related to the parameters of rock mass. Unlike the example in Section 3.7 where the sample was created using MCS, in this example, a sample of 48 data points obtained from uniaxial compression tests is employed to illustrate the ability of the maximum entropy quantile function to represent the data set in different truncation scenarios. The laboratory experiments detailed in Table 3.6 were carried out by Cui et al. (2017). The dataset follows a normal distribution, with a mean value of 129.64 MPa and a standard deviation of 30.41 MPa. For this example, seven different conditions are evaluated, including the original data set and different values for truncation including 4, 8.5 and 12.5 percent for both the left and right sides (Table 3.7).

Table 3.6. Illustrative sample (rock uniaxial compression strength), Cui et al. (2017)

No.	Value (MPa)	No.	Value (MPa)	No.	Value (MPa)	No.	Value (MPa)
1	61.2	14	112.00	27	136.40	40	159.10
2	63.2	15	114.60	28	137.40	41	162.60
3	66.6	16	114.90	29	139.00	42	165.30
4	86.5	17	115.00	30	140.00	43	165.50
5	90.8	18	118.70	31	140.70	44	167.90
6	97.7	19	119.70	32	142.20	45	174.70
7	98.0	20	123.20	33	142.60	46	177.20
8	99.7	21	125.80	34	144.40	47	191.70
9	102.4	22	128.90	35	147.50	48	191.90
10	104.3	23	129.20	36	148.90		
11	106.4	24	129.60	37	150.90		
12	109.7	25	129.60	38	152.50		
13	112.0	26	131.80	39	152.90		

Table 3.7. Removed sample elements for different truncation conditions

Truncation	12.5% left	8.5% left	4% left	4% right	8.5% right	12.5% right
Removed elements	61.2	61.2	61.2	191.70	174.70	165.50
	63.2	63.2	63.2	191.90	177.20	167.90
	66.6	66.6			191.70	174.70
	86.5	86.5			191.90	177.20
	90.8					191.70
	97.7					191.90

The equations used to obtain the maximum entropy quantile functions are the same as the previous example using PWMs and PPWMs provided in Table 3.8. Calculated Lagrangian multipliers for all the mentioned conditions are provided in Appendix B (Tables B.1 to B.7). The optimal order of the maximum entropy is also determined using the AIC method, as previously discussed, and results are provided in Appendix B (Figures B.1 to B.7). Using Appendix B, the optimal order of the maximum entropy quantile function and the optimal order of the extended maximum entropy quantile functions are obtained from the original and truncated samples which are provided in Eqs. (3.69) to (3.75).

Table 3.8. PWMs and PPWMs for the original and truncated samples

Truncation		12.5% left	8.5% left	4% left	original	4% right	8.5% right	12.5% right
PWM and PPWM Order (K)	1	119.93	123.86	127.05	129.64	121.65	114.32	107.37
	2	73.00	73.37	73.55	73.58	70.85	68.46	66.15
	3	51.85	51.88	51.89	51.89	49.89	48.35	47.00
	4	40.29	40.29	40.29	40.29	38.62	37.40	36.39
	5	33.03	33.03	33.03	33.03	31.56	30.53	29.71
	6	28.04	28.04	28.04	28.04	26.72	25.82	25.12
	7	24.40	24.40	24.40	24.40	23.19	22.38	21.77
	8	21.61	21.61	21.61	21.61	20.49	19.76	19.21
	9	19.41	19.41	19.41	19.41	18.36	17.69	17.20
	10	17.63	17.63	17.63	17.63	16.64	16.02	15.58

$$x(F)_{(\text{original})} = \exp\left(3.93388 + 8.1284\,F - 33.33669\,F^2 + 68.6233\,F^3 - 66.22578\,F^4 + 24.213\,F^5\right). \tag{3.69}$$

$$x(F)_{(4\%\text{left})} = \exp\left(4.342571932 + 2.264114601\,F - 3.383517329\,F^2 + 2.068215781F^3\right). \tag{3.70}$$

$$x(F)_{(8.5\%\text{left})} = \exp\left(4.491678097 + 1.440221537\,F - 1.920203797\,F^2 + 1.26471638\,F^3\right). \tag{3.71}$$

$$x(F)_{(12.5\%\text{left})} = \exp\left(4.54458762 + 1.270312731\,F - 1.693392812\,F^2 + 1.156148448\,F^3\right). \tag{3.72}$$

$$x(F)_{(4\%\text{right})} = \exp\left(3.927046646 + 7.990767102\,F - 32.06022243\,F^2 + 64.40627249\,F^3 - 60.57158758\,F^4 + 21.54440374\,F^5\right). \tag{3.73}$$

$$x(F)_{(8.5\%\text{right})} = \exp\left(3.913422134 + 8.044834257\,F - 32.23857336\,F^2 + 64.48164527\,F^3 - 60.28915933\,F^4 + 21.27158575\,F^5\right). \tag{3.74}$$

$$x(F)_{(12.5\%\text{right})} = \exp\left(3.887228146 + 8.444879131\,F - 34.90206209\,F^2 + 71.48686968\,F^3 - 68.20265127\,F^4 + 24.45233658\,F^5\right). \tag{3.75}$$

Table 3.9. Parameters for normal and lognormal distributions

Distribution	Normal		Lognormal	
	μ_X^P	σ_X^P	λ_X^P	ζ_X^P
12.5% left	130.3846	29.1462	4.8461	0.2208
8.5% left	130.1816	29.6649	4.8436	0.2250
4% left	129.7296	30.9249	4.8378	0.2351
original	129.64	30.41	4.8379	0.2314
4% right	129.5943	31.0176	4.8366	0.2360
8.5% right	129.2103	30.6061	4.8341	0.2336
12.5% right	129.1301	30.5341	4.8336	0.2333

Similar to the previous example, the parameters of the normal and lognormal distribution for truncated samples are calculated using the method introduced by Cohen (1959) and are provided in Table 3.9. As was mentioned in Section 3.7, the value of the random variable for various quantile amounts can be calculated using the *NORM.INV* and *LOGNORM.INV* functions in Microsoft Excel. These values from normal and lognormal distributions are then compared with those obtained from maximum entropy quantile functions (Eq. (3.69) to Eq. (3.75)) in the next section.

3.8.1. Comparison between fit lines obtained from different methods

In order to compare the effectiveness of the maximum entropy quantile function, a comparison is also conducted between results obtained from normal and lognormal distributions. For left truncated samples (Figures 3.11 to 3.13), from the truncation point to a probability of 0.6, the optimal order of maximum entropy quantile function leads to a better fit in comparison with normal and lognormal distributions. Within the range of 0.6 to 0.85, all quantile functions generate similar fit lines. Between 0.85 and 0.95, fit lines from normal and lognormal methods converge, presenting nearly identical results, while the optimal order of the maximum entropy fit line is less accurate than other methods. Ultimately, from 0.95 to the end, the fit lines from different methods are similar. Furthermore, for the right truncated samples (Figures 3.14 to 3.16), between 0 and 0.80, the optimal order of quantile functions results in a better fit line than that of normal and lognormal quantile functions.

However, in the interval from 0.80 to the truncation point, all quantile functions generate similar fit lines.

Table 3.10. Comparison for the residual sum of squares (RSS)

Distribution	Normal	Lognormal	Optimal order maximum entropy
12.5% left	3074.17	3707.80	2004.40
8.5% left	2276.97	3384.94	1330.41
4% left	1917.21	4299.85	1140.38
original	1638.94	6226.73	671.69
4% right	974.30	2220.46	495.28
8.5% right	1730.82	3147.43	885.94
12.5% right	2566.98	4151.02	1346.21

Similar to the previous example, the residual sum of squares (RSS) method is also employed in order to compare fit lines obtained from different methods. The results of calculating RSS for normal, lognormal, and optimal maximum entropy are provided in Table 3.10, which shows that the optimal order of maximum entropy is more capable of minimizing RSS in all conditions including the original and different truncated samples.

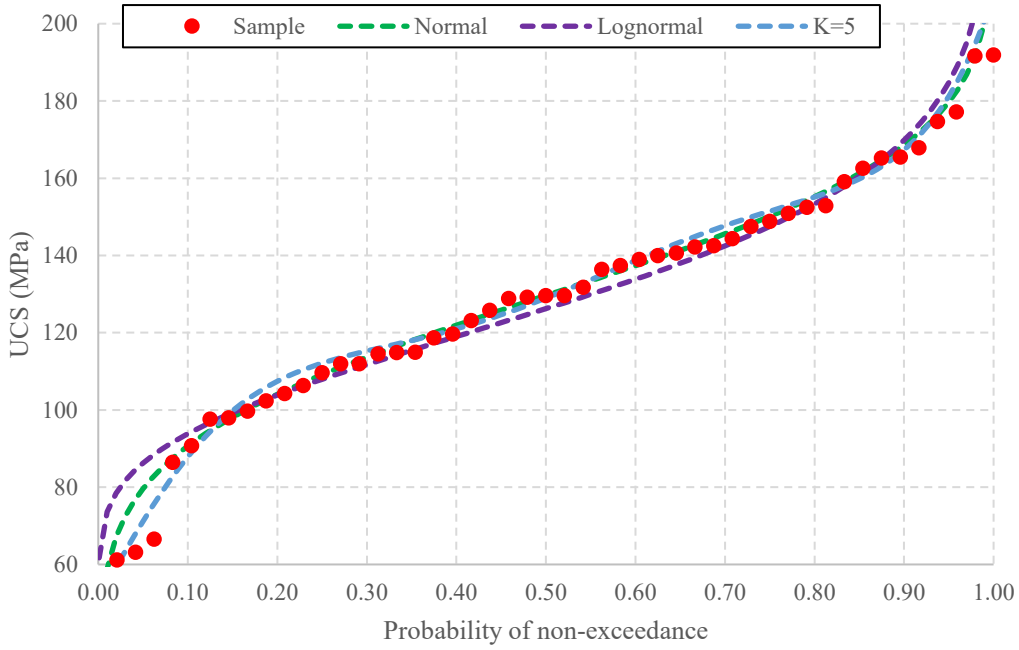

Figure 3.10. Maximum entropy quantile function for the original data set

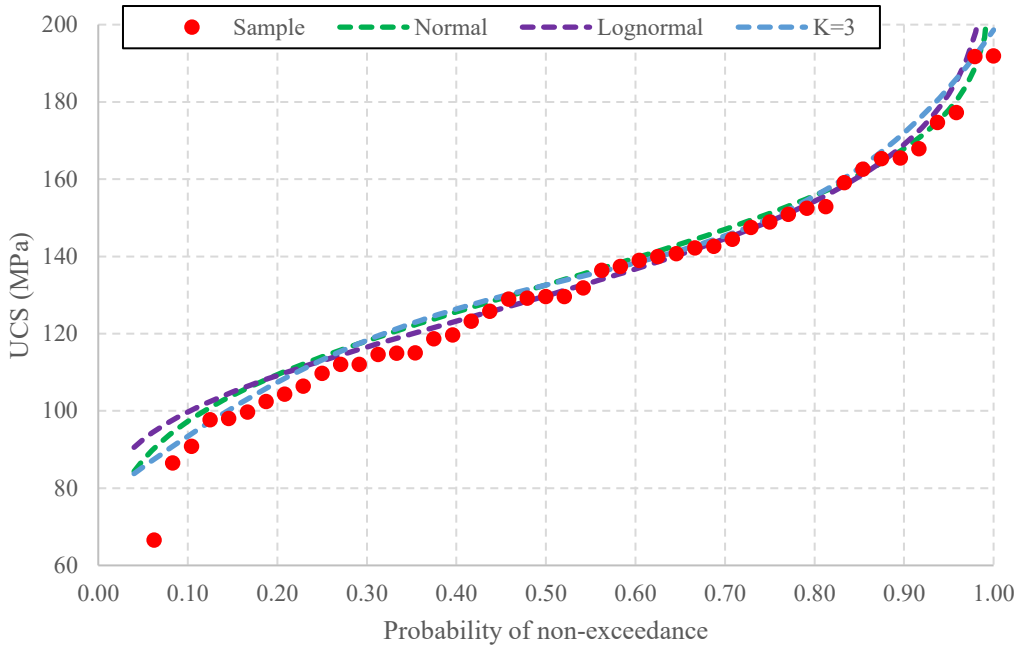

Figure 3.11. Maximum entropy quantile function for 4% left truncated data set

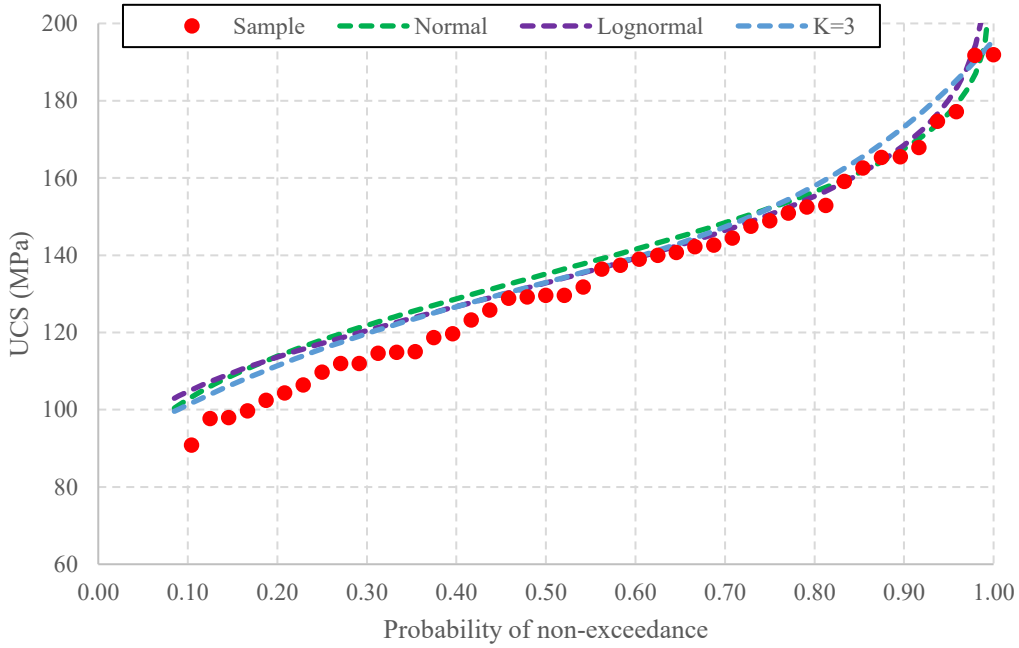

Figure 3.12. Maximum entropy quantile function for 8.5% left truncated data set

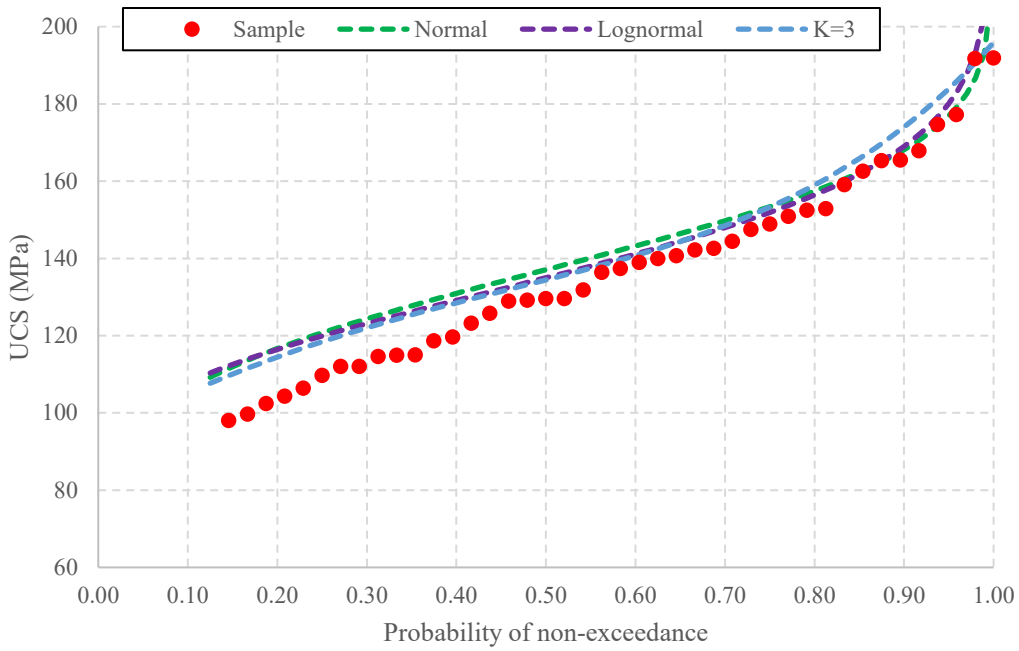

Figure 3.13. Maximum entropy quantile function for 12.5% left truncated data set

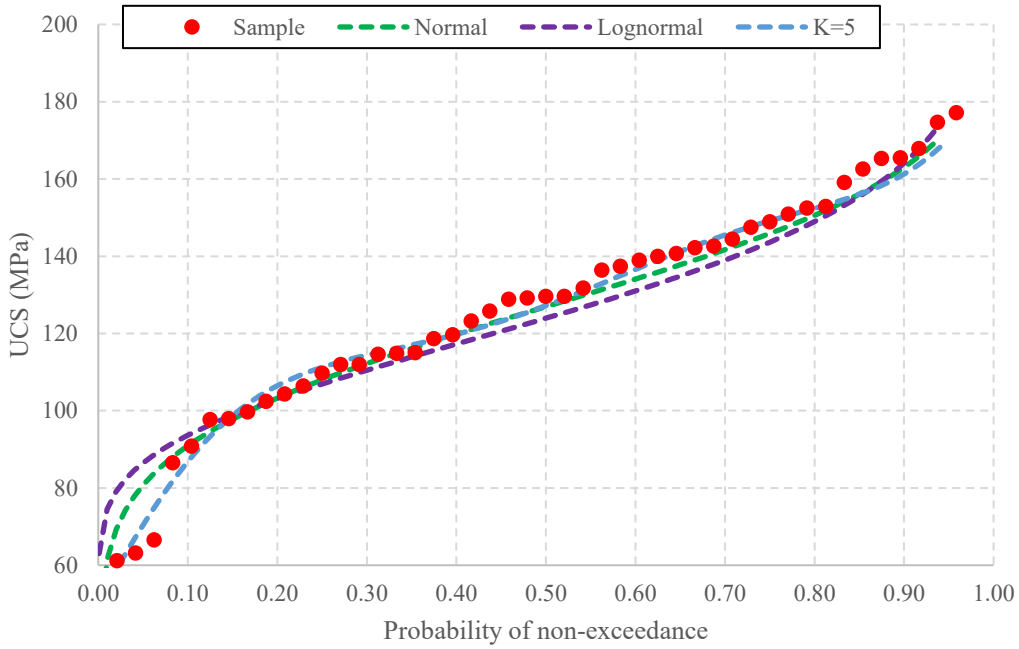

Figure 3.14. Maximum entropy quantile function for 4% right truncated data set

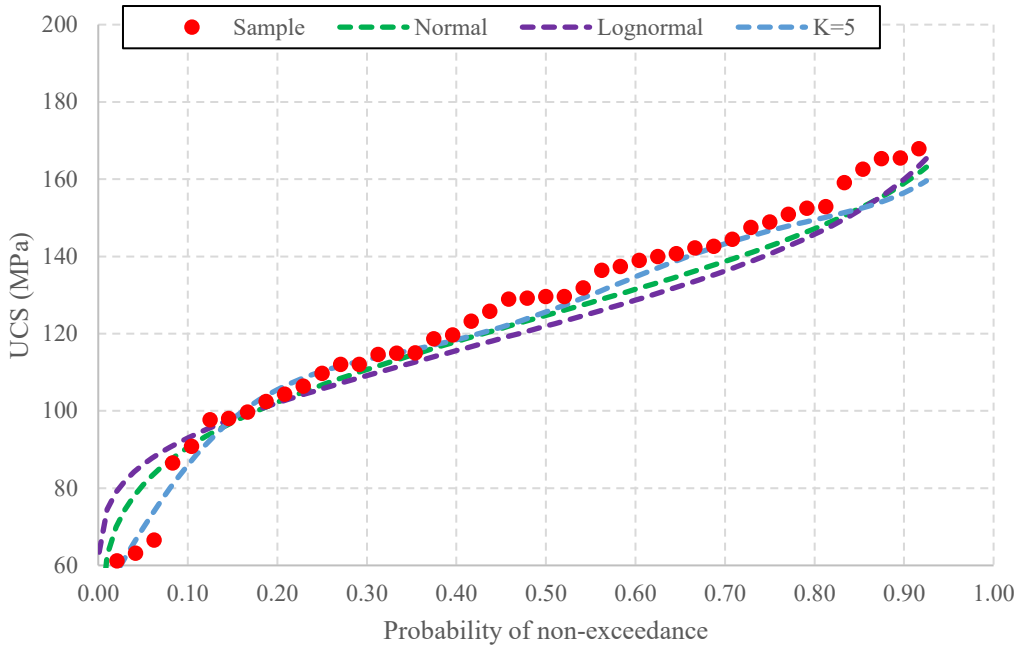

Figure 3.15. Maximum entropy quantile function for 8.5% right truncated data set

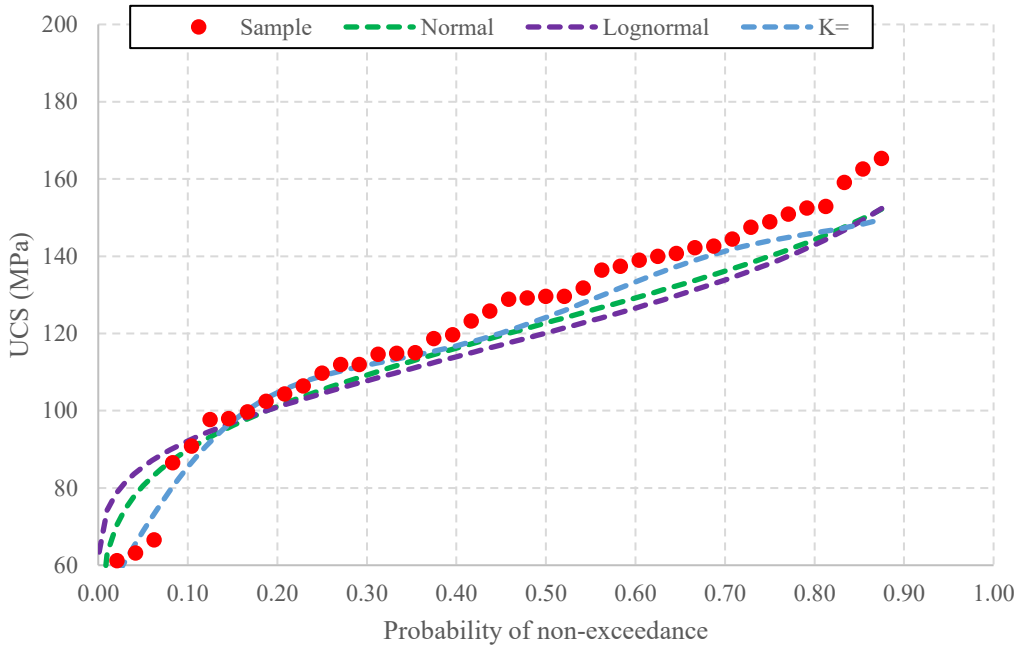

Figure 3.16. Maximum entropy quantile function for 12.5% right truncated data set

3.9. Summary

Chapter 3 focused on the application of MEPs in estimating quantile functions from truncated samples. Various methods are available to recover probability distribution functions from the moments of random variables. The MEPs is a method for calculating probability distribution functions from the moments of a random variable. This method is attractive because it allows for the creation of a probability distribution that is minimally biased, maximizing entropy while incorporating constraints provided by the available information (Rao and Hsieh, 1987).

PWMs were explained to address issues related to small sample sizes in maximum entropy applications. PWMs are robust against the impact of outliers or extreme observations in the dataset. This robustness stems from their formulation as linear combinations of observed data values. This feature of PWMs makes them more appropriate for presenting samples with a limited number of observations. Pandey's method of directly calculating quantile functions using PWMs was presented, emphasizing its advantages in handling higher-order moments accurately.

The chapter then presented PPWMs from truncated samples, explaining how to use the methodology to account for truncation in data. Then, the principles of extended quantile functions from truncated samples were explained to show the steps required to recover quantile functions from truncated samples using PPWMs. The optimal order for maximum entropy quantile functions was discussed, explaining the AIC as a tool for selecting the appropriate model order. Finally, two illustrative examples involving rock slope cohesion and rock uniaxial compression strength were provided, demonstrating the application of MEPs to estimate the extended quantile functions of truncated samples.

The chapter concludes by highlighting the benefits of maximum entropy quantile functions from a truncated sample, including their flexibility and objectivity in model selection based on sample information. The comparison with traditional distributions, such as normal and lognormal distributions, shows the effectiveness of MEPs in capturing distribution characteristics from limited and truncated data.

4. Reliability method with truncated quantile functions

Engineering design involves adjusting the components of a system to meet diverse requirements for performance, safety, usability, and longevity when subjected to different conditions (Haldar and Mahadevan, 2000). Over the past decades, there has been continuous research using probabilistic principles to assess the stability of slopes and embankments (Liang et al. 1999). This chapter focuses on the development of a quantile function-based FORM for truncated samples.

4.1. The application of reliability analysis in geotechnical engineering

Risk and safety analysis relies on the balance between the load and capacity of a structure. A structure can be considered secure when the capacity exceeds the load which can be described as follows (Haldar and Mahadevan, 2000)

$$Z = R - S, \tag{4.1}$$

where Z is the performance function, R is resistance and S is the applied load on the structure. Since R and S are both random variables, they possess mean (μ_R, μ_S) and standard deviations (σ_R, σ_S), which describe their randomness. The relationship between load and resistance, and the probability of failure can be expressed as a distribution function. The mean value represents the difference between the means of random variables, and the probability of failure is denoted by the intersection of the distribution functions for resistance and load (Baecher and Christian, 2005). Represented in Figure (4.1) are typical probability distributions for both R and S.

Deng and Pandey (2023) introduced a quantile-based FORM based on the approach introduced by Paloheimo and Hannus (1974). In this method, random variables that do not follow a normal distribution are converted into equivalent normal random variables using quantile functions and subsequently applied to the Hasofer-Lind method for reliability analysis.

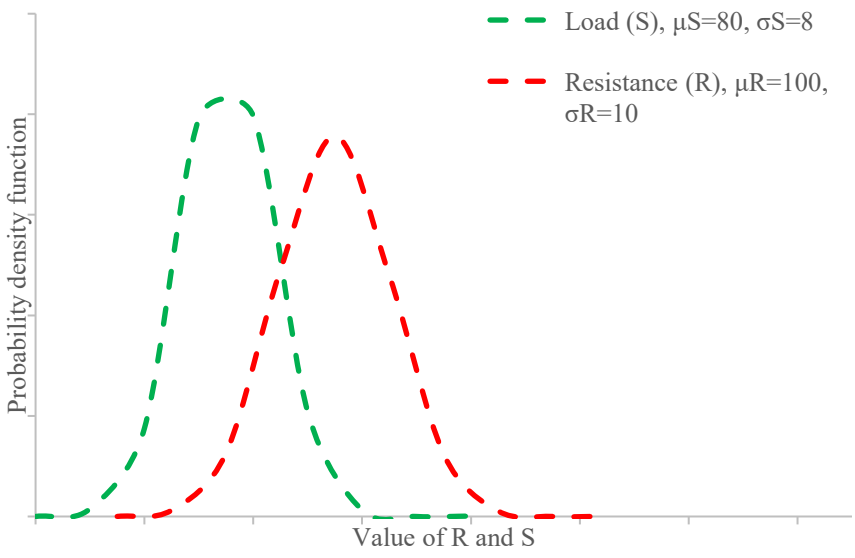

Figure 4.1. Fundamentals of Risk Evaluation

4.2. Quantile based FORM

Assume the limit state function in a reliability analysis is

$$g_X(X) = g_X(X_1, X_2, \dots, X_N) = 0, \tag{4.2}$$

here, $X = (X_1, X_2, \dots, X_N)$ denotes the basic random variables, with N being the count of these variables, and $g_X(X)$ represents the performance function's limit state. To convert the non-normally distributed variable X_i into a corresponding normalized variable X_i', two normalization conditions are imposed:

Firstly, the mean values are equal

$$\mu_{X_i'} = \mu_{X_i}, \tag{4.3}$$

and secondly: quantiles are equal at the design point, X_{iq},

$$F_{X_i'}(x_{iq}) = F_{X_i}(x_{iq}). \tag{4.4}$$

Condition 1 in Eq. (4.3) is utilized to derive the mean value of X_i', while condition two in Eq. (4.4) is designed for determining the standard deviation of X_i'. This can be elaborated into two scenarios, based on the role that the variable plays in the performance function: $\frac{\partial g_X(X)}{\partial X_i} > 0$ or $\frac{\partial g_X(X)}{\partial X_i} < 0$.

Case one is for $\frac{\partial g_X(X)}{\partial \mathrm{X}_i} > 0$,

$$x_{iq} = \begin{cases} \mu_{X_i} - \beta_i^- \sigma_{X_i}, & \text{for } X_i \\ \mu_{X_i'} - \beta\, \sigma_{X_i'}, & \text{for } X_i' \end{cases}, \tag{4.5}$$

$$F_{X_i}\left(\mu_{X_i} - \beta_i^- \sigma_{X_i}\right) = F_{X_i'}\left(\mu_{X_i'} - \beta\sigma_{X_i'}\right) = p_f, \tag{4.6}$$

where $F_{X_i}(.)$ and $F_{X_i'}(.)$ are the CDFs for X_i and X_i', respectively and β and β_i^- are indices for X_i and X_i'.

Case two is for $\frac{\partial g_X(X)}{\partial \mathrm{X}_i} < 0$,

$$x_{iq} = \begin{cases} \mu_{X_i} + \beta_i^+ \sigma_{X_i}, & \text{for } X_i \\ \mu_{X_i'} + \beta\, \sigma_{X_i'}, & \text{for } X_i' \end{cases}, \tag{4.7}$$

$$F_{X_i}\left(\mu_{X_i} + \beta_i^+ \sigma_{X_i}\right) = F_{X_i'}\left(\mu_{X_i'} + \beta\sigma_{X_i'}\right) = 1 - p_f, \tag{4.8}$$

Using Eqs. (4.6) and (4.8), the standard deviation of X'_i can be derived as

$$\sigma_{X_i'} = \frac{\beta_i \sigma_{X_i}}{\beta}, \tag{4.9}$$

where

$$\beta_i = \begin{cases} \dfrac{\mu_{X_i} - F_{X_i}^{-1}(p_f)}{\sigma_{X_i}}, & \text{for } \dfrac{\partial g_X(X)}{\partial \mathrm{X}_i} > 0 \\ -\dfrac{\mu_{X_i} - F_{X_i}^{-1}(1-p_f)}{\sigma_{X_i}}, & \text{for } \dfrac{\partial g_X(X)}{\partial \mathrm{X}_i} < 0 \end{cases}. \tag{4.10}$$

Given the maximum entropy quantile function as defined in Eq. (3.17), Eq. (4.10) can be expressed as

$$\beta_i = \begin{cases} \dfrac{\mu_{X_i} - \exp\left\{-\sum_{s=0}^{K}\left[\lambda_s (p_f)^s\right]\right\}}{\sigma_{X_i}}, & \text{for } \dfrac{\partial g_X(X)}{\partial \mathrm{X}_i} > 0 \\ -\dfrac{\mu_{X_i} - \exp\left\{-\sum_{s=0}^{K}\left[\lambda_s (1-p_f)^s\right]\right\}}{\sigma_{X_i}}, & \text{for } \dfrac{\partial g_X(X)}{\partial \mathrm{X}_i} < 0 \end{cases}. \tag{4.11}$$

4.3. Truncated quantile function-based FORM

Typically, the Rosenblatt or Nataf transformation is used to map the vector of all random variables from the X-space to the U-space (the standard normal random vector) (Melchers et al. 2003). For truncated distributions, it is possible for the (trial) design point mapped back to X-space to have the i-th component x_i^* fall in the inadmissible region $x_i^* > x_d$ since the corresponding point in U-space requires $\phi_{(u)} = 0$ which is undefined. x_d is also the truncation point.

Melchers et al. (2003) proposed that the problem can be avoided by modifying the iterative FORM for the truncated PDF algorithm as follows. Since points $x_i^* > x_d$ are not permitted, whenever the algorithm attempts to set a new trial design point with coordinates involving $x_i^* > x_d$, the value is instead set to $x_d + \delta x^*$, where δx^* is some arbitrarily small quantity.

Using the algorithm for quantile-based FORM proposed by Deng and Pandey (2023) and considering the modifications offered by Melchers et al. (2003) for conducting FORM for the truncated PDF, a modified algorithm for conducting truncated quantile-based FORM (Figure 4.2) can be summarized as follows,

Step 1. Formulate an appropriate limit state equation. Determine the probability distributions (i.e., quantile functions) for all basic random variables $X_i (i = 1.2. \ldots . N)$ and the correlation matrix ρ_X.

Step 2. Assume the initial design point, $x^* = x_i^* (i = 1.2. \ldots . N)$ and the initial reliability index, β, which are usually the mean values of random variables and $\beta = 3$, respectively.

Step 3. Calculate the probability of failure $p_f = \phi(-\beta)$.

Step 4. For non-normal random variable X_i, calculate the equivalent normalized variable X_i' using Eq. (4.3) for the equivalent mean value ($\mu_{X_i'}$) and Eq. (4.9) for the equivalent standard deviation ($\sigma_{X_i'}$). Replace μ_{X_i} and σ_{X_i} with $\mu_{X_i'}$ and $\sigma_{X_i'}$, respectively. In addition to this,

for $\dfrac{\partial g_X(X)}{\partial \mathrm{X}_i} > 0$,

$$\beta_i = \frac{\mu_{X_i} - F_{X_i}^{-1}(p_f)}{\sigma_{X_i}} = \frac{\mu_{X_i} - \exp\{-1 - \sum_{s=0}^{K}[\lambda_s (p_f)^s]\}}{\sigma_{X_i}}. \quad (4.12)$$

for $\frac{\partial g_X(X)}{\partial X_i} < 0$,

$$\beta_i = -\frac{\mu_{X_i} - F_{X_i}^{-1}(1-p_f)}{\sigma_{X_i}} = -\frac{\mu_{X_i} - \exp\{-1 - \sum_{s=0}^{K}[\lambda_s (1-p_f)^s]\}}{\sigma_{X_i}}. \quad (4.13)$$

Step 5. Compute the direction cosine, α_{X_i} at the design point as

$$\alpha_{X_i} = -\frac{\sum_{j=1}^{N}(\rho_{X_i X_j} \frac{\partial g_X(x^*)}{\partial X_i} \sigma_{X_j})}{\sqrt{\sum_{i=1}^{N}\sum_{j=1}^{N}\left(\rho_{X_i X_j} \frac{\partial g_X(x^*)}{\partial X_i} \frac{\partial g_X(x^*)}{\partial X_j} \sigma_{X_i}\sigma_{Xj}\right)}}, i = 1, 2, \dots, N, \quad (4.14)$$

where $\rho_{X_i X_j}$ is the correlation coefficient of the X_i and X_j variables, and $\rho_{X_i X_j} = 1$. For equivalent normal random variables, $\rho_{X_i X_j}$ can be determined through the Nataf transformation proposed by (Ang and Tang (1984).

Step 6. Compute the reliability index

$$\beta = \frac{g_X(x^*) + \sum_{i=1}^{N}\left[\frac{\partial g_X(x^*)}{\partial X_i}(\mu_{Xi} - x_i^*)\right]}{\sqrt{\sum_{i=1}^{N}\sum_{j=1}^{N}(\rho_{X_i X_j} \frac{\partial g_X(x^*)}{\partial X_i} \frac{\partial g_X(x^*)}{\partial X_j} \sigma_{X_i}\sigma_{Xj})}}. \quad (4.15)$$

Step 7. Determine the new design point $x^* = x_i^* (i = 1, 2, \dots, N)$ using Eq. (4.16).

$$x_i^* = \mu_{X_i} + \beta\alpha_{X_i}\sigma_{X_i}, i = 1, 2, \dots, N. \quad (4.16)$$

Step 8. If the updated design point is smaller than the truncation point, $x_i^* < x_d$, the value is adjusted to $x_d + \delta x^*$, where δx^* presented some arbitrarily small quantity. Conversely, if the new design point exceeds the truncation point, $x_i^* > x_d$, the value is modified to $x_d - \delta x^*$.

Step 9. Repeat Steps 2 through 8 until β converges to a predetermined tolerance level.

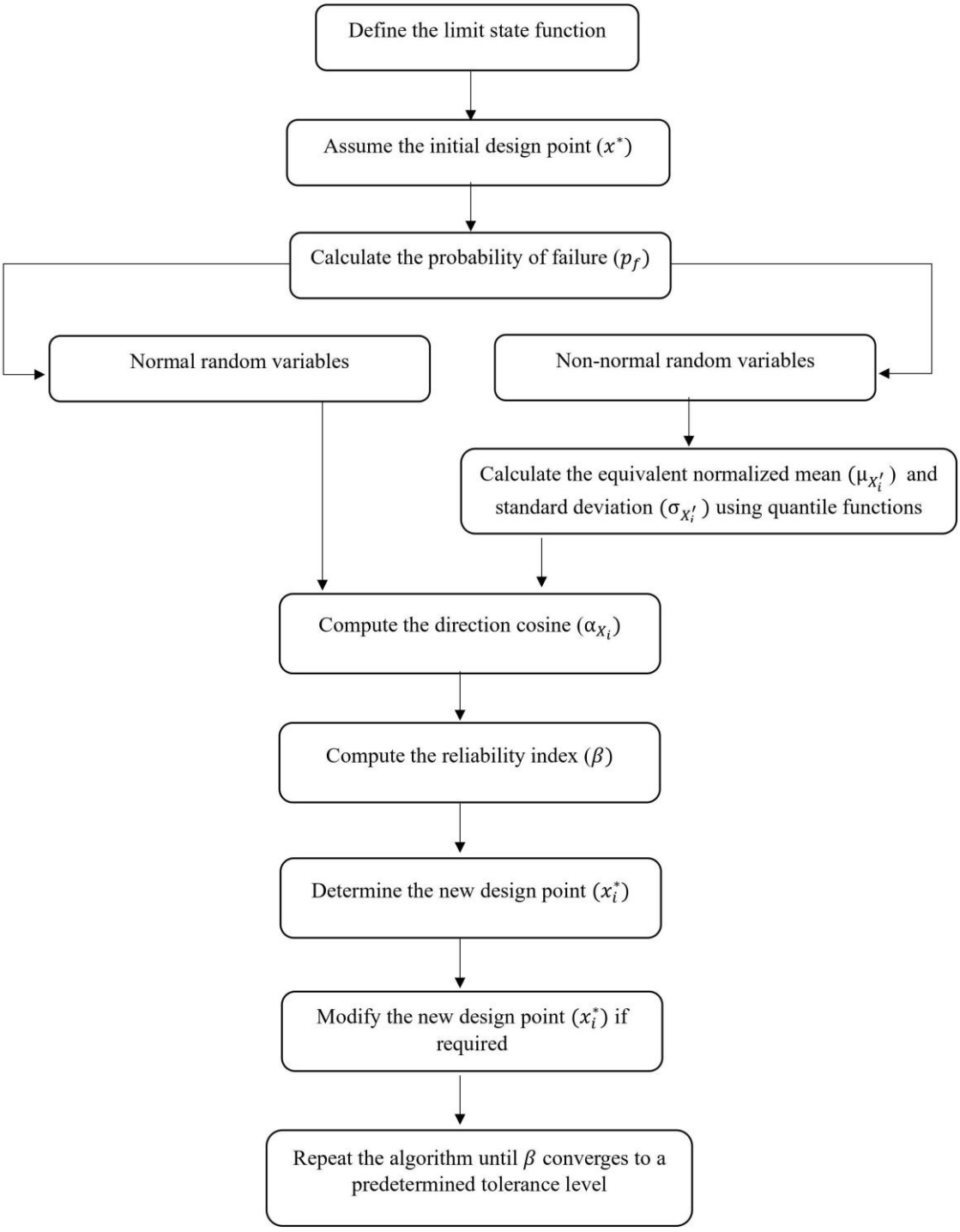

Figure 4.2. Truncated quantile function-based FORM

4.4. Illustrative example 1: FORM using truncated quantile Functions for Truncated Normal Samples

In this section the modified algorithm for conducting truncated quantile-based FORM for normal truncated samples is explained using the example provided by Melchers et al. (2003). The given equation represents a limit state function, expressed as $5X_1 + 3X_1X_2 - 240 = 0$, where X_1 has a truncated PDF. Distributions and parameters used in this example are provided in Table 4.1. Firstly, the initial design point was considered as the mean of random variable X_1 which is the usual in procedure of FORM. However, the algorithm broke down at iteration 2. The explanation for problem is that as the component X_1 of variable x_1^* approaches x_{d1} (the tail of the truncated distribution), there is a possibility that one of the iterations will search for a point where $x_1^* < x_{d1}$ which is not acceptable because the corresponding point in U space needs $\phi_{()} = 0$, which is not defined. The initial design point coordinate for X_1 in the first iteration was 10.29 (Melchers et al. 2003).

Table 4.1. Random variables and corresponding design point values at different stages of iteration, based on the example from Melchers et al. (2003)

Variable	Mean	St. deviation	Distribution	x_{d1}
X_1	10.29	0.794	truncated normal	9.0
X_2	12.0	1.5	normal	

Following the first iteration, the new design point for X_1 became 8.58. However, due to the PDF and CDF values of variable X_1 being zero, the algorithm could not continue with the second iteration. To overcome this issue, a modification can be made to the iterative FORM algorithm. In order to prevent points $x_1^* < x_{d1}$, whenever the algorithm tries to establish a new trial design point with coordinates involving $x_1^* < x_{d1}$, the value is instead set to x_{d1} + δx^*, where δx^* represents an extremely small value. This modification ensures that the algorithm avoids setting invalid points and continues its iterations successfully. By employing this strategy, the design point coordinate of 8.58 during the second iteration was substituted with a slightly higher value, just above 9.0 (in this example, the value chosen was 9.001). Following nine iterations, the routine successfully converged (Table 4.2) (Melchers et al. 2003).

Table 4.2. Design point values at various stages of iteration (Melchers et al. 2003)

Iteration no.	X_1	X_2
1	10.29	12.00
2	8.58	8.38
	9.00	8.38
3	9.01	7.15
4	9.12	7.11
5	9.43	6.81
6	9.35	6.89
7	9.40	8.84
8	9.37	6.87
9	9.39	6.85
Reliability index=3.61; Failure probability=1.55E-4		

Then random variables X_1 and X_2 are defined by normal quantile functions using function *norminv* in MATLAB. Using the algorithm suggested in Section 4.3. The FORM is conducted for a normal truncated sample using normal quantile functions. Based on this simulation, the reliability index (β) and probability of failure (p_f) are calculated as 3.57 and 1.74E-6, respectively, which are in close proximity to the result calculated by Melchers et al. (2003) (Table 4.3). In addition to this, the algorithm successfully converged in nine iterations providing the same number of required iterations as the original example.

Table 4.3. Comparing result of PDF based and QF based FORM with truncated normal random variables

	Reliability index (β)	Failure probability(p_f)	Number of iterations
PDF based FORM with truncated normal random variables (Melchers et al. 2003)	3.61	1.55E-4	9
QF based FORM with truncated normal random variables	3.57	1.74E-6	9

Table 4.4. Iterative calculations for illustrative example 1

Iteration no.		Assumed design point x^*	p_f	$\sigma^N_{X_i'}$	β_i	New β	New x^*
1	X_1	10.29	0.00135	0.794	3.000089	3.213425	9.001
	X_2	12.00	($\beta_0 = 3$)	1.50	3.000000		8.056817
2	X_1	9.001	655.80858E-6	0.794	3.213521	3.571480	9.001
	X_2	8.056817		1.50	3.213425		7.349416
3	X_1	9.001	177.484355E-6	0.794	3.571480	3.575155	9.001
	X_2	7.349416		1.50	3.571491		7.262066
4	X_1	9.001	175.010231E-6	0.794	3.575155	3.575359	9.001
	X_2	7.262066		1.50	3.575158		7.251739
5	X_1	9.001	174.873391E-6	0.794	3.575359	3.575380	9.001
	X_2	7.251739		1.50	3.575359		7.250525
6	X_1	9.001	174.859738E-6	0.794	3.57536	3.575382	9.001
	X_2	7.250525		1.50	3.57536		7.250382
7	X_1	9.001	174.858168E-6	0.794	3.57537	3.575382	9.001
	X_2	7.250382		1.50	3.57537		7.250366
8	X_1	9.001	174.857984E-6	0.794	3.57538	3.575382	9.001
	X_2	7.250366		1.50	3.57538		7.250364
9	X_1	9.001	174.857963E-6	0.794	3.57538	3.575381	9.001
	X_2	7.250364		1.50	3.57538		7.250363

4.5. Illustrative example 2: truncated maximum entropy quantile-based FORM for a truncated sample

In this section, an example from rock slope stability is used in order to demonstrate the application of maximum entropy quantile-based FORM for a truncated sample. The Sau Mau Ping rock slope in Hong Kong (Figure 4.3) was initially documented by Hoek and Bray (1974). Subsequent investigations by various researchers have taken place (Low, 2007; Wang et al. 2013; Deng and Pandey, 2023). This slope is situated in a region characterized by high rainfall but low seismic activity. Anxiety has arisen due to a minor slide on a nearby

slope, prompting worries that a significant slide could potentially occur at the Sau Mau Ping rock slope.

Figure 4.3. A view down Sau Mau Ping Road in Kowloon showing apartment blocks across the road from the steep rock slopes (Hoek and Bray, 1974)

The rock formation from which the adjacent slope to Sau Mau Ping Road was excavated consists of unweathered granite exhibiting exfoliation or sheet joints (Figure 4.4). These joints run parallel to the granite surface, and the gap between successive joints widens as one moves deeper into the rock mass. The undermining of these sheet joints has the potential to trigger a rockslide (Hoek and Bray, 1974). The required information related to the geometry of the slope and the physical properties of the rock mass is provided in Table 4.5. In order to conduct the reliability analysis in this example, the geotechnical properties of the sliding surface are considered random variables, which are summarized in Table 4.6.

Table 4.5. Basic parameters of the slope geometry (Hoek and Bray, 1974)

H (m)	ψ_f (degree)	ψ_p (degree)	a (g)	γ_r (KN/m3)	γ_w (KN/m3)	z (m)	z_w (m)	T (KN/m)	ψ_T (degree)
60	50	35	0.08	26	9.81	14	7	0	0

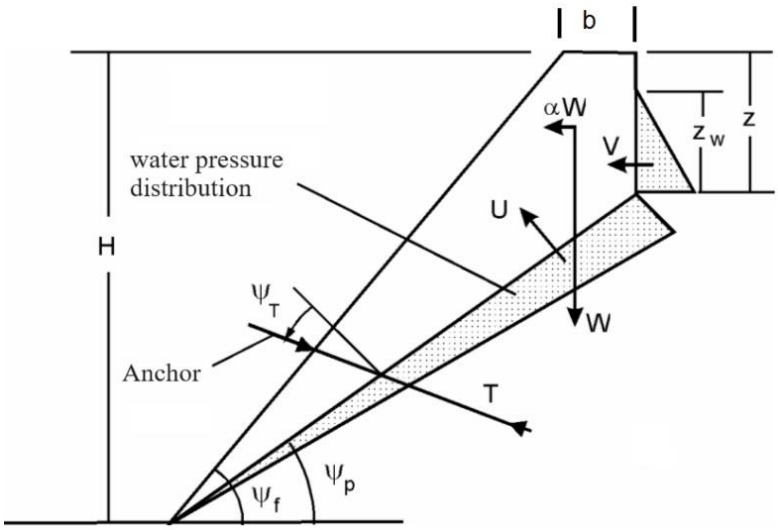

Figure 4.4. Sau Mau Ping rock slope

As mentioned in Chapter 3, a data set including 50 samples (Table 3.1) is created to evaluate the ability of maximum entropy quantile functions to represent truncated samples. This data represents the cohesion of rock discontinuities on the Sau Mau Ping rock slope in Hong Kong, as suggested by Hoek (2006).

Table 4.6. Random variables of rock slope Wang et al. 2013

Variable	c (KN/m2)	φ (degree)
Mean	100	35
Standard deviation	20	5
Distribution	Normal	Normal

Following the algorithm in Section 4.3 a limit state function needs to be defined. Eq. (4.17) represents the two-dimensional limit equilibrium analysis where the FOS is the ratio of the restoring forces to the disturbing forces.

$$FOS = \frac{cA + [W\ (\cos\psi_p - \alpha \sin\psi_p) - U - V \sin\psi_p + T \cos\psi_T] \tan\varphi}{W\ (\sin\psi_p + \alpha \cos\psi_p) + V \cos\psi_p - T \sin\psi_T}, \qquad (4.17)$$

and

$$A = \frac{H - z}{\sin\psi_p}, \qquad (4.18)$$

$$z = H(1 - \sqrt{\tan\psi_p \cot\psi_f}), \tag{4.19}$$

$$W = \frac{H^2\gamma_r}{2}\left\{\left[1 - \left(\frac{z}{H}\right)^2\right]\cot\psi_p - \cot\psi_f\right\}, \tag{4.20}$$

$$U = \frac{1}{2}(\gamma_w z_w)A, \tag{4.21}$$

$$V = \frac{1}{2}(\gamma_w z_w)z_w. \tag{4.22}$$

where FOS is the the factor of safety of the slope sliding along the sheet joint; W is the weight of rock wedge resting on the failure surface (KN); c is the cohesive strength along the sliding surface (KN/m^2); A is the base area of the wedge (m^2); φ is the friction angle of the sliding surface (degree); ψ_p is the angle of failure surface from horizontal (degree); ψ_f is the angle of the slope face from horizontal (degree), α is the horizontal earthquake acceleration (m/s^2); U is the uplift force due to water pressure on the failure surface (KN); V is the horizontal force due to water in the tension crack (KN); T is the force applied by the anchor system (KN); ψ_T is the inclination of the anchor, anti-clockwise from normal (degree); z is the depth of the tension crack (m); z_w is the depth of water in the tension crack (m); γ_w is the unit weight of water (KN/m^3); γ_r is the unit weight of rock granite (KN/m^3); and H is the height of the overall slope (m).

In reliability analysis, the performance function for slopes is defined as

$$g(x) = FOS - 1. \tag{4.23}$$

Traditionally, the approach of employing the method of moments has been used for estimating the PDF of a random variable. Subsequently, the PDF is integrated to derive the CDF, requiring inversion to obtain the quantile function (QF). In contrast, maximum entropy quantile functions are directly recovered from a given sample. This represents a notable advantage compared to traditional distributions, as mentioned in Chapter 3.

As well as the maximum entropy quantile functions, the distribution of random variable c was also determined by conventional methods from the sample of elements in Section 3.7. All three types of distributions are employed in the reliability analysis and the results are compared with those of the parent normal distribution.

Following the calculations related to truncated maximum entropy quantile functions and normal and lognormal truncated functions in Section 3.7, the algorithm suggested for conducting quantile function based FORM for a truncated sample, the reliability analysis for different amounts of truncation, including 4%, 6%, 8%, and 10% for both left and right truncation is conducted using quantile functions obtained from normal (Eq. 3.60), lognormal (Eq. 3.61), and maximum entropy (Table B.1 to B.7) distributions, and the results are provided in Table 4.7. The reference value for the reliability index is also calculated by using the function *norminv* in MATLAB and directly using parameters for the normal distribution provided in Table 4.5. This distribution is called the parent normal quantile function as the random variable evaluated in this example is originally a normal random variable. The details regarding the iterations of each distribution with different degrees of truncation are provided in Tables 4.7 to 4.10.

Table 4.7. Results of reliability analysis with different degrees of truncations

(Parent normal)

	β	p_f	Total Iter No.	Final design point c, φ
10% left	2.1521	16.57E-3	10	89.97, 25.95
8% left	1.792	36.56E-3	7	80.60, 28.47
6% left	1.7675	38.56E-3	7	80.18, 28.47
4% left	1.7609	39.12E-3	5	80.21, 28.47
original	1.6819	44.28E-3	6	78.48, 28.87
4% right	1.6806	45.63E-3	5	79.12, 28.70
6% right	1.6768	46.78E-3	5	79.11, 28.70
8% right	1.6557	48.88E-3	5	78.70, 28.70
10% right	1.6359	50.92E-3	5	78.34, 28.93

Table 4.8. Results of reliability analysis with different degrees of truncations (normal quantile functions)

	β	p_f	Total Iter No.	Final design point c, φ
10% left	2.2295	12.88E-3	10	90.66, 25.78
8% left	1.9646	24.72E-3	7	83.71, 27.55
6% left	1.9129	27.87E-3	6	82.93, 27.78
4% left	1.8563	31.69E-3	6	81.93, 28.01
original	1.5520	58.92E-3	6	75.03, 29.73
4% right	1.5756	57.55E-3	6	75.93, 29.50
6% right	1.5657	58.70E-3	6	75.96, 29.50
8% right	1.5561	59.84E-3	6	75.86, 29.50
10% right	1.5472	59.95E-3	5	78.31, 29.50

Table 4.9. Results of reliability analysis with different degrees of truncations (lognormal quantile functions)

	β	p_f	Total Iter No.	Final design point c, φ
10% left	2.0544	19.96E-6	6	85.63, 27.10
8% left	1.9449	25.89E-6	7	83.19, 27.73
6% left	1.907	28.25E-3	6	82.82, 27.78
4% left	1.8876	29.53E-3	6	82.85, 27.78
original	1.7819	37.37E-3	6	81.33, 28.18
4% right	1.7876	36.91E-3	7	81.70, 28.07
6% right	1.7667	38.63E-3	7	81.45, 28.13
8% right	1.7497	40.08E-3	7	81.16, 28.18
10% right	1.7285	41.94E-3	7	80.75, 28.30

Table 4.10. Results of reliability analysis with different degrees of truncations (optimal order of maximum entropy quantile functions)

	β	p_f	Total Iter No.	Final design point c, φ
10% left	2.1678	15.08E-3	9	91.16, 25.66
8% left	1.9074	28.22E-6	6	83.93, 27.50
6% left	1.7939	36.41E-3	6	80.93, 28.24
4% left	1.7858	43.37E-3	6	78.86, 28.76
original	1.6217	56.34E-3	6	75.86, 29.50
4% right	1.7574	39.41E-3	11	81.10, 28.24
6% right	1.7347	41.39E-3	10	80.80, 28.30
8% right	1.7188	59.18E-3	7	76.06, 29.45
10% right	1.7003	60.72E-3	7	75.89, 29.50

By comparing the outcomes derived from the reliability analysis employing normal, lognormal, and maximum entropy quantile functions (Table 4.11 and Figure 4.5), it can be concluded that the results obtained from maximum entropy quantile functions are the closest results to the values derived from the parent normal quantile functions, which is considered the benchmark in this analysis.

This observation suggests that maximum entropy exhibits capabilities in modeling and representing the random variable under consideration throughout the conducted reliability analysis, considering both the original and truncated sample scenarios. Moreover, the quantile functions of lognormal and normal distributions exhibit more deviations from the corresponding values of the parent normal distribution, indicating a less effective performance in this example. The lognormal distribution yields a reliability index that is the least conservative when compared to the maximum entropy quantile functions. Meanwhile, the normal distribution results in smaller reliability indices for the right-truncated sample and greater reliability indices for the left-truncated sample compared with the parent normal quantile functions.

Furthermore, when evaluating six out of the nine distinct conditions for maximum entropy quantile functions applied to both the original and truncated samples, it is noteworthy that the optimal order identified through the AIC yields results closest to those obtained from the

parent normal distribution. This implies that selecting the optimal order, as determined by AIC, in the context of maximum entropy quantile functions is advantageous for optimizing calculations and mitigating the need for higher orders that entail computationally intensive procedures.

Consequently, using the optimal order of the maximum entropy quantile function, along with the algorithm outlined in Section 4.3, enables the acceptable estimation of the reliability index (β) based on maximum entropy quantile functions for truncated samples. This approach not only enhances the efficiency of calculations but also ensures a robust and reliable estimation of the reliability index in the given context.

Table 4.11. Reliability index ($\boldsymbol{\beta}$) calculated from parent normal, normal, lognormal, and maximum entropy quantile functions for the original and different degrees of truncations

distribution		10% left	8% left	6% left	4% left	original	4% right	6% right	8% right	10% right
Parent normal QF		**2.1521**	**1.792**	**1.7675**	**1.7609**	**1.6819**	**1.6806**	**1.6768**	**1.6557**	**1.6359**
Normal QF		2.2295	1.9646	1.9129	1.8563	1.5520	1.5756	1.5657	1.5561	1.5472
Lognormal QF		2.0544	1.9449	1.907	1.8876	1.7819	1.7876	1.7667	1.7497	1.7285
	Order									
	1	2.1955	2.114	2.0469	1.9848	1.8578	1.8368	1.8241	1.816	1.8078
	2	2.2703	2.1569	2.0554	1.9643	1.7875	**1.7574**	**1.7347**	1.7288	1.7203
	3	**2.1678**	2.0171	1.8864	1.8558	**1.6217**	1.5907	1.575	**1.7188**	**1.7003**
Maximum	4	2.0717	1.9150	**1.7939**	**1.7858**	1.5520	1.5686	1.5574	1.5489	1.5399
entropy	5	2.1086	1.924	1.7954	1.7155	1.5833	1.5644	1.5518	1.5434	1.5345
QF	6	2.1061	1.9136	1.7941	1.7188	1.5769	1.5568	1.5468	1.5359	1.524
	7	2.1099	1.9137	1.8006	1.7244	1.5436	1.5171	1.4945	1.4789	1.4621
	8	2.1015	1.9089	1.8002	1.7264	1.5273	1.5227	1.4978	1.5231	1.4668
	9	2.1264	1.9012	1.7898	1.6771	1.5281	1.4833	1.471	1.4604	1.4635
	10	2.1207	**1.9074**	1.7908	1.6917	1.5349	1.4844	1.4698	1.4702	1.449

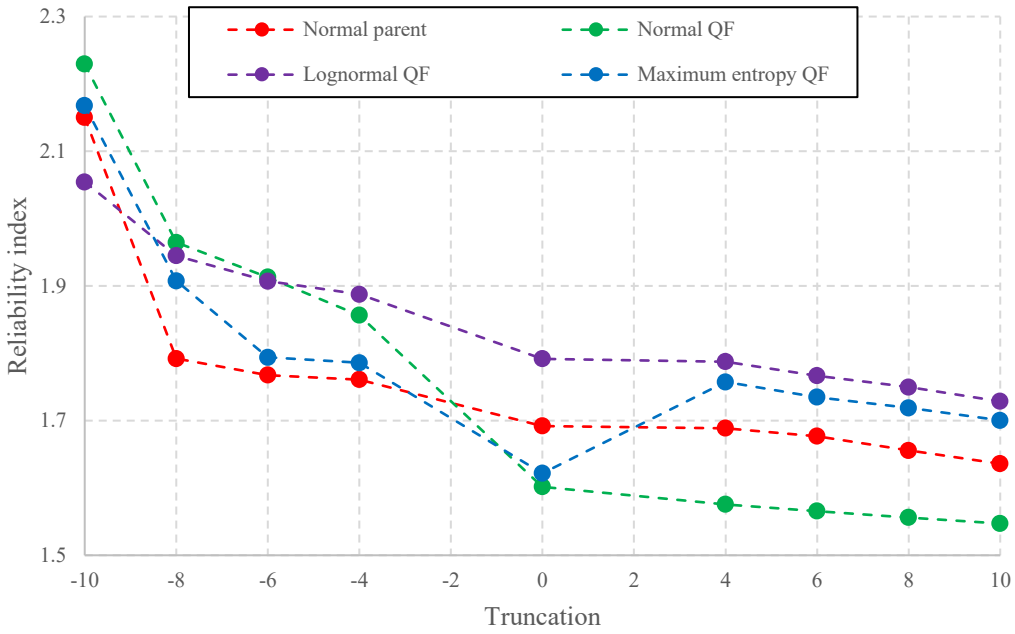

Figure 4.5. Comparison between reliability index ($\boldsymbol{\beta}$) for the original and different degrees of truncations (parent normal, normal, lognormal, and maximum entropy quantile functions)

4.6. Summary

Chapter 4 discussed the application of reliability methods with truncated quantile functions in the context of geotechnical engineering. The primary focus is on developing a quantile function-based FORM approach for truncated samples.

The quantile-based FORM is then introduced, building upon the work of Deng and Pandey (2023). The method involves converting non-normally distributed random variables into equivalent normal variables using quantile functions. The chapter further extends the methodology to handle truncated samples using the modifications proposed by Melchers et al. (2003) for conducting FORM for the truncated PDF in the algorithm proposed by Deng and Pandey (2023) for quantile-based FORM.

The chapter concluded with two illustrative examples. The first example demonstrated the modified algorithm for normal truncated samples, comparing results with a previous approach. This example was used to verify the suggested modified method for conducting reliability analysis with truncated samples. The second example applied the methodology to rock slope stability analysis, showcasing the reliability analysis for different degrees of

truncation using normal, lognormal, and maximum entropy quantile functions. Based on the results, the optimal order or maximum entropy quantile functions are able to provide the closest answers to the reference results (parent normal) while working with truncated samples. The closeness of results obtained from maximum entropy distribution with the reference values reflects in the ability of maximum entropy distribution to present the samples with higher precision compared with normal and lognormal distributions. The presented algorithm is illustrated through practical examples, demonstrating its effectiveness in estimating reliability indices for different scenarios.

5. Reliability analysis of slopes in the Nipigon River Landslide

A landslide took place in the vicinity of Nipigon, Ontario, Canada, during the early hours of April 23, 1990 (Figures 5.1 and 5.2). The landslide covered an area of nearly 350 meters inland and had a maximum width of approximately 290 meters (Dodds et al. 1993).

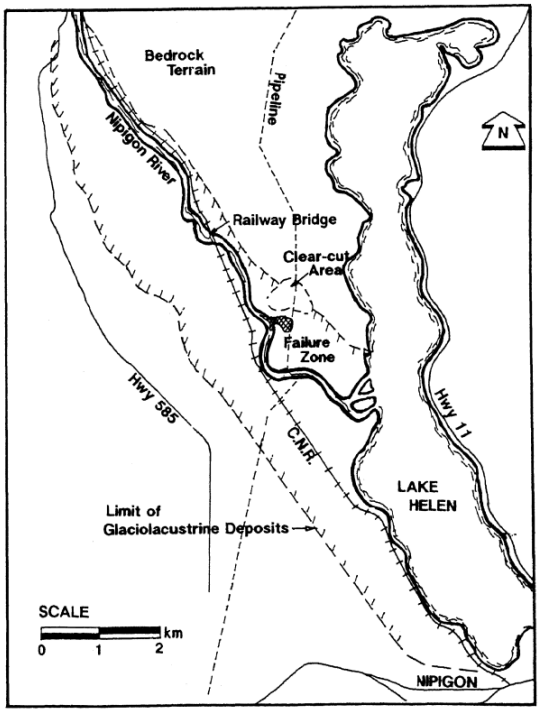

Figure 5.1. Location of the landslide (Dodds et al. 1993)

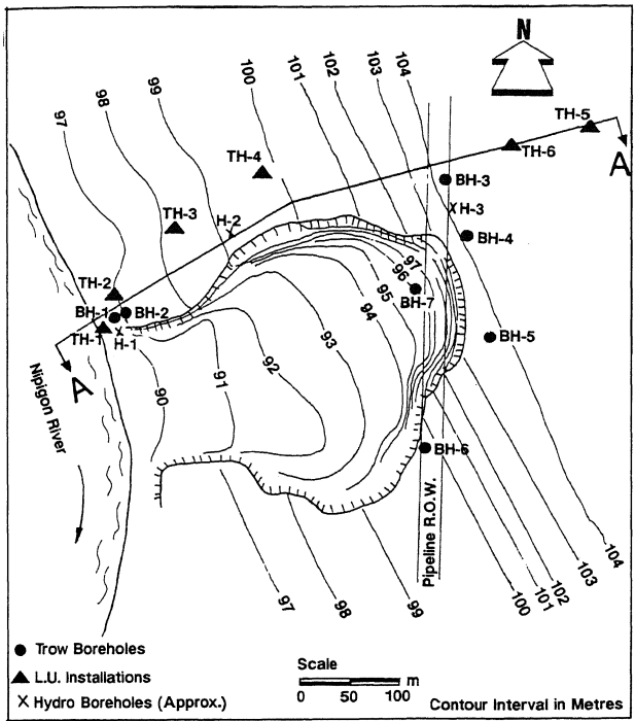

Figure 5.2. Site Plan (Dodds et al. 1993)

The intensity of the landslide resulted in soil being forcefully pushed both upstream and downstream along the Nipigon River for approximately 300 meters in each direction. The shear force behind this movement was so significant that piles of debris were discovered flattened in the trees on the opposite riverbank, presumably thrown there when the soil collided with that bank. At the site of the incident, the Nipigon River measured about 100 meters in width. Islands formed by the displaced soil altered the river's flow, leading to subsequent erosion on the western bank across from the landslide. This altered current likely played a role in triggering several additional landslides further south, all occurring within one month of the initial event (Dodds et al. 1993).

5.1. Geology

The region examined surrounds the segment of the Nipigon River extending from where it flows into Lake Helen to an upstream railway bridge located beyond the site of the landslide. This area's primary topographical feature consists of a glaciolacustrine plain and delta sediments of sand and silt deposits. The local terrain is generally flat, resulting in inadequate drainage conditions. The sides of river valleys that have been deeply carved into these fine-grained deposits often display patterns of erosion, including rill and gully formation, especially on newly excavated ditch slopes and highway embankments. Additionally, higher, and steeper natural or human-made slopes are susceptible to minor failures (Dodds et al. 1993).

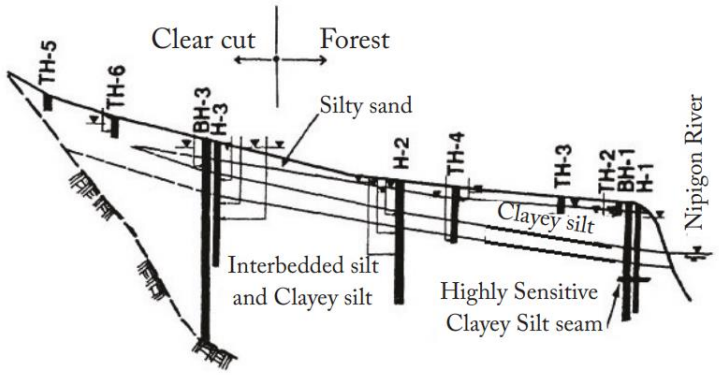

Figure 5.3. Stratigraphic Section (Dodds et al. 1993)

In July of 1991, the drilling of three boreholes, specifically labeled H.1, H.2, and H.3 was conducted (Figure 5.3). These boreholes were used to collect undisturbed soil samples using a piston sampler. To gain insights into the soil's layering and its undrained shear strength, the team employed an electric piezocone and conducted shear-vane tests. Additionally, pore pressure dissipation tests were carried out within clayey layers using the piezocone to estimate the coefficient of consolidation for the deposits present in their natural state (Dodds et al. 1993). Based on the samples obtained from the boreholes, four main soil types were recognized, including sandy silt (upper and lower), clayey silt, and very soft clayey silt (Figure 5.4). In addition to this, soil parameters for different soil layers of the geological section based on studies conducted by Dodds et al. (1993) and Barros et al. (2023) are summarized in Table 5.1.

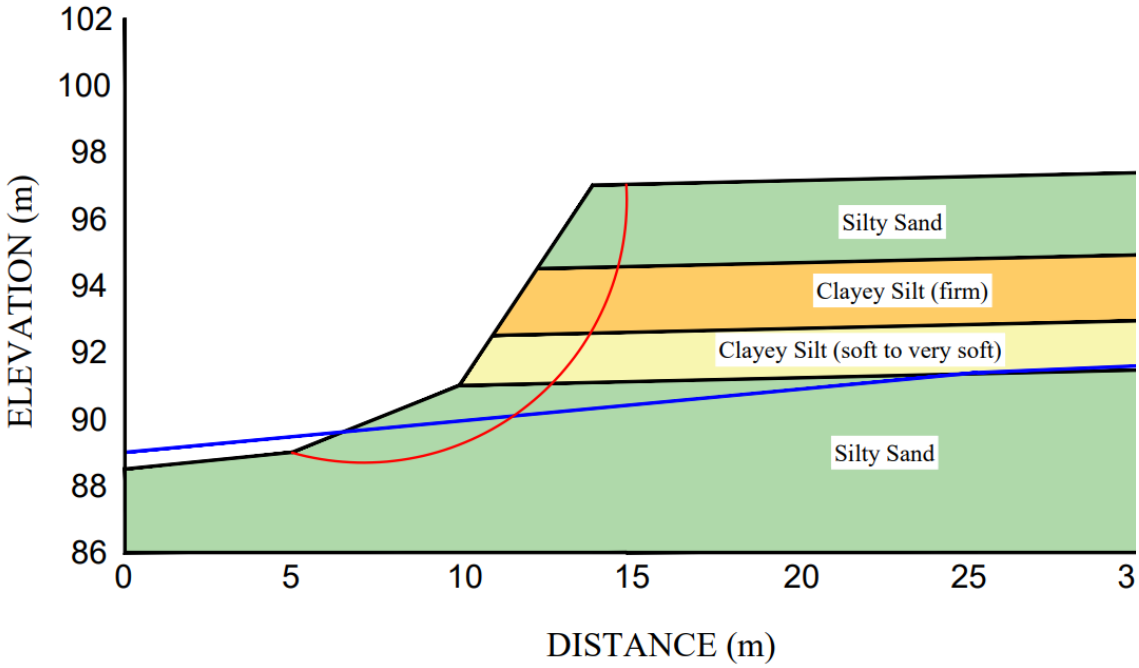

Figure 5.4. Geological section of Nipigon River Landslide (Fs=1.08 for the failure surface based on (Dodds et al. 1993))

Table 5.1. Soil parameters (Dodds et al. (1993) and Barros et al. (2023))

Soil type	Unit weight (KN/m^3)	Friction angle (degree)	Cohesion (kPa)
Silty sand (upper)	17.6	30	53
Clayey silt (firm)	19	28	30
Clayey silt (soft to very soft)	18.2	28	0
Silty sand (lower)	18	30	10

5.2. Truncated maximum entropy quantile functions for Nipigon River Landslide

To obtain the soil parameters required for the reliability analysis, the cohesion of the upper silty sand layer is employed. The laboratory investigations involved the use of unconfined compression tests, which were conducted by civil engineering undergraduate students (Maria Barros, Kamal Mistry, Justin Plummer, and Chris Pyykkonen), under the supervision of Dr. Jian Deng (Table 5.2).

Table 5.2. Undrained shear strength (kPa) of upper silty sand layer (Barros et al. 2023)

No.	c_u(kPa)	No.	c_u (kPa)
1	10.53	19	55.01
2	16.73	20	56.33
3	17.97	21	57.83
4	18.75	22	60.49
5	19.87	23	61.33
6	38.23	24	65.14
7	38.41	25	65.22
8	38.64	26	67.44
9	39.65	27	69.12
10	43.37	28	69.25
11	44.61	29	73.48
12	48.32	30	74.76
13	48.94	31	75.04
14	49.95	32	75.71
15	51.03	33	77.61
16	52.27	34	82.33
17	53.05	35	96.71
18	53.5		

Using the data provided in Table 5.2, it is possible to derive PWMs (Table 5.4) by using Eq. (3.11). Then, solving Eq. (3.17) with these sample PWMs allows for the determination of maximum entropy quantile functions. In the next step, the effects of different truncation percentages on maximum entropy quantile functions are evaluated. Once again, using the data provided in Table 5.2 and considering different amounts for truncation, including 6, 8.5, and 11.5 percent for both the left and right sides (Table 5.3), it is possible to derive PPWMs (Table 5.4) through using Eqs. (3.23) and (3.25). Subsequently, solving Eqs. (3.32) and (3.38) with corresponding PPWMs allows for the determination of extended maximum entropy quantile functions for the left and right truncated samples, respectively. Calculated Lagrangian multipliers (λ_s) for all the mentioned conditions are provided in Appendix C

(Tables C.1 to C.7). The optimal order of calculated quantile functions is also obtained from the AIC method (Appendix C, Figures C.1 to C.7).

Table 5.3. Removed sample elements for different truncation conditions

Truncation	11.5% left	8.5% left	6% left	6% right	8.5% right	11.5% right
Removed elements	10.53	10.53	10.53	82.33	77.61	75.71
	16.73	16.73	16.73	96.71	82.33	77.61
	17.97	17.97			96.71	82.33
	18.75					96.71

Table 5.4. PWMs and PPWMs for the original and truncated samples

Truncation		11.5% left	8.5% left	6% left	original	6% right	8.5% right	11.5% right
PWM and PPWM Order (K)	1	51.50	52.04	52.55	53.33	48.22	46.00	43.84
	2	32.37	32.41	32.44	32.46	30.25	29.38	28.51
	3	23.41	23.42	23.42	23.42	21.85	21.33	20.82
	4	18.39	18.39	18.39	18.39	17.10	16.72	16.35
	5	15.19	15.19	15.19	15.19	14.05	13.76	13.47
	6	12.96	12.96	12.96	12.96	11.93	11.69	11.46
	7	11.33	11.33	11.33	11.33	10.37	10.17	9.97
	8	10.07	10.07	10.07	10.07	9.17	8.99	8.83
	9	9.07	9.07	9.07	9.07	8.22	8.06	7.92
	10	8.26	8.26	8.26	8.26	7.45	7.31	7.19

Using Appendix C, the optimal order of the maximum entropy quantile function and the optimal order of the extended maximum entropy quantile functions are obtained, which are provided in Eqs. (5.1) to (5.7) for the original and truncated samples.

$$x(F)_{(\text{original})} = \exp\left(2.19450 + 5.93016\,F - 39.22736\,F^2 - 259.44085\,F^3 + 556.77689\,F^4 - 516.65614\,F^5 + 176.70074\,F^6\right). \tag{5.1}$$

$$x(F)_{(6\%\text{left})} = \exp\left(2.44480 + 11.58056\,F - 23.84183\,F^2 - 31.12163\,F^3 + 176.56807\,F^4 - 217.23964\,F^5 + 86.32414\,F^6\right). \tag{5.2}$$

$$x(F)_{(8.5\%\text{left})} = \exp(2.0583 + 34.43353F - 285.8893\,F^2 + 1236.28301\,F^3 - 2946.22996\,F^4 + 3901.91994\,F^5 - 2683.94515\,F^6 + 746.19766\,F^7). \quad (5.3)$$

$$x(F)_{(11.5\%\text{left})} = \exp(2.40199 + 34.09024\,F - 322.50317\,F^2 + 1498.60360\,F^3 - 3711.09919\,F^4 + 2011.61669\,F^5 - 3477.77315\,F^6 + 969.53782\,F^7). \quad (5.4)$$

$$x(F)_{(6\%\text{right})} = \exp(1.95718 + 13.42584\,F - 34.35133\,F^2 + 38.99374F^3 - 15.70810\,F^4). \quad (5.5)$$

$$x(F)_{(8.5\%\text{right})} = \exp(1.93977 + 13.32295F - 33.65947\,F^2 + 37.73970F^3 - 15.03231\,F^4). \quad (5.6)$$

$$x(F)_{(11.5\%\text{right})} = \exp(1.93494 + 13.00362\,F - 32.04852\,F^2 + 35.08405F^3 - 13.65815\,F^4). \quad (5.7)$$

Similar to the examples in Chapter 3, the parameters of the normal and lognormal distributions for truncated samples are calculated using the method introduced by Cohen (1959) and are provided in Table 5.5. As was mentioned in Section 3.7, the value of the random variable for various quantile amounts can be calculated using the *NORM.INV* and *LOGNORM.INV* functions in Microsoft Excel. These values from normal and lognormal distributions are then compared with those obtained from maximum entropy quantile functions.

Table 5.5. Parameters for normal and lognormal distributions

Distribution	Normal		Lognormal	
	μ_X^P	σ_X^P	λ_X^P	ζ_X^P
11.5% left	53.4493	20.7505	3.9085	0.3746
8.5% left	53.0500	20.9157	3.8989	0.3801
6% left	52.9565	20.7526	3.8980	0.3779
6% right	53.3096	19.9417	3.9106	0.3618
8.5% right	53.2674	20.0830	3.9088	0.3645
11.5% right	53.0796	20.2240	3.9040	0.3681

For samples with the left truncation (Figures 5.6 to 5.8), from the truncation point to the probability of 0.15, the optimal order of maximum entropy offers a better fit line than normal and lognormal quantile functions. Between the probability of 0.15 and 0.3, the normal quantile function is the best fit line for the data set. From 0.3 to 0.7, the optimal order of maximum entropy and the normal quantile functions led to nearly the same fit lines. In the interval of 0.7 and 0.85 the optimal order of the maximum entropy yields a closer fit line. Finally, from 0.85 to the probability equaling to 1, the fit lines obtained from different methods overlap.

For samples with the right truncation (Figure 5.9 to 5.11), in the range of 0 to 0.55, the optimal order of quantile functions produces a more accurate fit line compared to both normal and lognormal quantile functions. Within the interval of 0.55 to 0.75, the optimal order of maximum entropy and normal quantile functions yields similar fit lines, while the lognormal quantile function results in a less accurate fit for this range. Finally, from 0.75 to the truncation point, fit lines obtained from the optimal order of maximum entropy are better than those derived from normal and lognormal quantile functions.

Similar to the previous examples, the residual sum of squares (RSS) method is also employed in order to compare fit lines obtained from different methods. The results of calculating RSS for normal, lognormal, and optimal maximum entropy are provided in Table 5.6, which shows that the optimal order of maximum entropy is more capable of minimizing RSS in all conditions, including the original and different truncated samples.

As outlined in Chapter 3, the optimal order of maximum entropy can generate satisfactory fit lines for truncated samples, as it is not constrained by the requirement of considering only two ordinary moments inherent in normal or lognormal distributions. Additionally, the proposed model offers an advantage in that maximum entropy quantile functions are not restricted to conventional probability distributions such as normal or lognormal functions. The decision to employ a maximum entropy quantile function is solely based on sample information, rendering it an objective choice rather than a subjective one.

Table 5.6. Comparison for the residual sum of squares (RSS)

Distribution	Normal	Lognormal	Optimal order maximum entropy
11.5% left	1454.95	1999.97	1406.19
8.5% left	1555.58	2635.06	1488.60
6% left	1125.88	3246.23	1004.58
original	934.20	4895.84	620.18
6% right	2506.33	5990.19	765.13
8.5% right	1522.54	3463.17	508.97
11.5% right	925.12	1949.69	377.32

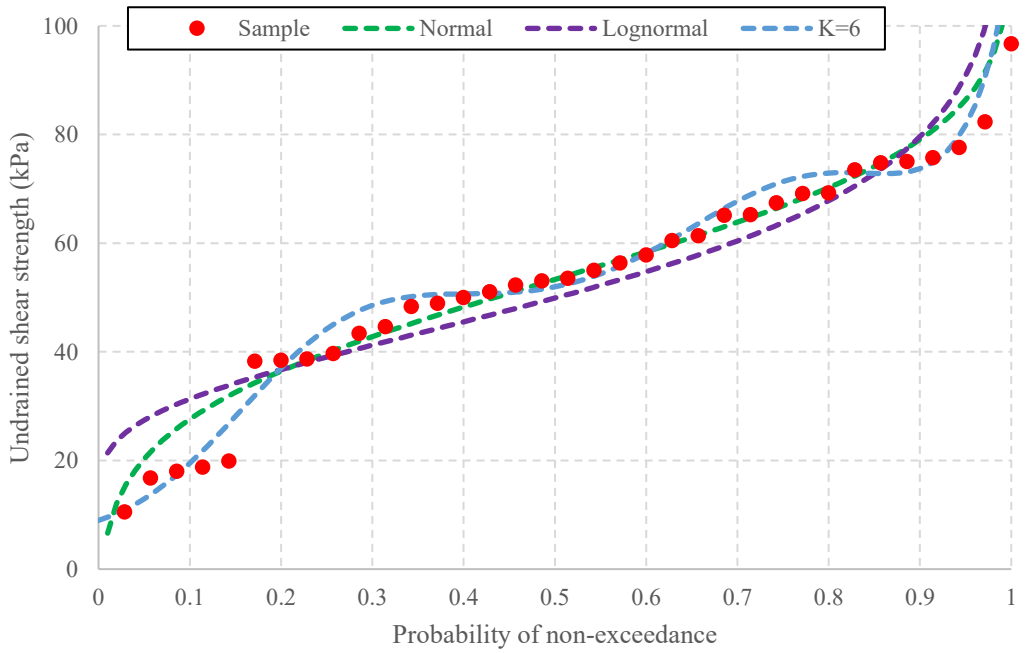

Figure 5.5. Maximum entropy quantile function for the original data set (Undrained shear strength of upper silty sand layer from Nipigon River Landslide)

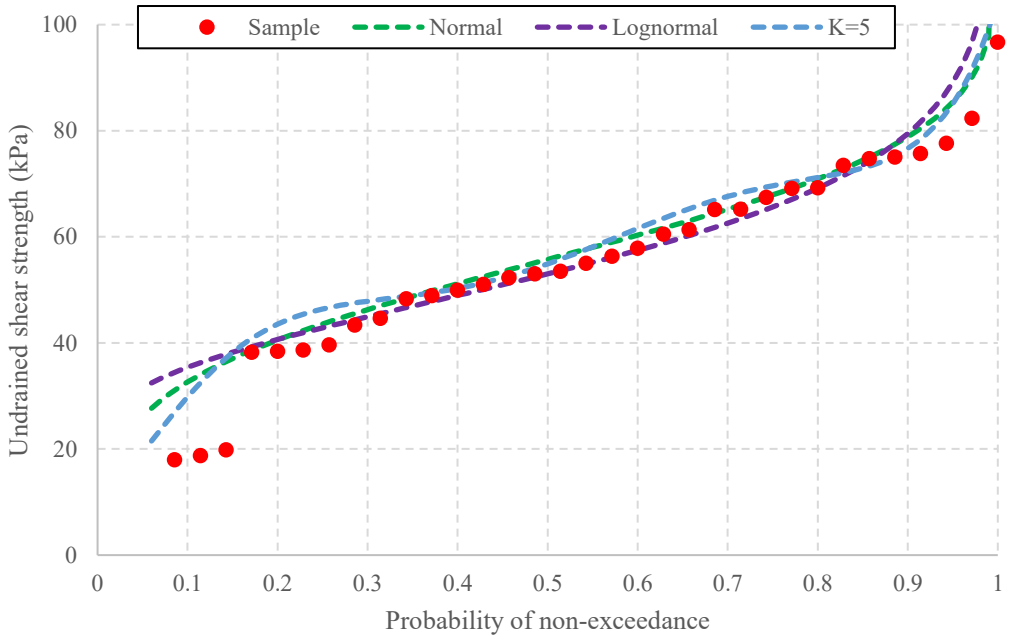

Figure 5.6. Maximum entropy quantile function for 6% left truncated data set (Undrained shear strength of upper silty sand layer from Nipigon River Landslide)

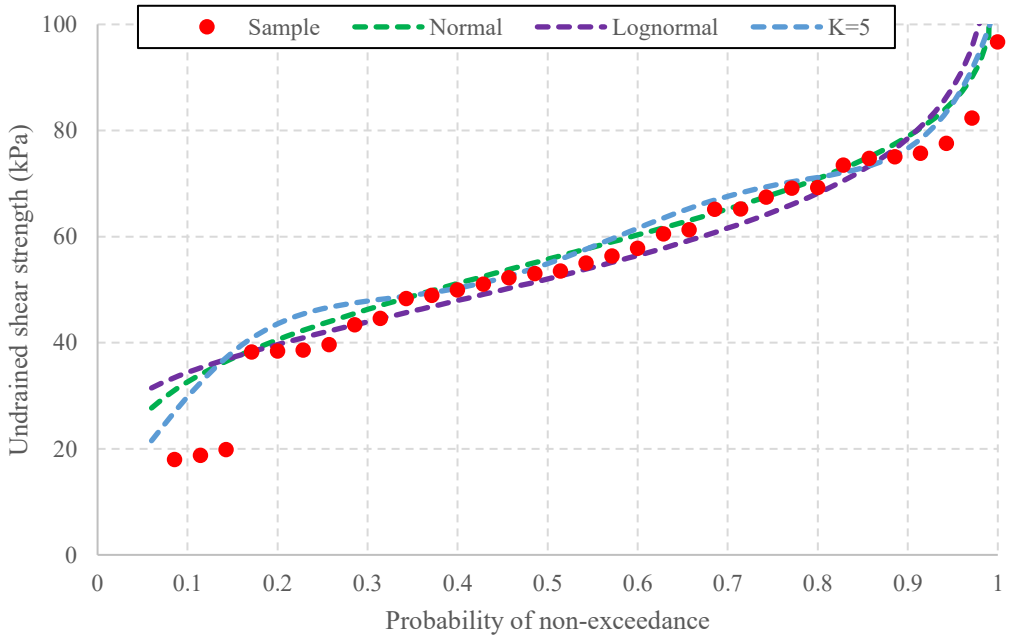

Figure 5.7. Maximum entropy quantile function for 8.5% left truncated data set (Undrained shear strength of upper silty sand layer from Nipigon River Landslide)

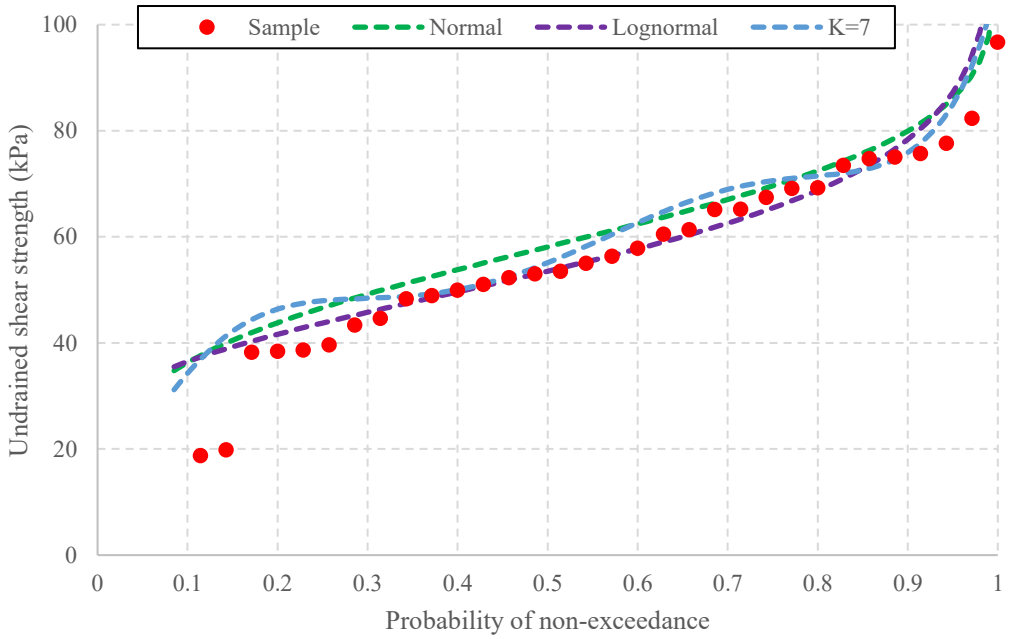

Figure 5.8. Maximum entropy quantile function for 11.5% left truncated data set (Undrained shear strength of upper silty sand layer from Nipigon River Landslide)

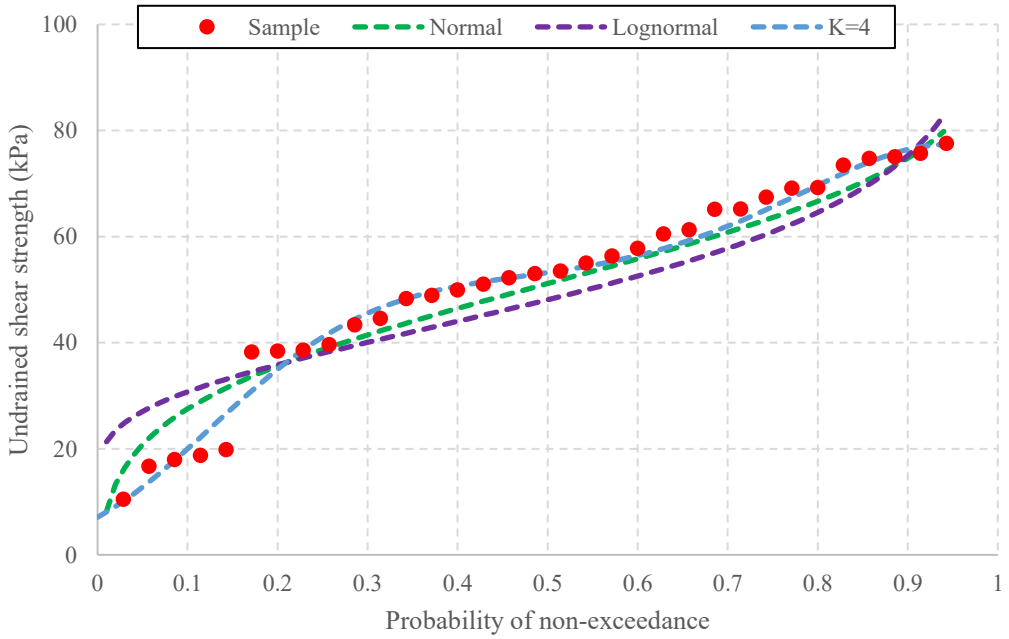

Figure 5.9. Maximum entropy quantile function for 6% right truncated data set (Undrained shear strength of upper silty sand layer from Nipigon River Landslide)

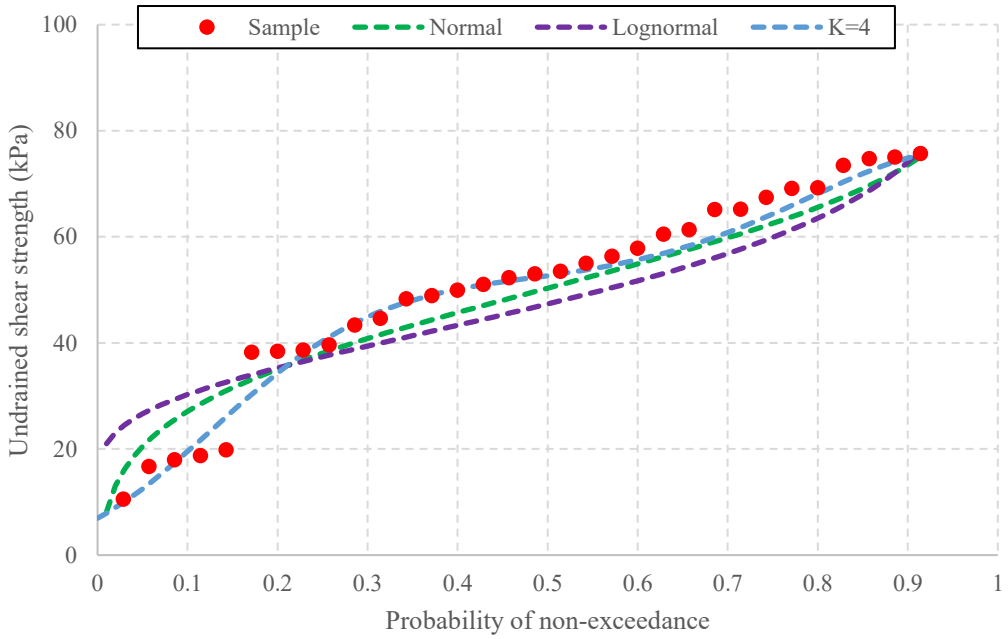

Figure 5.10. Maximum entropy quantile function for 8.5% right truncated data set (Undrained shear strength of upper silty sand layer from Nipigon River Landslide)

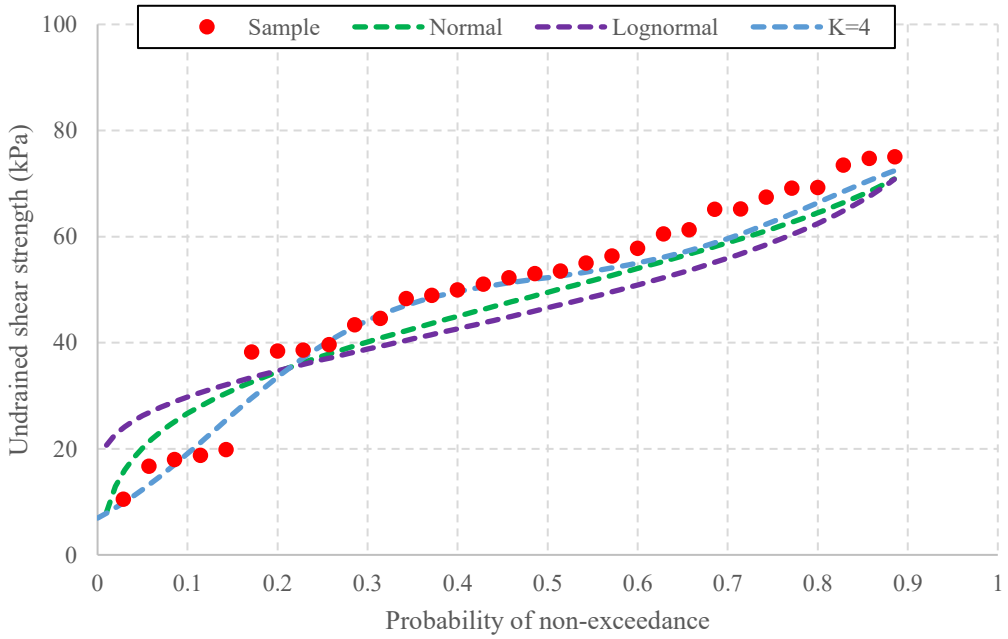

Figure 5.11. Maximum entropy quantile function for 11.5% right truncated data set (Undrained shear strength of upper silty sand layer from Nipigon River Landslide)

5.3. Reliability analysis of Nipigon River landslide with truncated samples

The examination of slope stability relies on integrating the LEM with a quantile-based reliability approach. Based on the algorithm proposed in Section 4.3, the first step in quantile function-based FORM for truncated samples is to define the limit state function. Furthermore, it was mentioned that the limit state function used for slope stability is generally written as $g_{(X)} = FOS - 1$. In order to simplify the calculation of the FOS as the first part of the limit state function, the explicit equation proposed by Low (1989) (Eq. 5.8) is used. This equation is primarily offered to calculate the FOS of an embankment on soft ground (Figure 5.12).

$$FOS = N_1 \frac{C_A}{\gamma H} + N_2 \left(\frac{C_m}{\gamma H} + \lambda \tan \varphi_m\right), \tag{5.8}$$

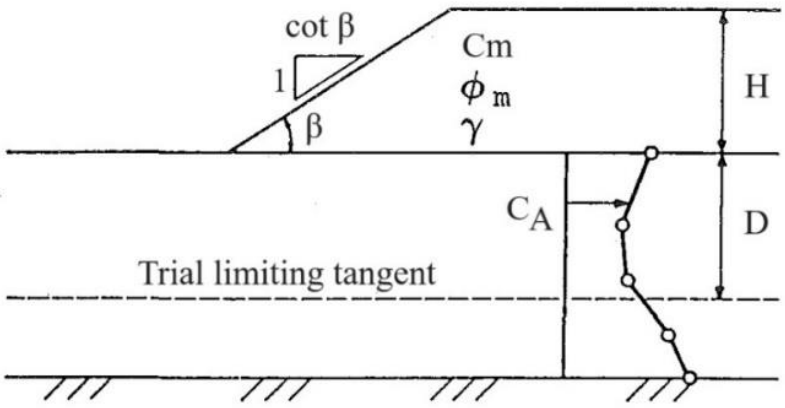

Figure 5.12. Embankment for the FOS calculation Low (1989)

where H is the height of the embankment, C_A is the equivalent undrained shear strength in the foundation soil, $C_m$is the cohesion of embankment soil, φ_m is the friction angle of embankment soil and γ is the unit weight of embankment soil. In addition to this, N_1 (stability number for the foundation soil), N_2 (stability number for the embankment soil) and λ (coefficient of tan φ_m) can be calculated by the following equations

$$N_1 = 3.06 \frac{C_A}{\gamma H} + \left(\frac{D}{H}\right)^{0.53} \alpha_1^{1.47/\alpha_2}, \tag{5.9}$$

$$N_2 = 1.53\frac{C_A}{\gamma H} + \left[\left(\frac{D}{H}+1\right)^{0.53} - \left(\frac{D}{H}\right)^{0.53}\right]\alpha_1^{1.47/\alpha_2}, \tag{5.10}$$

$$\lambda = 0.19 + \frac{0.02\cot\beta}{\frac{D}{H}}, \tag{5.11}$$

$$\alpha_1 = 1.564\left(\frac{D}{H}+0.5\right)0.1303\frac{\cot^2\beta+1}{\frac{D}{H}+0.5}, \tag{5.12}$$

$$\alpha_2 = \alpha_1\left(\frac{D}{H}+0.5\right) - 0.5\left(\frac{D}{H}+0.5\right)^2 - \frac{1}{24}(\cot^2\beta+1). \tag{5.13}$$

In order to verify the accuracy of Eq. (5.8), the FOS for Nipigon River landslide is calculated by using the soil properties provided in Table 5.1 and the geological section in Figure 5.4. Based on this calculation the FOS calculated from Eq. (5.8) is equal to 1.097 (Table 5.7), which is close to 1.08 reported by Dodds et al. (1993). In conclusion, Eq. (5.8) is capable of calculating the FOS with acceptable accuracy and can be used as the first part of the limit state function in the reliability analysis of Nipigon River landslide.

Table 5.7. Calculation of the FOS for Nipigon River landslide

Parameter	Notations	Amount
depth of trial limiting tangent in the foundation soil	D (m)	3
height of embankment	H (m)	6
Cot of slope angle	β	0.67
stability number for the foundation soil	N_1	3.98
stability number for the embankment soil	N_2	1.81
equivalent undrained shear strength in the foundation soil	C_A (kPa)	10
unit weight of embankment soil	γ (KN/m^3)	18
cohesion of embankment soil	C_m (kPa)	31.58
friction angle of embankment soil	φ_m (deg)	27
tan friction angle of embankment soil	$\tan\varphi_m$	0.51
coefficient of $\tan\Phi_m$	λ	0.216
lowest FOS corresponding to trial limiting tangent of depth D	FOS	1.097

Comparing the results obtained from normal, lognormal, and maximum entropy quantile functions for the original and various degrees of truncation (Figure 5.13 and Table 5.12) demonstrates that maximum entropy quantile function-based FORM closely approximates the outcomes derived from the parent normal quantile function-based approach which can be considered as the reference number. This trend persists across various levels of truncation, with the maximum entropy quantile functions offering reasonable estimations of reliability indices. Meanwhile, in five out of seven different conditions evaluated in this section, the optimal order of maximum entropy provides the closest results to the parent normal quantile functions. Therefore, using the optimal order of the maximum entropy quantile function along with AIC can be effective in optimizing the calculations and prevent using higher orders, which require heavy calculations. Furthermore, the lognormal and normal quantile functions show more significant deviations from the parent normal values, suggesting a less robust performance in these scenarios. For example, the lognormal distribution produces a reliability index that is the least conservative when contrasted with the maximum entropy quantile functions, despite the fact that all these quantile functions are derived from the same dataset. Meanwhile, the normal distribution results in lower reliability indices for right-truncated samples and higher reliability indices for left-truncated samples when compared to the parent normal quantile functions. The details regarding the iterations of each distribution with different degrees of truncation are provided in Tables 5.8 to 5.11.

Table 5.8. Results of reliability analysis with different degrees of truncations (Parent normal)

	β	p_f	Total Iter No.	Final design point c_u
11.5% left	1.1052	134.54E-3	3	38.53
8.5% left	1.0800	140.07E-3	3	38.53
6% left	0.9784	163.94E-3	3	38.53
original	0.7372	230.51E-3	3	38.53
6% right	0.6483	258.38E-3	3	38.53
8.5% right	0.6109	270.64E-3	3	38.53
11.5% right	0.5868	278.66E-3	3	38.53

Table 5.9. Results of reliability analysis with different degrees of truncations (normal)

	β	p_f	Total Iter No.	Final design point c_u
11.5% left	1.0348	138.99E-3	3	38.53
8.5% left	0.9652	167.21E-3	3	38.53
6% left	0.9025	183.38E-3	3	38.53
original	0.7075	239.59E-3	3	38.53
6% right	0.6863	246.25E-3	3	38.53
8.5% right	0.6562	255.83E-3	3	38.53
11.5% right	0.5907	277.36E-3	3	38.53

Table 5.10. Results of reliability analysis with different degrees of truncations (lognormal)

	β	p_f	Total Iter No.	Final design point c_u
11.5% left	0.9353	174.82E-3	3	38.53
8.5% left	0.8775	190.11E-3	3	38.53
6% left	0.8599	194.92E-3	3	38.53
original	0.8454	198.93E-3	3	38.53
6% right	0.7613	223.24E-3	3	38.53
8.5% right	0.7314	232.28E-3	3	38.53
11.5% right	0.6805	248.08E-3	3	38.53

Table 5.11. Results of reliability analysis with different degrees of truncations (maximum entropy)

	β	p_f	Total Iter No.	Final design point c_u
11.5% left	1.0464	147.67E-3	3	38.53
8.5% left	1.0863	138.67E-3	3	38.53
6% left	0.9630	167.76E-3	3	38.53
original	0.7092	239.11E-3	3	38.53
6% right	0.6217	267.07E-3	3	38.53
8.5% right	0.6061	272.22E-3	3	38.53
11.5% right	0.5874	278.45E-3	3	38.53

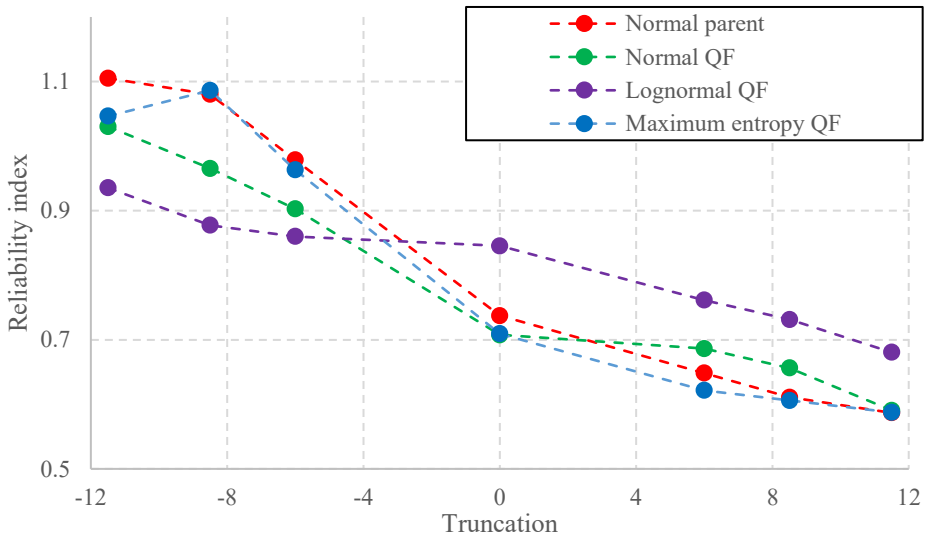

Figure 5.13. Comparison between reliability index ($\boldsymbol{\beta}$) for the original and different degrees of truncations (parent normal, normal, lognormal, and maximum entropy quantile functions)

Table 5.12. Reliability index ($\boldsymbol{\beta}$) calculated from normal and maximum entropy quantile functions for the original and different degrees of truncations

distribution		11.5% left	8.5% left	6% left	original	6% right	8.5% right	11.5% right
Parent normal QF		**1.1052**	**1.0800**	**0.9784**	**0.7372**	**0.6483**	**0.6109**	**0.5868**
Normal QF		1.0348	0.9652	0.9025	0.7075	0.6863	0.6562	0.5907
Lognormal QF		0.9353	0.8775	0.8599	0.8454	0.7613	0.7314	0.6805
	Order							
Maximum entropy QF	1	1.9163	1.4852	1.2205	0.9030	0.8896	0.8657	0.8344
	2	1.5294	**1.0863**	0.8701	0.6373	0.8882	0.5895	0.5735
	3	1.0974	0.8489	0.7313	0.5792	0.5579	0.5481	0.5359
	4	**1.0464**	0.8800	0.7871	0.627	**0.6217**	**0.6061**	**0.5874**
	5	1.3082	1.3259	**0.9630**	0.6242	0.6207	0.6020	0.5801
	6	1.3366	1.3202	0.9288	**0.7092**	0.5933	0.5732	0.5515
	7	1.6822	1.3519	0.9629	0.6241	0.5761	0.5559	0.5378
	8	1.2657	1.3563	0.9977	0.6641	0.5813	0.5595	0.5387
	9	1.4266	1.3433	0.9996	0.6104	0.5666	0.5488	0.5311
	10	1.5792	1.2848	0.9545	0.6111	0.5707	0.5462	0.5423

In addition to this, based on values offered by Christian et al. (1994) (Table 2.1) regarding the expected performance level for different values of the reliability index and the probability of failure in slope stability analysis, the studied section from the Nipigon River has hazardous and unsatisfactory performance levels (for all the analyses including the original and truncated samples), which eventually led to the landslide happening on April 23, 1990.

5.4. Higher levels of truncation

In this section, the effect of higher levels of truncation (20% and 28.5% from left and right) on the reliability indexes calculated from different methods is evaluated (Table 5.13).

Table 5.13. Reliability index (β) calculated from normal and maximum entropy quantile functions for higher levels of truncation

distribution	28.5% left	20% left	20.5% right	28.5.% right
Parent normal QF	1.9925	1.6280	0.4974	0.3611
Normal QF	2.2913	1.8435	0.2311	-0.1991
Lognormal QF	1.6442	1.2699	0.1661	-0.3190
Maximum entropy QF (Optimal order)	1.9233	1.6020	0.4501	0.3400

Based on the results, it is evident that as the level of truncation in samples increases, the disparity between the calculated reliability indexes and the original values for the reliability index markedly rises. This exclusion can lead to a distortion of the statistical properties of the sample, affecting the calculated reliability indexes.

The reliability indexes obtained from higher levels of truncation, especially in left-truncated samples, can lead to an overestimation of the reliability index. Consequently, this may cause the reliability index to fall to different performance levels than the original set, resulting in misleading conclusions from the reliability analysis. Therefore, in the case of truncated samples in geotechnical engineering, the general geological knowledge of evaluated soil and rock formations is of significant importance as it can prevent engineers and designers from conducting the reliability analyses with highly truncated samples which can eventually provide inaccurate results. Finally, the accuracy of reliability analysis decreases with increasing levels of truncation, a threshold that varies depending on the characteristics of the data samples. Consequently, the critical truncation percentage, beyond which reliability analysis becomes less accurate, may differ across different examples.

The details regarding the iterations of each distribution with different degrees of truncation are provided in Tables 5.14 to 5.17.

Table 5.14. Results of reliability analysis with different degrees of truncations (Parent normal)

	β	p_f	Total Iter No.	Final design point c_u
28.5 % left	1.9925	23.15E-3	3	38.53
20 % left	1.6280	51.76E-3	3	38.53
20 % right	0.4974	309.42E-3	3	38.53
28.5% right	0.3611	358.98E-3	3	38.53

Table 5.15. Results of reliability analysis with different degrees of truncations (normal)

	β	p_f	Total Iter No.	Final design point c_u
28.5 % left	2.2913	10.97E-3	3	38.53
20 % left	1.8435	32.62E-3	3	38.53
20 % right	0.2311	408.58E-3	3	38.53
28.5% right	-0.1991	547.57E-3	3	38.53

Table 5.16. Results of reliability analysis with different degrees of truncations (lognormal)

	β	p_f	Total Iter No.	Final design point c_u
28.5 % left	1.6442	50.05E-3	3	38.53
20 % left	1.2699	102.06E-3	3	38.53
20 % right	0.1661	434.02E-3	3	38.53
28.5% right	-0.3190	625.14E-3	3	38.53

Table 5.17. Results of reliability analysis with different degrees of truncations (maximum entropy)

	β	p_f	Total Iter No.	Final design point c_u
28.5 % left	1.9233	26.13E-3	3	38.53
20 % left	1.6020	54.96E-3	3	38.53
20 % right	0.4501	325.27E-3	3	38.53
28.5% right	0.3400	372.18E-3	3	38.53

5.5. Remedial measures for improving slope stability

In this section, various methods available for improving the stability of the Nipigon River landslide are discussed.

5.5.1. Reducing the coefficient of variation (COV)

Reducing the coefficient of variation (COV) of the undrained shear strength in soil yields multiple benefits for slope stability. Firstly, it promotes consistency in material properties across the slope, enhancing predictability and reducing the risk of localized failure zones. Secondly, it ensures a more uniform resistance to shear forces, thereby improving overall stability against gravity, water flow, and external loads. Moreover, by reducing variability in the undrained shear strength, slope design accuracy is improved, leading to more reliable stability analyses. Lastly, a lower COV of the undrained shear strength enhances the slope's resilience to changing environmental conditions, minimizing sensitivity to factors like water content fluctuations and load variations.

Reliability analyses with different COVs for the upper silty sand layer are conducted and results are provided in Table 5.18. It resulted in a decrease in the COV of the undrained shear strength of the upper silty sand layer, which can effectively increase the reliability index and reduce the probability of failure, both of which contribute to the stability of the slope.

Table 5.18. The result of reliability analyses with different COV

COV	β	P_f
0.375	0.7371	0.2305
0.300	0.9257	0.1773
0.250	1.110	0.1334
0.200	1.388	0.0825
0.150	1.852	0.0319

Reducing COV can also be achieved through different methods including soil stabilization techniques, drainage, vegetation, and erosion control.

Drainage: higher pore water pressure as a result of the saturation of the subsoil can be considered one of the major causes of slope instability. Therefore, designing a comprehensive surface and subsurface drainage system is required. Another significant point regarding the drainage system is that the efficiency of the system usually reduces after several years, and long-term maintenance plans should be conducted in order to guarantee the function of the drainage system (Kazmi et al. 2017).

Erosion control: it plays a vital role in maintaining slope stability by preventing the degradation of soil structure and the loss of surface material due to the action of wind, water, or gravity. By implementing erosion control measures such as vegetation, geotextiles, or terracing, the forces of erosion can be minimized, thus reducing the likelihood of slope failure.

5.5.2. Geometrical Method

This method can be considered one of the most effective ways to increase the FOS on slopes. By converting steep slopes into gentle slopes, the FOS can be increased. (Kazmi et al. 2017). Reliability-based slope optimization can be considered a method in order to determine the safe slope angle in slope stability analyses. In this section, this analysis is conducted for the Nipigon River landslide, and the reliability indexes are calculated after considering different amounts of reduction in the slope angle and various percentages of truncation in the sample of data. Based on the results (Table 5.19 and Figure 5.14), the reduction in the slope angle will increase the value of the reliability index.

According to the results provided in Figure 5.15, the percentage of the increase in the reliability index is different for left and right-truncated samples. The increase in reliability indexes obtained for left truncated samples is smaller than the original sample, while the increase in reliability indexes obtained for right truncated samples is greater than the original sample. For instance, with a 20% reduction in slope angle, the reliability index from an 11.5% left-truncated sample is 6.41% lower than the original, whereas the index from an 11.5% right-truncated sample is 6.45% higher. The reason for this difference also lies in how the truncation affects the distribution of the reliability index. Therefore, knowledge of the

truncation condition plays a significant role in evaluating the results of the reliability analysis with truncated samples and prevents engineers from using misleading results.

By understanding the relationship between the percentage of the slope angle reduction and the reliability index, engineers can calculate the required slope angle reduction to satisfy the requirement of stability in slope stability projects.

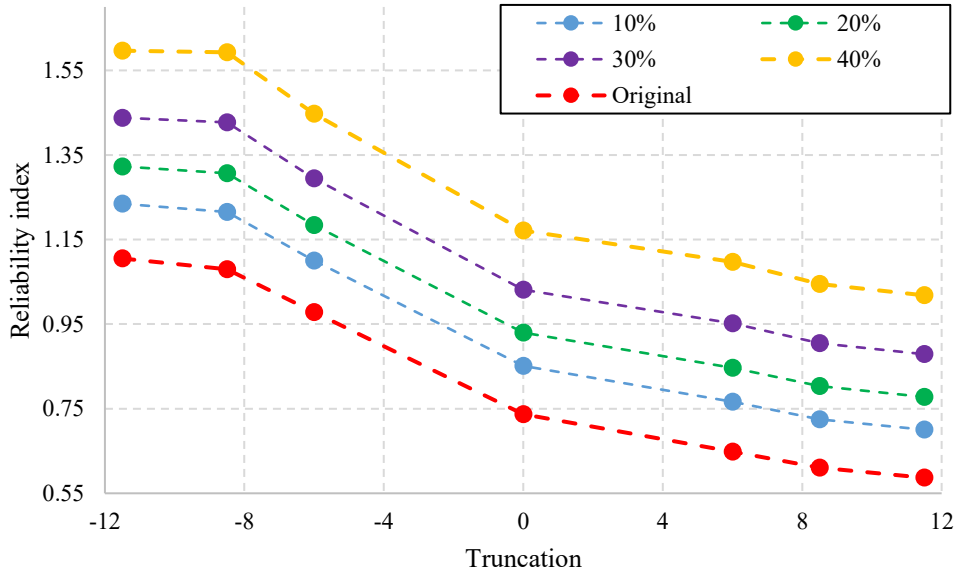

Figure 5.14. Variations in the reliability index with differing percentages of the slope angle reduction across various truncation levels

Table 5.19. Variations in the reliability index with differing percentages of the slope angle reduction across various truncation levels

slope angle reduction	11.5% left	8.5% left	6% left	original	6% right	8.5% right	11.5% right
Original slope angle	1.1052	1.0800	0.9784	0.7372	0.6483	0.6109	0.5868
10%	1.2346	1.2149	1.1003	0.8515	0.7664	0.7252	0.7004
20%	1.3228	1.3069	1.1844	0.9296	0.8470	0.8032	0.7778
30%	1.4380	1.4270	1.2949	1.0314	0.9522	0.9050	0.8789
40%	1.5966	1.5924	1.4478	1.1716	1.0969	1.0452	1.0181

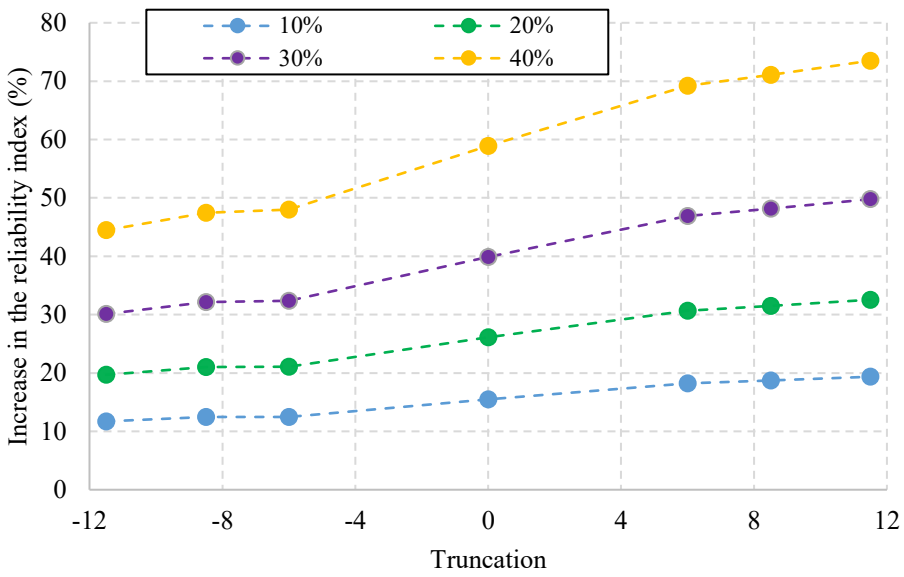

Figure 5.15. The increase in the reliability index (%) for differing percentages of the slope angle reduction across various truncation levels

5.6. Summary

This chapter discussed the reliability analysis of slopes in the Nipigon River Landslide. The landslide, which occurred in 1990 near Nipigon, Ontario, Canada. The chapter discussed the concept of truncated maximum entropy quantile functions for the reliability analysis of the Nipigon River Landslide. Using the undrained shear strength values determined through laboratory tests by Barros et al. (2023), for for the upper silty sand layer, maximum entropy quantile functions were derived. The effects of different truncation percentages on these functions were evaluated.

The reliability analysis involves the integration of the LEM with a quantile-based approach. A limit state function for slope stability was defined using an equation proposed by Low (1989). The accuracy of this equation was verified by calculating the FOS for the Nipigon River landslide, showing close agreement with previous reports.

The reliability analysis was performed for various levels of truncation, considering both left and right truncation scenarios. The results, obtained from parent normal, normal, lognormal, and maximum entropy quantile functions, demonstrated that the maximum entropy approach closely approximates the outcomes derived from the parent normal distribution. The

reliability indices were compared, indicating that maximum entropy quantile functions provide reasonable estimations.

This chapter also suggests that the maximum entropy quantile function-based FORM is effective in assessing slope stability while working with truncated samples. The findings reveal hazardous and unsatisfactory performance levels for the Nipigon River Landslide, contributing to the understanding of the landslide event that occurred in 1990.

Remedial measures for improving the stability of the slope include reducing the COV of the undrained shear strength, geometrical methods, and the construction of retaining walls. Finally, reliability-based slope optimization can be carried out for both the original and truncated samples to identify the optimal reduction in slope angle necessary to achieve the desired reliability index.

6. Conclusion and recommendations

The conclusion of this research is summarized in this chapter and recommendations are suggested for further research on this topic.

6.1. Conclusions

This research focused on the application of truncated quantile functions in the reliability analysis of slopes. Based on the results, the optimal order of the maximum entropy quantile function is more capable of representing truncated samples compared to normal and lognormal distributions. Furthermore, a modified truncated quantile function-based FORM was introduced. This new approach was verified and applied to rock and soil slope stability examples. The detailed conclusions of each chapter are provided in the following sections.

6.1.1. General concepts

This study highlighted the significance of landslides as a prevalent and impactful disaster in Canada, particularly concerning human lives and infrastructure sustainability. The incorporation of reliability analysis, specifically using the reliability index (β), emerged as a valuable tool in evaluating engineering uncertainties, particularly in slope stability. The discussion on truncated distributions explained the challenges posed by limitations in the domain of probability distributions, emphasizing the relevance of truncated random variables in engineering scenarios.

6.1.2. Truncated quantile function from a truncated sample

Chapter 3 focused on the application of MEPs in estimating quantile functions from truncated samples. Using MEPs along with PPWMs, the extended quantile functions of a truncated sample can be obtained. Meanwhile by using the AIC, one can obtain the optimal order of maximum entropy quantile functions for reliability analyses. The optimization of the quantile functions prevents us from utilizing excessively complex models, which have numerous adjustable parameters that may not adequately capture the sample information, as well as simplistic models, which lack sufficient adjustable parameters to fully incorporate the sample information.

This method demonstrated the ability to handle issues related to truncated, small sample sizes effectively. Chapter 3 also showcased the application of these principles in two illustrative examples involving cohesion of rock discontinuities and rock uniaxial compression strength, highlighting their flexibility and objectivity of the optimal order of maximum entropy in comparison with normal and lognormal quantile functions in model selection.

6.1.3. Reliability method with truncated quantile functions

Chapter 4 explored the application of reliability methods incorporating truncated quantile functions within the field of geotechnical engineering. The primary emphasis was on proposing a FORM based on quantile functions for truncated samples. This modified version is based on the quantile-based FORM introduced by Deng and Pandey (2023) and modifications suggested by Melchers et al. (2003) for the FORM for truncated PDFs. The suggested algorithm was verified by repeating the results of an example provided by Melchers et al. (2003). In addition to this, an illustrative example, including rock slope stability analysis using the optimal order of maximum entropy quantile functions with different amounts of the truncation was used to calculate the reliability index. This example substantiated the effectiveness of the proposed algorithm in estimating reliability indices for various scenarios. It was also observed that the optimal order of maximum entropy quantile functions provides more accurate results compared to normal and lognormal distributions based on the reference values, which is related to the ability of maximum entropy quantile functions to better present the sample of data.

6.1.4. Reliability analysis of slopes in the Nipigon River Landslide

In Chapter 5, the reliability analysis of slopes in the Nipigon River Landslide, a 1990 incident near Nipigon, Ontario, Canada, was discussed. It applied the concept of truncated maximum entropy quantile functions for reliability analysis in this context. Utilizing the undrained shear strength values obtained from laboratory tests conducted by Barros et al. (2023) for the upper silty sand layer, maximum entropy quantile functions and the extended maximum entropy quantile functions were derived, and the effect of various truncation percentages on these functions was assessed.

The reliability analysis integrated the LEM with a quantile-based approach. A limit state function for slope stability in soft soils was formulated using an equation proposed by Low (1989), and its accuracy was confirmed by calculating the FOS for the Nipigon River landslide, aligning closely with previous reports.

Then, the reliability analysis was conducted using the modified algorithm proposed in Chapter 4 for the FORM method based on quantile functions for truncated samples using normal, lognormal, and maximum entropy quantile functions and finally the results were compared, which showed an agreement between the parent normal distribution and the maximum entropy quantile functions.

The chapter asserted the effectiveness of the maximum entropy quantile function-based FORM method in evaluating slope stability with truncated samples. The findings disclosed hazardous and unsatisfactory performance levels for the Nipigon River Landslide, contributing to a comprehensive understanding of the 1990 landslide event.

Remedial measures for improving slope stability can be different. For example, by decreasing the coefficient of variation of the undrained shear strength using various methods, the reliability index can be improved. Finally, reliability-based slope optimization was conducted for the original and truncated samples to discover the optimal slope angle reduction value for achieving the required reliability index.

6.2. Recommendations for further research

Following the conclusion of this study some recommendations can be made in order to help future research in this area.

Exploring the broader application of truncated quantile functions in geotechnical engineering beyond slope stability analysis and investigating how these functions can be utilized in different geological settings and materials, assessing their flexibility and reliability in various scenarios.

Investigating the impact of time-dependent factors on slope stability, such as long-term weathering effects and progressive changes in geological conditions. Meanwhile try to

develop models that consider the dynamic nature of slope stability and assess how these factors influence the reliability of predictions over extended periods.

Conducting more laboratory tests on other layers of the Nipigon River Landslide including clayey silt layers (firm and soft) and the lower silty sand layer, can provide more information regarding the properties of soil layers. Then, using the obtained information reliability analyses can be conducted by considering multiple random variables at the same time.

Furthermore, by accessing the information of each layer, the sensitivity analysis can be included to evaluate the effect of each individual layer on the final result of reliability analyses and eventually the stability of the slope.

Finally, long-term monitoring of slopes, combined with comprehensive data collection efforts, can provide valuable insights into the evolving nature of slope stability, and contribute to refining and improving reliability analysis methodologies.

Appendix A Cohesion of rock discontinuities

Table A.1. Parameters of maximum entropy quantile functions for the original data set (moment order K =1-10)

	$K=1$	$K=2$	$K=3$	$K=4$	$K=5$
λ_0	-5.2626882	-5.2280893	-5.0956121	-5.0092606	-5.0547986
λ_1	-0.6648717	-0.8543543	-2.3028578	-3.8578940	-2.6214904
λ_2		0.1813725	3.6341409	10.2766906	2.0612773
λ_3			-2.2323814	-12.2222074	8.9503519
λ_4				4.8745441	-18.3591676
λ_5					9.1164231
	$K=6$	$K=7$	$K=8$	$K=9$	$K=10$
λ_0	-5.0692247	-5.1174012	-5.1514348	-5.1139361	-5.1267004
λ_1	-2.0644365	0.4390965	2.7679954	0.0555016	-0.1610275
λ_2	-3.2409252	-35.3959279	-73.6886583	-18.0732638	-5.7828058
λ_3	29.4619934	201.9130124	471.0728738	-31.0031714	-166.5357729
λ_4	-55.8775852	-517.6349250	-1496.7179550	922.6616700	1484.3992991
λ_5	41.4983924	692.5032583	2682.6427916	-4091.2482848	-4766.9608566
λ_6	-10.6254127	-472.7049289	-2752.8845302	8603.1900766	6741.3334086
λ_7		130.1124367	1505.7207284	-9715.0182374	-2277.1334419
λ_8			-339.6625270	5678.5925911	-4710.5454464
λ_9				-1349.9291652	5431.1802358
λ_{10}					-1730.7547993

Table A.2. Parameters of maximum entropy quantile functions for 4% left truncated data set (moment order K =1-10)

	$K=1$	$K=2$	$K=3$	$K=4$	$K=5$
λ_0	-5.3069207	-5.2971817	-5.1849162	-5.0876968	-5.1005867
λ_1	-0.6125828	-0.6664118	-1.9097222	-3.6828816	-3.3304937
λ_2		0.0517106	3.0305700	10.6501344	8.2970277
λ_3			-1.9313308	-13.4299657	-7.3462676
λ_4				5.6234915	-1.0670326
λ_5					2.6293947
	$K=6$	$K=7$	$K=8$	$K=9$	$K=10$
λ_0	-5.0778512	-5.0809623	-5.0611251	-5.1458262	-5.1257584
λ_1	-4.2067008	-4.0494727	-5.1236360	0.0524326	-1.5481314
λ_2	16.6615408	14.6638133	29.2892657	-49.3858623	-17.2373797
λ_3	-39.7853467	-29.1438333	-114.7171219	386.6782121	100.3019473
λ_4	58.3803874	30.0290942	290.0894651	-1303.5093664	77.0458186
λ_5	-48.7535761	-8.9405577	-450.7860132	2156.7250363	-1751.7498599
λ_6	16.8793092	-11.2886581	410.3767111	-1460.3971402	5188.6261570
λ_7		7.9102198	-202.2910077	-353.2601700	-6962.1405745
λ_8			42.3133147	999.4076689	4427.5842074
λ_9				-377.1170094	-977.2537919
λ_{10}					-84.5395505

Table A.3. Parameters of maximum entropy quantile functions for 6% left truncated data set (moment order K =1-10)

	$K=1$	$K=2$	$K=3$	$K=4$	$K=5$
λ_0	-5.3290228	-5.3330524	-5.2352130	-5.1401158	-5.1438195
λ_1	-0.5862353	-0.5638566	-1.6552459	-3.4042983	-3.3023368
λ_2		-0.0215371	2.6005344	10.1430734	9.4598145
λ_3			-1.7025078	-13.1071950	-11.3370699
λ_4				5.5845901	3.6352793
λ_5					0.7668157
	$K=6$	$K=7$	$K=8$	$K=9$	$K=10$
λ_0	-5.1056493	-5.0790367	-5.0807333	-5.1058578	-5.1036084
λ_1	-4.7788175	-6.1505088	-6.0551634	-4.5186405	-4.6608442
λ_2	23.5959989	41.3139525	39.8430517	16.7813130	18.9642212
λ_3	-66.2648740	-161.8336699	-151.7442052	-11.5268846	-23.6188991
λ_4	104.4281440	361.5325521	325.0065274	-71.3685855	-57.4669270
λ_5	-86.4365696	-450.2962921	-375.6569090	83.4271739	205.0781380
λ_6	28.6673221	287.7392499	201.3357156	333.3188750	-251.8080776
λ_7		-73.1391474	-20.3479640	-889.0022358	293.5951754
λ_8			-13.2144444	783.3430850	-485.0303371
λ_9				-241.2855742	465.1844280
λ_{10}					-161.0729722

Table A.4. Parameters of maximum entropy quantile functions for 8% left truncated data set (moment order K =1-10)

	$K=1$	$K=2$	$K=3$	$K=4$	$K=5$
λ_0	-5.3524225	-5.3731472	-5.2965107	-5.2160008	-5.2280663
λ_1	-0.5578491	-0.4421343	-1.3045974	-2.8031746	-2.4664493
λ_2		-0.1115818	1.9671430	8.4590028	6.1901561
λ_3			-1.3519865	-11.1917928	-5.2964259
λ_4				4.8256582	-1.6786073
λ_5					2.5619382
	$K=6$	$K=7$	$K=8$	$K=9$	$K=10$
λ_0	-5.1986223	-5.1732659	-5.1897071	-5.2103765	-5.2113336
λ_1	-3.6222658	-4.9488674	-3.8381773	-2.3696374	-2.6784264
λ_2	17.3247994	34.5741802	15.8281671	-10.4073157	0.9551104
λ_3	-48.7097031	-142.1014144	-8.0267230	194.8954334	63.9808774
λ_4	78.1587508	330.0151673	-163.2956768	-993.1698528	-289.3908983
λ_5	-66.6159181	-423.6513897	586.8746935	2550.3169439	518.9536651
λ_6	22.7670249	277.2975731	-886.7445771	-3661.7993993	-384.5734725
λ_7		-71.9262062	633.0634960	2939.4598329	129.0424187
λ_8			-174.5975344	-1211.6053076	-261.9600090
λ_9				193.9545465	380.4766133
λ_{10}					-155.5406187

Table A.5. Parameters of maximum entropy quantile functions for 10% left truncated data set (moment order K =1-10)

	$K=1$	$K=2$	$K=3$	$K=4$	$K=5$
λ_0	-5.3743870	-5.4109758	-5.3564738	-5.2951913	-5.3255674
λ_1	-0.5313517	-0.3260287	-0.9447177	-2.0997012	-1.2384335
λ_2		-0.1983515	1.2973951	6.3234585	0.4861521
λ_3			-0.9743802	-8.6104990	6.6039391
λ_4				3.7504555	-13.0675619
λ_5					6.6331029
	$K=6$	$K=7$	$K=8$	$K=9$	$K=10$
λ_0	-5.3229811	-5.3293783	-5.3069180	-5.3467361	-5.3754607
λ_1	-1.3421388	-0.9980437	-2.4003678	-0.2790712	2.2876786
λ_2	1.4933774	-3.0283870	18.6047578	-9.2980346	-59.1788981
λ_3	2.6593334	27.2844902	-115.4321120	8.7651405	424.3898767
λ_4	-5.7928053	-72.4517400	415.6057518	344.1116408	-1474.4182575
λ_5	0.3171325	95.0647633	-839.7606012	-1865.9166901	2693.0910158
λ_6	2.0817025	-65.5978243	946.0234771	4362.4131397	-2345.9662422
λ_7		19.1546781	-558.4837999	-5320.6231977	245.0976954
λ_8			135.2423821	3309.4777830	1140.5983963
λ_9				-829.2561838	-772.6532313
λ_{10}					146.1778432

Table A.6. Parameters of maximum entropy quantile functions for 4% right truncated data set (moment order K =1-10)

	$K=1$	$K=2$	$K=3$	$K=4$	$K=5$
λ_0	-5.2629705	-5.2226093	-5.0787458	-5.0165635	-5.0562204
λ_1	-0.6381325	-0.8598286	-2.4335708	-3.5545724	-2.4745453
λ_2		0.2125623	3.9678913	8.7606811	1.5757337
λ_3			-2.4301120	-9.6435757	8.8888084
λ_4				3.5218959	-16.8276305
λ_5					7.9886064
	$K=6$	$K=7$	$K=8$	$K=9$	$K=10$
λ_0	-5.0720411	-5.1276942	-5.1243089	-5.1767001	-5.1678493
λ_1	-1.8621015	1.0564313	0.9617142	3.8451541	3.1706063
λ_2	-4.2599509	-41.9330969	-43.0718392	-78.8248783	-64.8859431
λ_3	31.4808090	234.2526652	257.8768475	403.0802364	283.2952513
λ_4	-58.1754209	-602.6473251	-736.0631354	-742.7159642	-224.7444758
λ_5	43.6925756	813.0690686	1166.4721418	-363.0238242	-1554.5737299
λ_6	-11.7198929	-558.8591120	-1045.4706173	3588.7040172	4921.0797779
λ_7		154.3113710	491.4192502	-5730.4513922	-5954.2855779
λ_8			-92.9037221	3959.9819660	2915.1479693
λ_9				-1041.3752499	-25.6386273
λ_{10}					-299.3683090

Table A.7. Parameters of maximum entropy quantile functions for 6% right truncated data set (moment order K =1-10)

	$K=1$	$K=2$	$K=3$	$K=4$	$K=5$
λ_0	-5.2642115	-5.2175484	-5.0728289	-5.0181202	-5.0596746
λ_1	-0.6218679	-0.8785746	-2.4622539	-3.4492908	-2.3156213
λ_2		0.2463754	4.0279858	8.2505635	0.7031257
λ_3			-2.4485860	-8.8072646	10.6710134
λ_4				3.1059729	-18.2921352
λ_5					8.4035392
	$K=6$	$K=7$	$K=8$	$K=9$	$K=10$
λ_0	-5.0695082	-5.1428903	-5.1387673	-5.1732062	-5.1744372
λ_1	-1.9344514	1.9234084	1.8014666	3.6619062	3.6831518
λ_2	-2.9312334	-52.7759778	-52.7402662	-74.5852275	-74.7128743
λ_3	24.7478069	293.1949164	304.1061987	378.5985275	388.4457097
λ_4	-44.0662879	-765.2348849	-838.1156063	-721.5120971	-866.5075068
λ_5	30.6678830	1050.1546667	1254.2499833	-129.2460811	740.1208315
λ_6	-7.3107131	-732.5836305	-1020.3485011	2707.8092936	-10.9667748
λ_7		204.6190865	405.9631139	-4394.0154081	440.0945539
λ_8			-55.6324520	3005.1002011	-1923.6191220
λ_9				-776.5318458	1909.7121242
λ_{10}					-606.9809478

Table A.8. Parameters of maximum entropy quantile functions for 8% right truncated data set (moment order K =1-10)

	$K=1$	$K=2$	$K=3$	$K=4$	$K=5$
λ_0	-5.2647087	-5.2132410	-5.0653499	-5.0229222	-5.0585916
λ_1	-0.6076369	-0.8911761	-2.5098953	-3.2759999	-2.3013771
λ_2		0.2723674	4.1398364	7.4190151	0.9263926
λ_3			-2.5054175	-7.4457027	9.3177623
λ_4				2.4140267	-16.0081783
λ_5					7.2368614
	$K=6$	$K=7$	$K=8$	$K=9$	$K=10$
λ_0	-5.0729658	-5.1522888	-5.0962461	-5.1836503	-5.1548302
λ_1	-1.7434671	2.4376546	-1.1799736	4.4598704	2.0460778
λ_2	-4.3961419	-58.4624593	-2.3508770	-90.2509245	-40.9997264
λ_3	29.9412042	321.2516130	-50.2525529	526.2876783	103.0043593
λ_4	-53.7806925	-836.5876548	437.1578485	-1477.7159757	389.7373162
λ_5	39.8740422	1146.7014799	-1296.3761239	2113.5663174	-2442.8566645
λ_6	-10.7189977	-798.2211443	1844.8046098	-1245.1346539	4814.4898495
λ_7		222.1909976	-1283.3841269	-319.1728632	-3895.9413446
λ_8			350.7915651	740.5443645	225.5341301
λ_9				-253.2858617	1438.4484847
λ_{10}					-594.2154080

Table A.9. Parameters of maximum entropy quantile functions for 10% right truncated data set (moment order K =1-10)

	$K=1$	$K=2$	$K=3$	$K=4$	$K=5$
λ_0	-5.2656296	-5.2077484	-5.0591499	-5.0271329	-5.0576367
λ_1	-0.5923040	-0.9116261	-2.5385064	-3.1172031	-2.2824192
λ_2		0.3070288	4.1964208	6.6749543	1.1101745
λ_3			-2.5210470	-6.2570809	8.1178532
λ_4				1.8263845	-13.9773834
λ_5					6.2103607
	$K=6$	$K=7$	$K=8$	$K=9$	$K=10$
λ_0	-5.0771054	-5.1630282	-5.1554221	-5.1685494	-5.1872465
λ_1	-1.5256743	3.0147709	2.5866651	2.8302081	4.5095041
λ_2	-6.1138393	-64.8800107	-58.7016317	-55.3779011	-87.8984507
λ_3	36.1213089	352.9428312	314.3023205	224.1175947	499.4499257
λ_4	-65.2851118	-917.0625067	-790.5443926	-124.9030079	-1377.6777538
λ_5	50.5562358	1255.4353163	1021.6682896	-1363.0678974	2006.0223886
λ_6	-14.5683146	-872.1859929	-626.7130868	4090.9754158	-1484.5504370
λ_7		242.0666869	105.3868033	-5159.3180471	521.4610762
λ_8			31.3387370	3138.6671475	-271.8642363
λ_9				-754.6927105	313.7414915
λ_{10}					-123.8899934

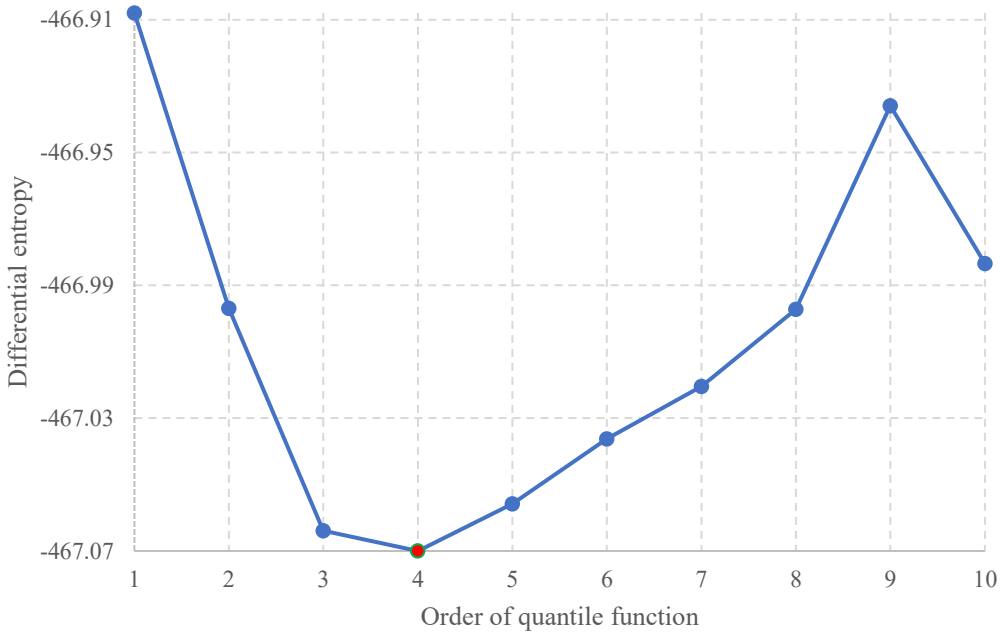

Figure A.1. Differential entropy versus order of quantile function for the original data set

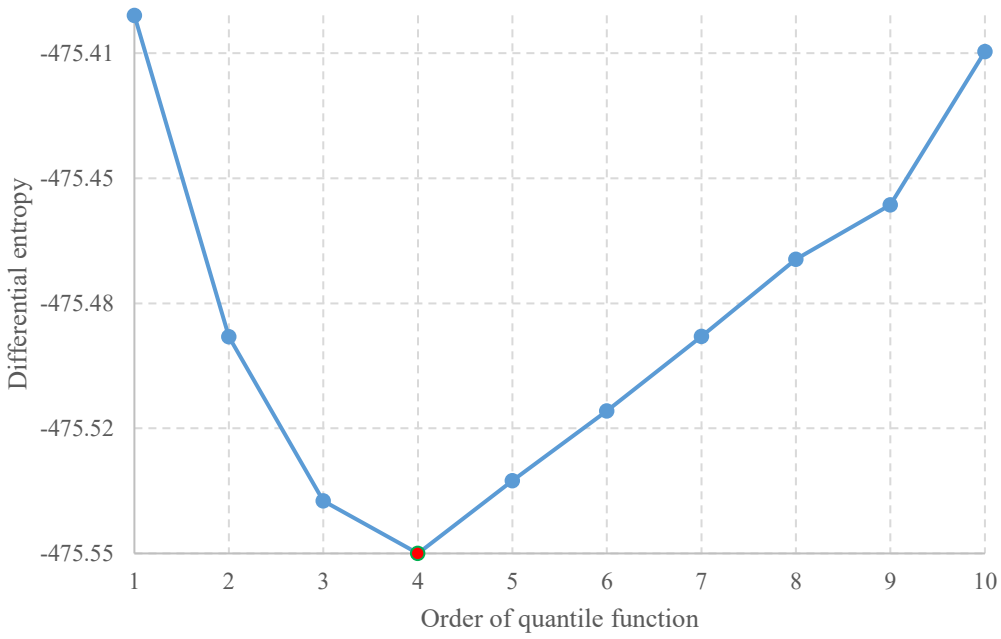

Figure A.2. Differential entropy versus order of quantile function for 4% left truncated data set

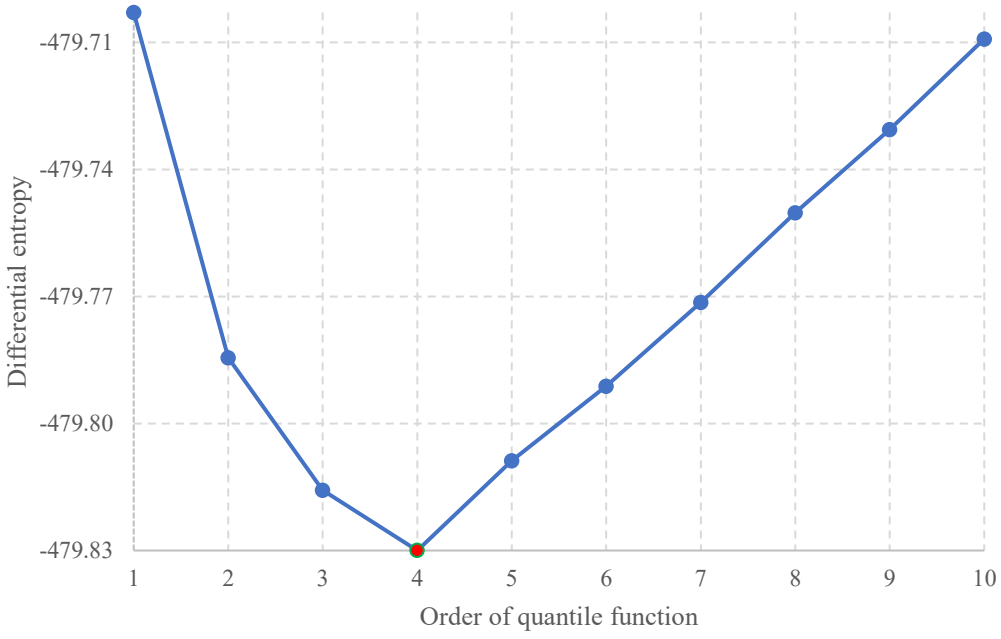

Figure A.3. Differential entropy versus order of quantile function for 6% left truncated data set

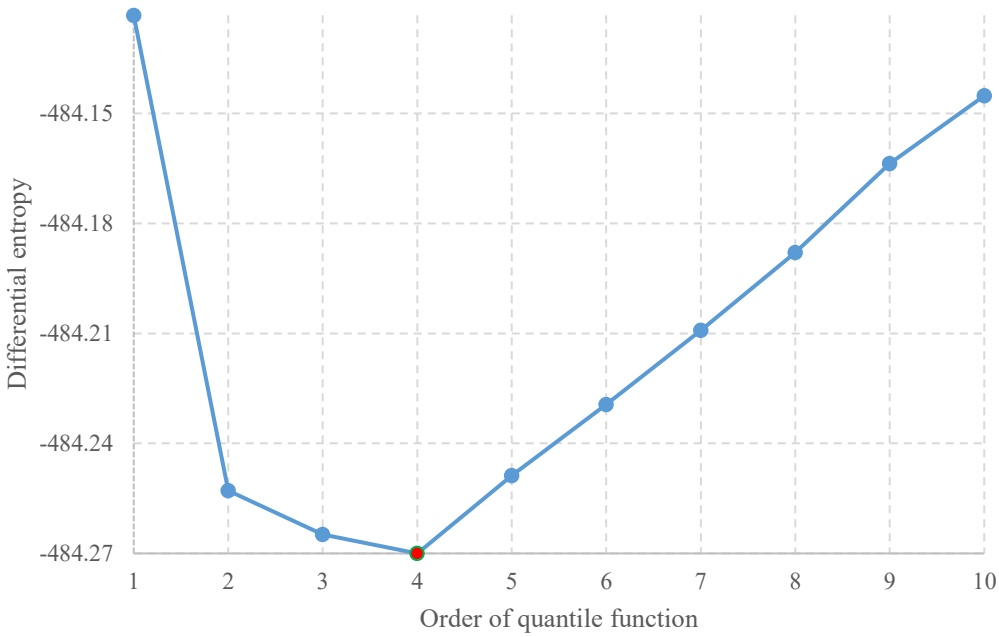

Figure A.4. Differential entropy versus order of quantile function for 8% left truncated data set

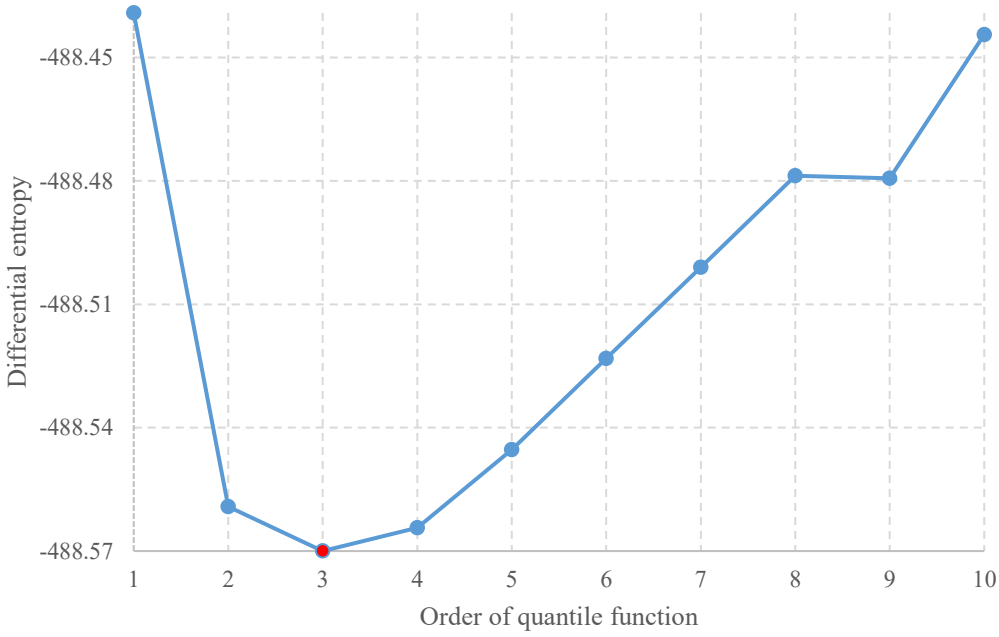

Figure A.5. Differential entropy versus order of quantile function for 10% left truncated data set

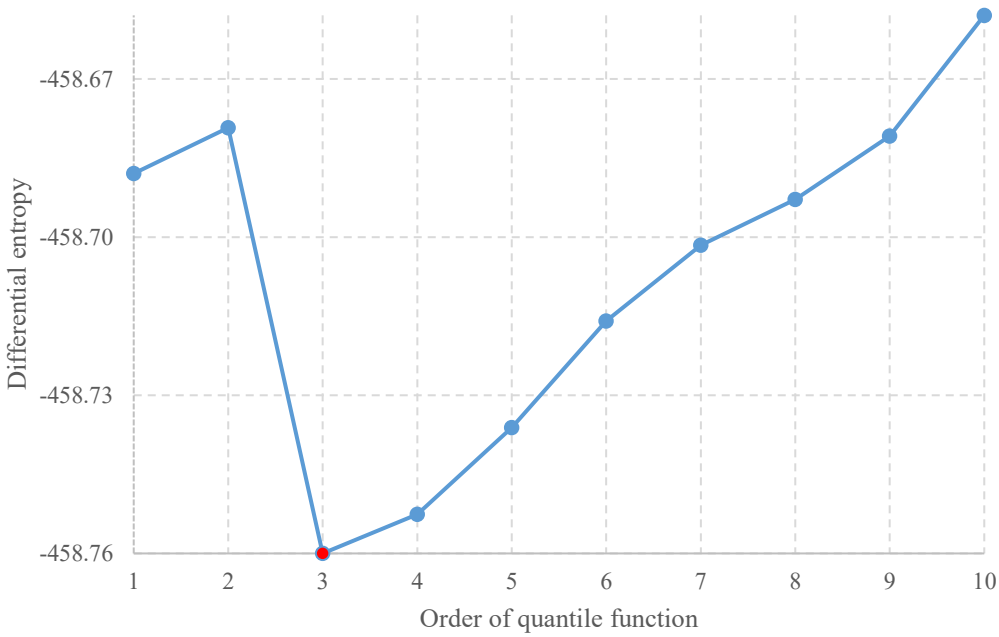

Figure A.6. Differential entropy versus order of quantile function for 4% right truncated data set

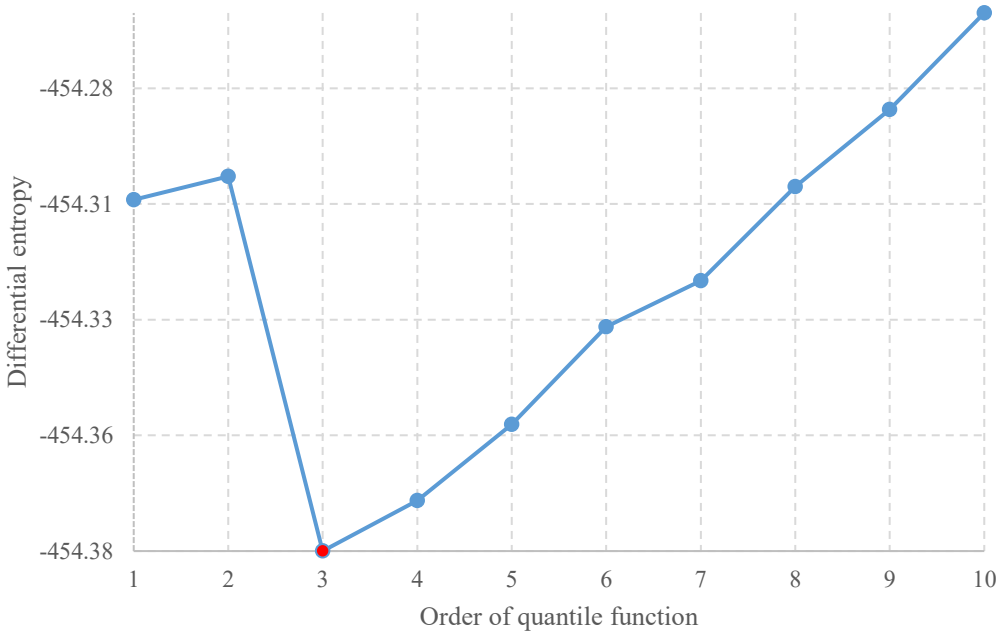

Figure A.7. Differential entropy versus order of quantile function for 6% right truncated data set

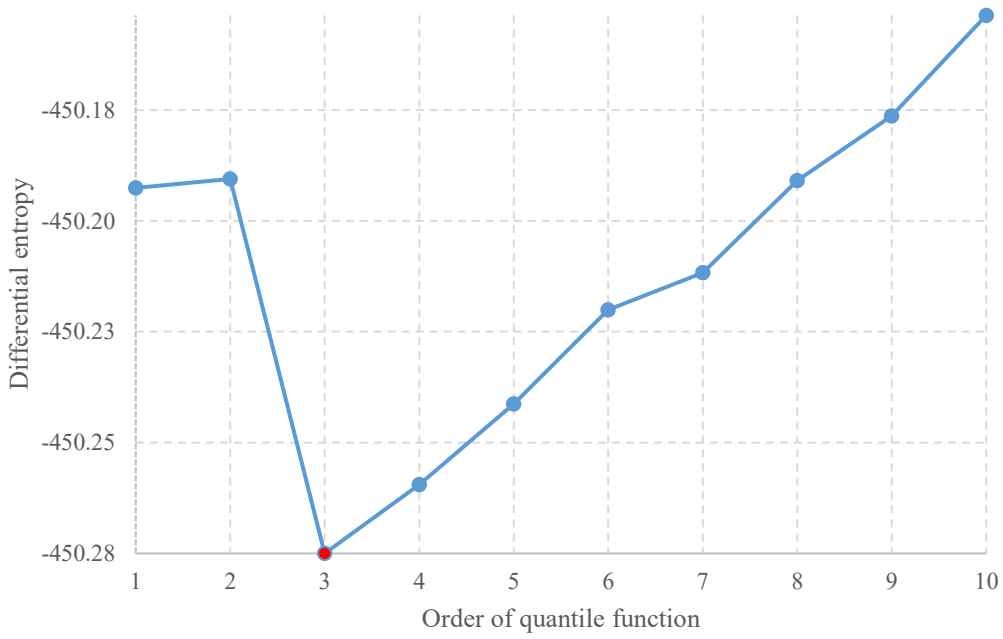

Figure A.8. Differential entropy versus order of quantile function for 8% right truncated data set

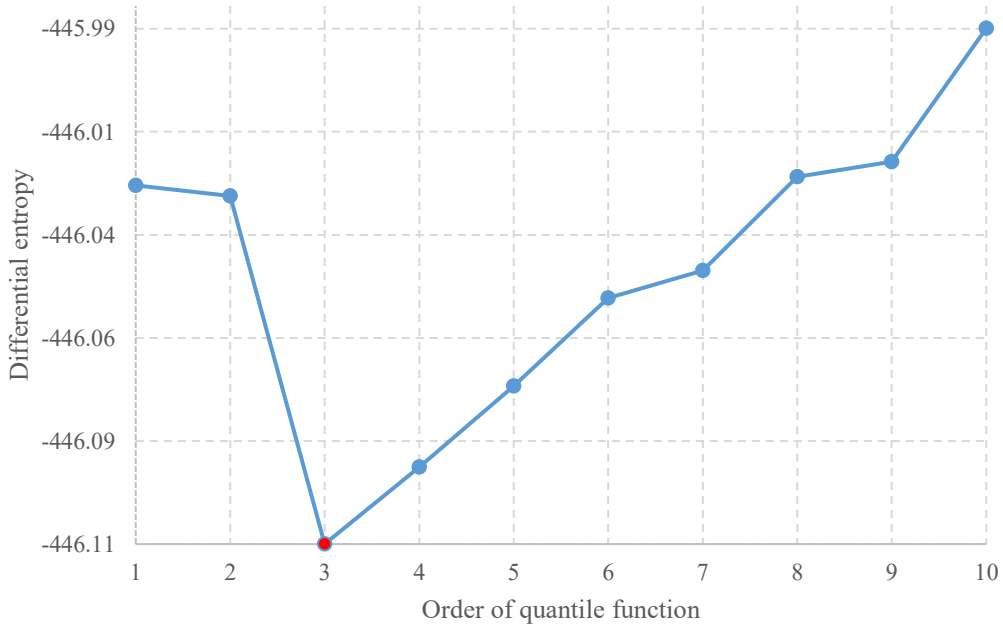

Figure A.9. Differential entropy versus order of quantile function for 10% right truncated data set

Appendix B Rock uniaxial compression strength

Table B.1. Parameters of maximum entropy quantile functions for the original sample of data (moment order K =1-10)

	$K=1$	$K=2$	$K=3$	$K=4$	$K=5$
λ_0	-5.427238247	-5.335919249	-5.145608035	-5.067352413	-4.93388029
λ_1	-0.819426759	-1.307024013	-3.319137541	-4.678907794	-8.128401952
λ_2		0.461829665	5.190020755	10.90201472	33.33668791
λ_3			-3.03229702	-11.53804572	-68.62328201
λ_4				4.12287573	66.22578045
λ_5					-24.21298961
	$K=6$	$K=7$	$K=8$	$K=9$	$K=10$
λ_0	-4.854620766	-4.834278655	-4.862891804	-4.857471011	-4.865609413
λ_1	-10.96579952	-11.93635924	-10.03648694	-10.67571622	-9.840435157
λ_2	59.56942747	71.65924504	39.61717024	57.69207756	35.61869714
λ_3	-168.4287845	-232.2102206	-2.036953757	-197.6120771	31.99470348
λ_4	246.7639027	415.7570053	-435.7227315	617.4631391	-590.3611377
λ_5	-178.778684	-415.2716609	1338.196464	-1832.689289	1770.448596
λ_6	50.40140783	217.3319687	-1812.328431	3775.748035	-2631.130831
λ_7		-46.79959421	1187.763781	-4536.038619	2288.175099
λ_8			-306.9143552	2847.741918	-1320.828891
λ_9				-723.1164238	561.8496927
λ_{10}					-137.4154334

Table B.2. Parameters of maximum entropy quantile functions for 4% left truncated data set (moment order K =1-10)

	$K=1$	$K=2$	$K=3$	$K=4$	$K=5$
λ_0	-5.500903027	-5.466794199	-5.342571932	-5.316687608	-5.223102966
λ_1	-0.728448709	-0.913709406	-2.264114601	-2.731265009	-5.260786173
λ_2		0.17660859	3.383517329	5.375231722	22.12977727
λ_3			-2.068215781	-5.057935131	-48.11779124
λ_4				1.456493396	48.59783014
λ_5					-18.45992451
	$K=6$	$K=7$	$K=8$	$K=9$	$K=10$
λ_0	-5.134572587	-5.03985237	-5.095100293	-4.991788346	-5.041789189
λ_1	-8.577079048	-13.25468628	-9.938171315	-16.16592734	-12.75601054
λ_2	53.41461917	112.7779493	58.14891479	158.0109789	97.522094
λ_3	-168.5070004	-485.1950989	-103.527279	-778.3578938	-322.0546357
λ_4	267.9712821	1113.253338	-265.4258664	2049.21175	313.6113166
λ_5	-207.2388217	-1396.327782	1392.354335	-2895.53177	517.4585848
λ_6	61.79173641	904.3857681	-2290.149108	1849.605	-904.2292669
λ_7		-236.935101	1703.183624	123.6421419	-1319.776735
λ_8			-486.0802588	-777.1425049	3999.193555
λ_9				285.4203523	-3314.911531
λ_{10}					944.7010885

Table B.3. Parameters of maximum entropy quantile functions for 8.5% left truncated data set (moment order K =1-10)

	$K=1$	$K=2$	$K=3$	$K=4$	$K=5$
λ_0	-5.558966493	-5.565157443	-5.491678097	-5.519669665	-5.497277766
λ_1	-0.65840512	-0.624340307	-1.440221537	-0.919226886	-1.550699011
λ_2		-0.032632971	1.920203797	-0.326465859	3.921046283
λ_3			-1.26471638	2.128116233	-8.877286776
λ_4				-1.659124243	10.45075529
λ_5					-4.758645278
	$K=6$	$K=7$	$K=8$	$K=9$	$K=10$
λ_0	-5.483159774	-5.466017698	-5.480870942	-5.472168663	-5.480414321
λ_1	-2.109891113	-3.017287502	-1.984608277	-2.64190157	-1.936495699
λ_2	9.303730898	21.11380268	3.314686599	15.7692918	1.183646458
λ_3	-29.81144757	-93.65422494	35.49922909	-65.13018438	60.24331253
λ_4	48.84962125	220.660115	-259.6450954	165.9384877	-379.1958546
λ_5	-37.95232327	-281.0082204	711.066106	-323.2718211	958.245694
λ_6	10.9011406	183.8408176	-966.5583626	528.6101187	-1023.918983
λ_7		-48.78305417	651.7431512	-615.9185636	-11.84241838
λ_8			-174.2808058	406.5244132	1033.11834
λ_9				-110.7298606	-870.6093066
λ_{10}					233.8754779

Table B.4. Parameters of maximum entropy quantile functions for 12.5% left truncated data set (moment order K =1-10)

	$K=1$	$K=2$	$K=3$	$K=4$	$K=5$
λ_0	-5.594296072	-5.61096175	-5.54458762	-5.575277542	-5.561386167
λ_1	-0.620373051	-0.528120568	-1.270312731	-0.694878848	-1.089722519
λ_2		-0.088598743	1.693392812	-0.796664991	1.869195146
λ_3			-1.156148448	2.612102134	-4.311218543
λ_4				-1.84530835	5.784971661
λ_5					-3.001879663
	$K=6$	$K=7$	$K=8$	$K=9$	$K=10$
λ_0	-5.552275504	-5.535757391	-5.551104755	-5.537895867	-5.535323537
λ_1	-1.453756942	-2.33585265	-1.275846026	-1.715291423	-2.252886049
λ_2	5.387711843	16.91707274	-1.106032502	1.186770998	13.79462723
λ_3	-18.03014971	-80.52056329	48.72897676	72.98803903	-45.76690073
λ_4	30.9937066	199.4774989	-276.4955256	-553.0918055	20.71381703
λ_5	-24.82205937	-263.5034328	711.6189801	1804.173424	231.2849018
λ_6	7.173277778	177.1848833	-945.8165262	-3144.328351	-597.6272692
λ_7		-47.99904983	631.8629526	3041.511407	620.119576
λ_8			-168.2919991	-1536.427612	-266.5313136
λ_9				314.8638406	7.590506324
λ_{10}					17.89329201

Table B.5. Parameters of maximum entropy quantile functions for 4% right truncated data set (moment order K =1-10)

	$K=1$	$K=2$	$K=3$	$K=4$	$K=5$
λ_0	-5.432228626	-5.312292653	-5.146632378	-5.045104816	-4.927046646
λ_1	-0.773363296	-1.415947077	-3.170462537	-4.93795531	-7.990767102
λ_2		0.610252582	4.741727855	12.180024	32.06022243
λ_3			-2.654830544	-13.75066835	-64.40627249
λ_4				5.387207036	60.57158758
λ_5					-21.54440374
	$K=6$	$K=7$	$K=8$	$K=9$	$K=10$
λ_0	-4.838830027	-4.844886816	-4.901396187	-4.91166555	-4.882278566
λ_1	-11.15231231	-10.85635327	-7.280363668	-6.82621652	-8.842575105
λ_2	61.32560263	57.57366881	-1.479924121	-5.082047298	31.97446776
λ_3	-175.8903051	-155.8261648	262.7661171	259.729415	-56.04820097
λ_4	262.4862568	208.744412	-1327.58767	-1194.858742	314.9078252
λ_5	-194.6206958	-118.7377146	3032.549356	2435.257199	-1971.292193
λ_6	56.50328559	2.536690561	-3641.404347	-2385.656516	5730.94644
λ_7		15.2271782	2234.518124	829.3199036	-8575.399503
λ_8			-553.4247599	254.8188691	6829.871633
λ_9				-188.0142402	-2681.993549
λ_{10}					384.4999778

Table B.6. Parameters of maximum entropy quantile functions for 8.5% right truncated data set (moment order K =1-10)

	$K=1$	$K=2$	$K=3$	$K=4$	$K=5$
λ_0	-5.430567481	-5.29590434	-5.139319591	-5.029623329	-4.913422134
λ_1	-0.744847703	-1.468058441	-3.128183979	-5.039772291	-8.044834257
λ_2		0.687993111	4.60226487	12.65564431	32.23857336
λ_3			-2.518224298	-14.54401109	-64.48164527
λ_4				5.844256321	60.28915933
λ_5					-21.27158575
	$K=6$	$K=7$	$K=8$	$K=9$	$K=10$
λ_0	-4.828291577	-4.871305645	-4.864984384	-4.898884956	-4.879036027
λ_1	-11.0970502	-9.030793868	-9.146988014	-7.274583125	-8.514239496
λ_2	60.509938	34.69364017	33.39160317	5.756770967	28.98455234
λ_3	-172.2542567	-35.73199306	-9.601570498	166.5943173	-27.07308998
λ_4	255.6174054	-106.875573	-250.5614003	-828.3295745	49.11643548
λ_5	-188.8140639	319.4630166	691.6745006	1721.674393	-660.1379393
λ_6	54.73136983	-304.7010186	-807.2911388	-1762.364295	2297.34821
λ_7		100.9435424	442.9571933	780.0612574	-3617.912615
λ_8			-92.6820104	-10.22077571	2945.821494
λ_9				-67.14118882	-1199.599571
λ_{10}					190.7255416

Table B.7. Parameters of maximum entropy quantile functions for 12.5% right truncated data set (moment order K =1-10)

	$K=1$	$K=2$	$K=3$	$K=4$	$K=5$
λ_0	-5.425296202	-5.283133194	-5.126287219	-5.020721476	-4.887228146
λ_1	-0.725423755	-1.490328362	-3.154147846	-4.994959029	-8.444879131
λ_2		0.72852496	4.654798097	12.41533033	34.90206209
λ_3			-2.527802489	-14.12370933	-71.48686968
λ_4				5.638483559	68.20265127
λ_5					-24.45233658
	$K=6$	$K=7$	$K=8$	$K=9$	$K=10$
λ_0	-4.840339371	-4.871607757	-4.878607687	-4.845593394	-4.912684099
λ_1	-10.12749905	-8.619767412	-7.932941856	-10.68541811	-6.037446556
λ_2	50.49463002	31.63544662	17.57857068	76.50383669	-10.04553613
λ_3	-130.951238	-31.15405022	82.51486026	-421.2477085	253.5152861
λ_4	176.0157316	-89.09171038	-545.0725853	1706.746531	-1072.479101
λ_5	-116.9583557	254.9071877	1251.346995	-4595.225313	2070.46784
λ_6	30.22738327	-232.8205235	-1440.012761	7757.617432	-1924.537107
λ_7		73.89313609	835.2994175	-7883.083365	581.7007573
λ_8			-194.9840555	4420.787445	294.7717318
λ_9				-1053.008197	-203.3501939
λ_{10}					14.74765663

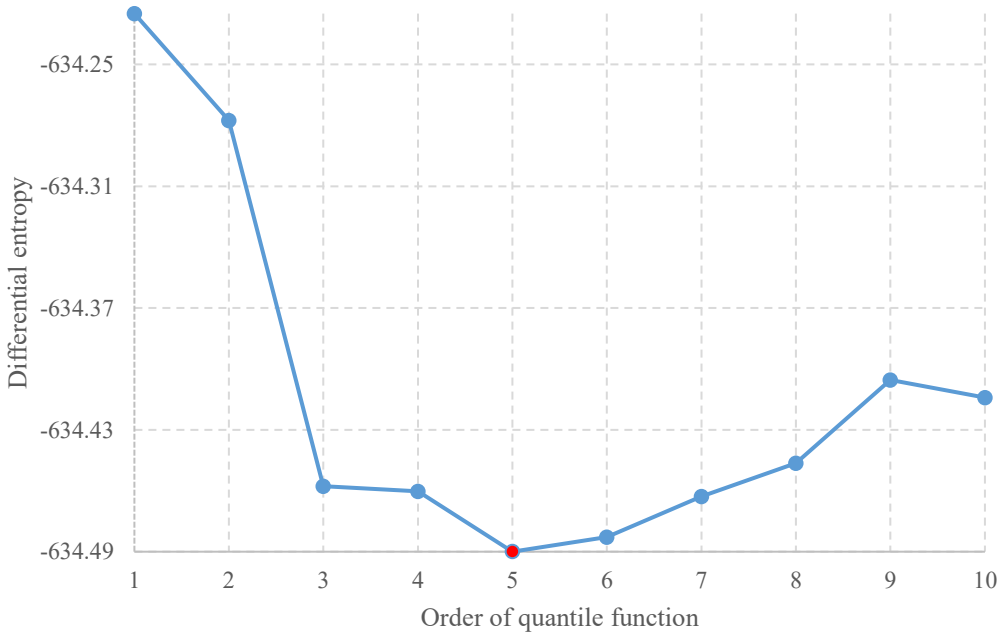

Figure B.1. Differential entropy versus order of quantile function for the original data set

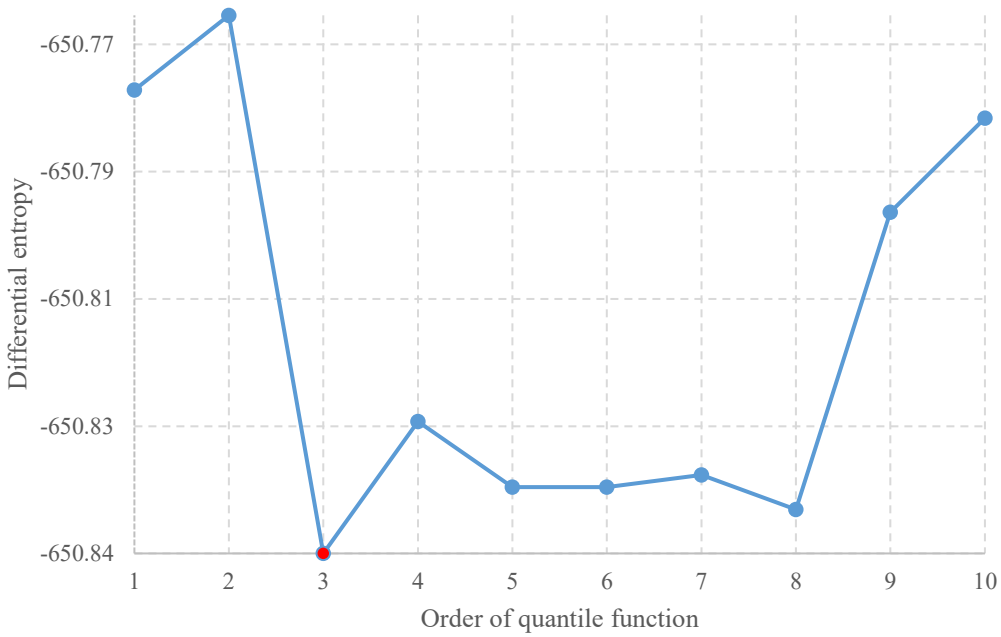

Figure B.2. Differential entropy versus order of quantile function for 4% left truncated data set

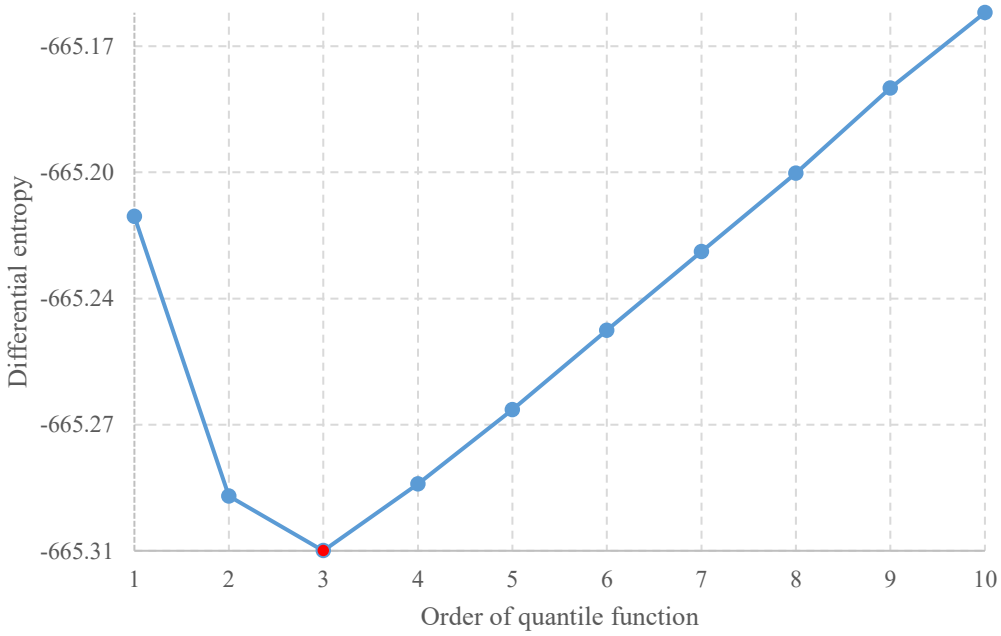

Figure B.3. Differential entropy versus order of quantile function for 8.5% left truncated data set

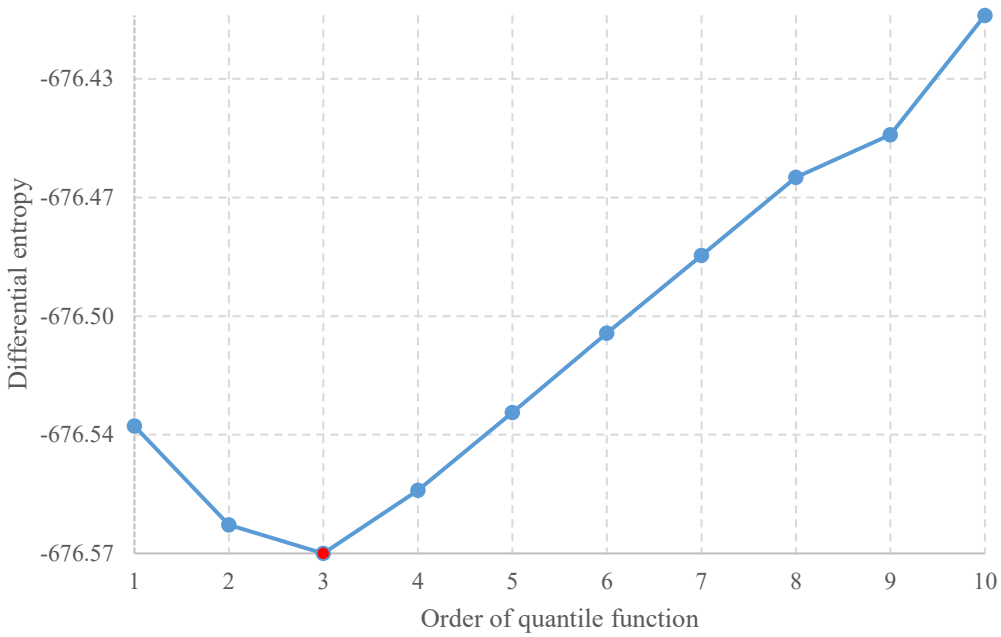

Figure B.4. Differential entropy versus order of quantile function for 12.5% left truncated data set

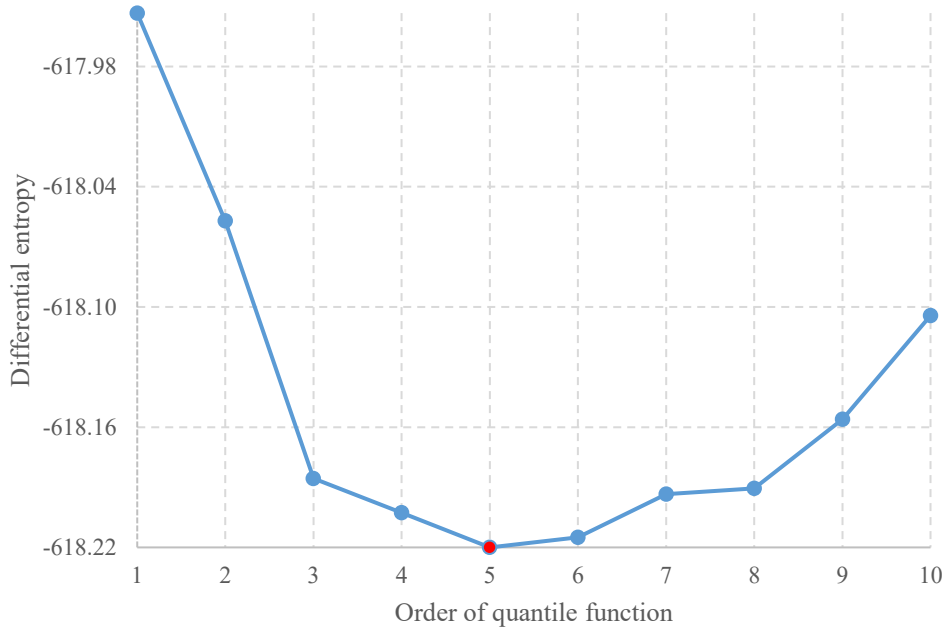

Figure B.5. Differential entropy versus order of quantile function for 4% right truncated data set

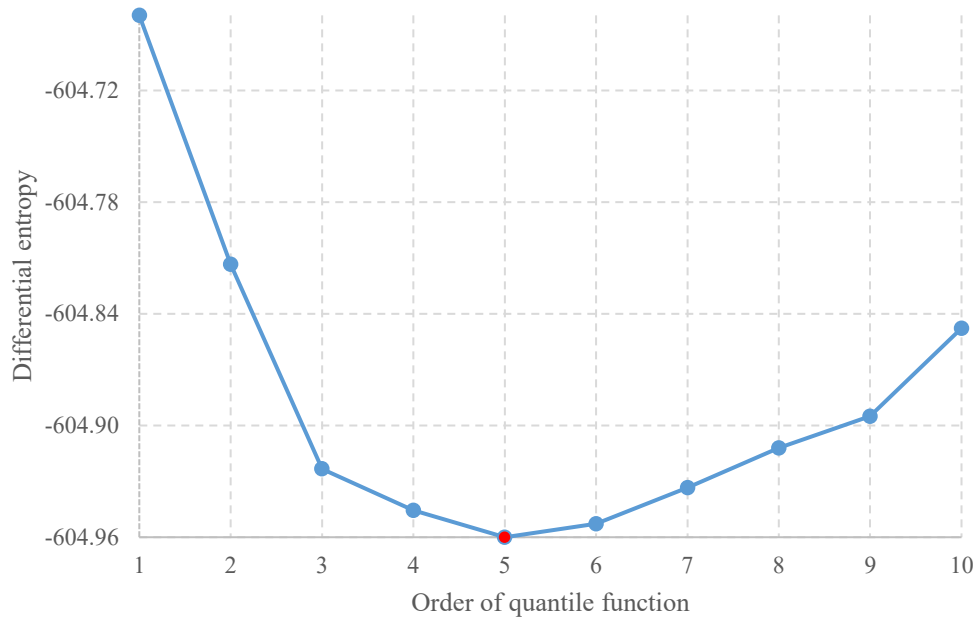

Figure B.6. Differential entropy versus order of quantile function for 8.5% right truncated data set

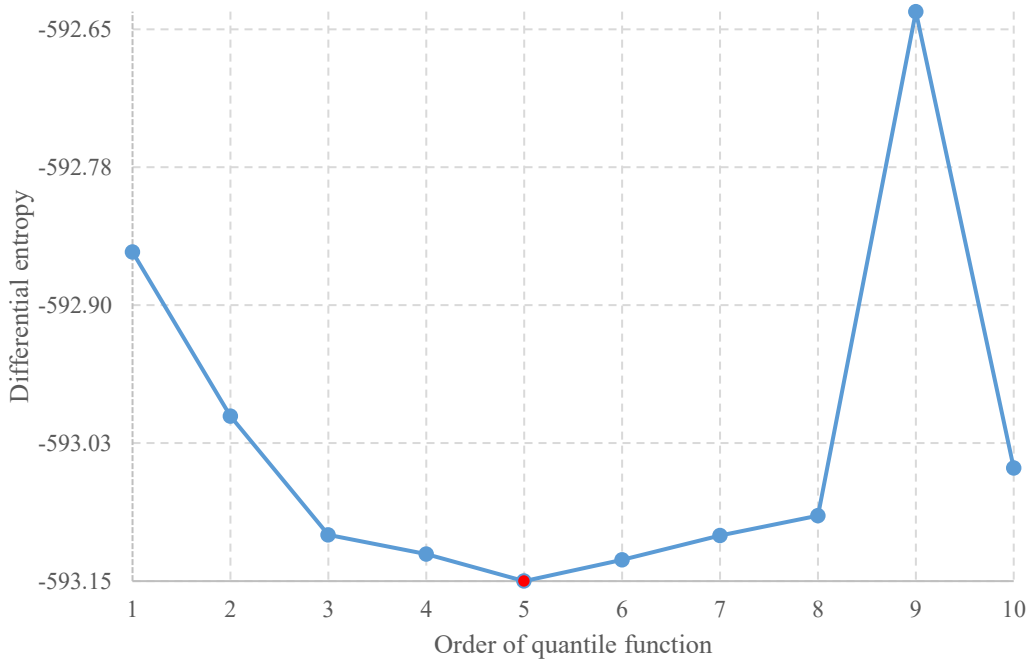

Figure B.7. Differential entropy versus order of quantile function for 12.5% right truncated data set

Appendix C Nipigon River Landslide

Table C.1. Parameters of maximum entropy quantile functions for the original data set for undrained shear strength of upper silty sand layer from Nipigon River Landslide (moment order K =1-10)

	$K=1$	$K=2$	$K=3$	$K=4$	$K=5$
λ_0	-4.23178	-3.88399	-3.36789	-3.08505	-2.79376
λ_1	-1.34169	-3.04279	-7.83755	-11.99874	-18.24268
λ_2		1.55246	12.20816	28.43261	65.64615
λ_3			-6.62046	-29.76126	-119.70755
λ_4				10.90290	105.47299
λ_5					-35.98218
	$K=6$	$K=7$	$K=8$	$K=9$	$K=10$
λ_0	-3.19450	-3.19546	-2.95078	-3.46828382	-3.465513439
λ_1	-5.93016	-5.88849	-18.72629	8.958978943	9.486164665
λ_2	-39.22736	-39.71251	127.28923	-253.1607117	-262.2489828
λ_3	259.44085	261.88420	-716.14487	1582.375519	1635.395343
λ_4	-556.77689	-563.03809	2493.08881	-4709.268961	-4839.031564
λ_5	516.65614	525.20051	-4919.34745	7356.714433	7465.517629
λ_6	-176.70074	-182.61431	5359.90874	-5377.65732	-5358.83445
λ_7		1.63179	-2994.82647	222.1263055	355.9137907
λ_8			665.77848	2013.892085	1453.637957
λ_9				-846.4319607	-269.534758
λ_{10}					-192.7595596

Table C.2. Parameters of maximum entropy quantile functions for 6% left truncated data set for undrained shear strength of upper silty sand layer from Nipigon River Landslide (moment order K =1-10)

	$K=1$	$K=2$	$K=3$	$K=4$	$K=5$
λ_0	-4.39388	-4.18975	-3.83642	-3.62426	-3.27095
λ_1	-1.14541	-2.18059	-5.66164	-9.02400	-17.14902
λ_2		0.95876	8.88841	22.44831	72.63599
λ_3			-4.99425	-24.71086	-148.63249
λ_4				9.40624	141.54857
λ_5					-50.78203
	$K=6$	$K=7$	$K=8$	$K=9$	$K=10$
λ_0	-3.44480	-3.33275	-3.22271	-3.35253	-3.45540
λ_1	-11.58056	-16.47141	-21.17589	-15.07760	-10.41503
λ_2	23.84183	81.81663	136.21921	51.66506	10.68490
λ_3	31.12163	-265.26549	-537.45514	-16.67026	12.51891
λ_4	-176.56807	591.68938	1283.39915	-398.19287	587.10919
λ_5	217.23964	-840.44431	-1772.47574	1249.71293	-3547.72752
λ_6	-86.32414	650.78032	1280.13609	-1700.60584	8131.94004
λ_7		-204.52714	-365.41468	1046.05749	-8611.77273
λ_8			-5.80132	-147.29390	3263.87711
λ_9				-72.05099	917.67335
λ_{10}					-756.38258

Table C.3. Parameters of maximum entropy quantile functions for 8.5% left truncated data set for undrained shear strength of upper silty sand layer from Nipigon River Landslide (moment order K =1-10)

	$K=1$	$K=2$	$K=3$	$K=4$	$K=5$
λ_0	-4.46796	-4.32518	-4.04091	-3.86246	-3.47442
λ_1	-1.05534	-1.79160	-4.66871	-7.59554	-16.80645
λ_2		0.68642	7.31222	19.29325	77.09449
λ_3			-4.19786	-21.76518	-165.81247
λ_4				8.42607	162.95955
λ_5					-59.63900
	$K=6$	$K=7$	$K=8$	$K=9$	$K=10$
λ_0	-3.47829	-3.05831	-3.10385	-3.05638	-3.03898
λ_1	-16.68104	-34.43353	-33.03048	-34.42257	-36.38080
λ_2	75.98375	285.88931	271.69151	282.33332	333.66883
λ_3	-161.69041	-1236.28301	-1170.25164	-1178.51715	-1669.46981
λ_4	155.62684	2946.22996	2782.87763	2569.08114	4768.54626
λ_5	-53.43755	-3901.91994	-3670.03738	-2632.66476	-7488.98230
λ_6	-2.00314	2683.94515	2485.86821	286.28858	4398.90577
λ_7		-746.19766	-644.40560	1820.31827	4942.20512
λ_8			-25.52260	-1453.40645	-11091.87562
λ_9				338.21212	7935.37058
λ_{10}					-2094.89345

Table C.4. Parameters of maximum entropy quantile functions for 11.5% left truncated data set for undrained shear strength of upper silty sand layer from Nipigon River Landslide (moment order K =1-10)

	$K=1$	$K=2$	$K=3$	$K=4$	$K=5$
λ_0	-4.54439	-4.47010	-4.27748	-4.18773	-3.88738
λ_1	-0.96090	-1.35097	-3.36363	-4.90632	-12.47140
λ_2		0.36620	5.05787	11.49024	60.14212
λ_3			-2.99174	-12.51701	-135.39146
λ_4				4.59717	137.52596
λ_5					-51.59693
	$K=6$	$K=7$	$K=8$	$K=9$	$K=10$
λ_0	-3.88305	-3.40199	-3.22695	-3.40980	-3.31984
λ_1	-12.62082	-34.09024	-42.68114	-34.01031	-40.82240
λ_2	61.50375	322.50317	465.55265	323.10431	441.97443
λ_3	-140.52556	-1498.60360	-2534.83676	-1414.71222	-2383.00340
λ_4	146.75200	3711.09919	7597.72283	2712.77415	6941.79128
λ_5	-59.45462	-5011.61669	-13145.10381	-479.92177	-11064.23072
λ_6	2.55125	3477.77315	13050.64394	-6914.07760	8388.50350
λ_7		-969.53782	-6889.20941	11869.31966	-0.31819
λ_8			1495.46697	-8159.75468	-4767.57891
λ_9				2095.12952	3155.41600
λ_{10}					-674.41314

Table C.5. Parameters of maximum entropy quantile functions for 6% right truncated data set for undrained shear strength of upper silty sand layer from Nipigon River Landslide (moment order K =1-10)

	$K=1$	$K=2$	$K=3$	$K=4$	$K=5$
λ_0	-4.22587	-3.80785	-3.36410	-2.95718	-2.93345
λ_1	-1.28218	-3.33098	-7.45308	-13.42584	-13.93779
λ_2		1.87503	11.05187	34.35133	37.41220
λ_3			-5.71455	-38.99374	-46.41201
λ_4				15.70810	23.52777
λ_5					-2.98272
	$K=6$	$K=7$	$K=8$	$K=9$	$K=10$
λ_0	-3.14059	-3.33463	-3.35009	-3.48185	-3.37459
λ_1	-7.46851	1.12837	2.48119	9.23595	2.61879
λ_2	-18.03294	-118.76999	-146.53155	-230.01497	-123.68214
λ_3	154.84192	664.21033	889.39214	1297.63784	563.32051
λ_4	-329.14039	-1638.53988	-2550.99597	-3335.52856	-797.56889
λ_5	292.16823	2084.03106	4110.18181	3920.42971	-369.97171
λ_6	-94.62795	-1337.99775	-3843.48943	-604.38355	1211.33344
λ_7		343.94518	1962.26271	-3369.49366	2036.96510
λ_8			-425.39766	3285.84284	-6349.93978
λ_9				-975.65678	5387.40358
λ_{10}					-1562.52573

Table C.6. Parameters of maximum entropy quantile functions for 8.5% right truncated data set for undrained shear strength of upper silty sand layer from Nipigon River Landslide (moment order K =1-10)

	$K=1$	$K=2$	$K=3$	$K=4$	$K=5$
λ_0	-4.21128	-3.78845	-3.33042	-2.93977	-2.95851
λ_1	-1.27934	-3.35168	-7.59950	-13.32295	-12.91732
λ_2		1.89679	11.34907	33.65947	31.23236
λ_3			-5.88494	-37.73970	-31.85524
λ_4				15.03231	8.82804
λ_5					2.36691
	$K=6$	$K=7$	$K=8$	$K=9$	$K=10$
λ_0	-3.15430	-3.37243	-3.32747	-3.46705	-3.31495
λ_1	-6.76035	2.99253	0.75727	7.84218	-1.29951
λ_2	-21.64008	-136.21241	-106.58509	-195.00861	-53.35555
λ_3	160.23415	740.20563	565.38842	1002.48866	63.57686
λ_4	-327.96370	-1819.81854	-1271.49863	-2114.40504	1078.54769
λ_5	284.33685	2326.77883	1347.13454	1078.16551	-4682.40971
λ_6	-90.42753	-1508.14037	-507.33871	3297.65753	7958.51616
λ_7		392.27546	-152.08699	-6493.84288	-5669.57308
λ_8			122.26231	4627.87178	-17.23318
λ_9				-1212.67716	2123.58190
λ_{10}					-802.29746

Table C.7. Parameters of maximum entropy quantile functions for 11.5% right truncated data set for undrained shear strength of upper silty sand layer from Nipigon River Landslide (moment order K =1-10)

	$K=1$	$K=2$	$K=3$	$K=4$	$K=5$
λ_0	-4.19545	-3.76965	-3.29092	-2.93494	-2.97139
λ_1	-1.27836	-3.36502	-7.79582	-13.00362	-12.21236
λ_2		1.90994	11.76290	32.04852	27.31056
λ_3			-6.13235	-35.08405	-23.59392
λ_4				13.65815	1.54231
λ_5					4.62222
	$K=6$	$K=7$	$K=8$	$K=9$	$K=10$
λ_0	-3.18703	-3.38646	-3.39771	-3.52812	-3.42137
λ_1	-5.37991	3.61529	4.39531	11.49006	6.38936
λ_2	-31.48067	-137.39592	-151.07270	-250.74367	-182.49419
λ_3	190.17592	726.81224	827.89735	1433.51049	1024.34056
λ_4	-373.42152	-1754.41909	-2138.50788	-4018.29811	-2744.29166
λ_5	318.62568	2209.75400	3022.44281	6104.46677	3926.70969
λ_6	-100.71394	-1413.57018	-2381.09118	-4735.89919	-2686.21116
λ_7		363.28551	969.29641	1103.87425	-5.15328
λ_8			-155.30235	724.02973	1320.19783
λ_9				-374.33605	-834.35118
λ_{10}					172.91177

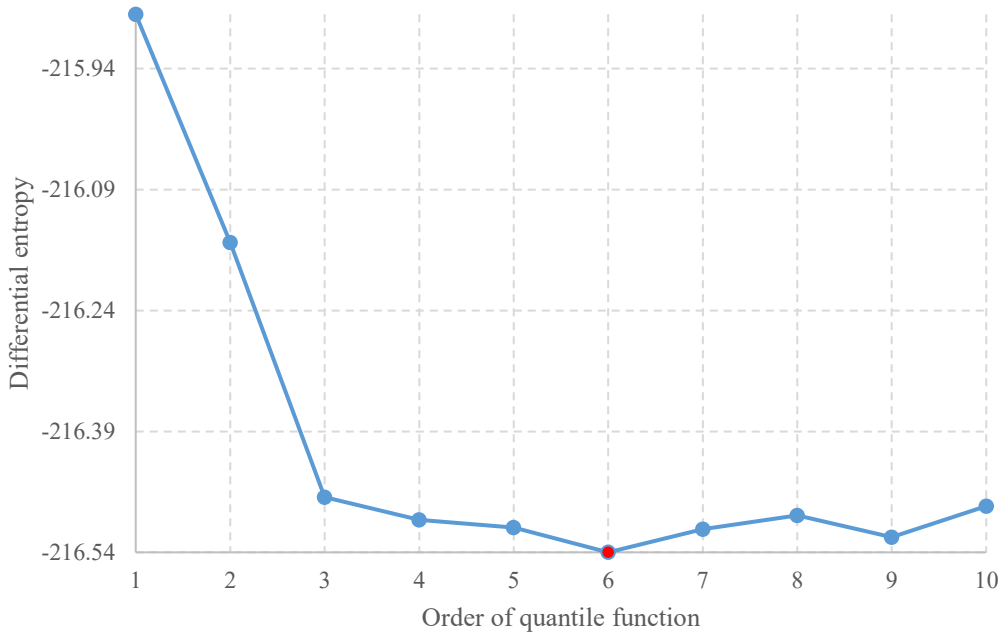

Figure C.1. Differential entropy versus order of quantile function for the original data set (undrained shear strength of upper silty sand layer from Nipigon River Landslide)

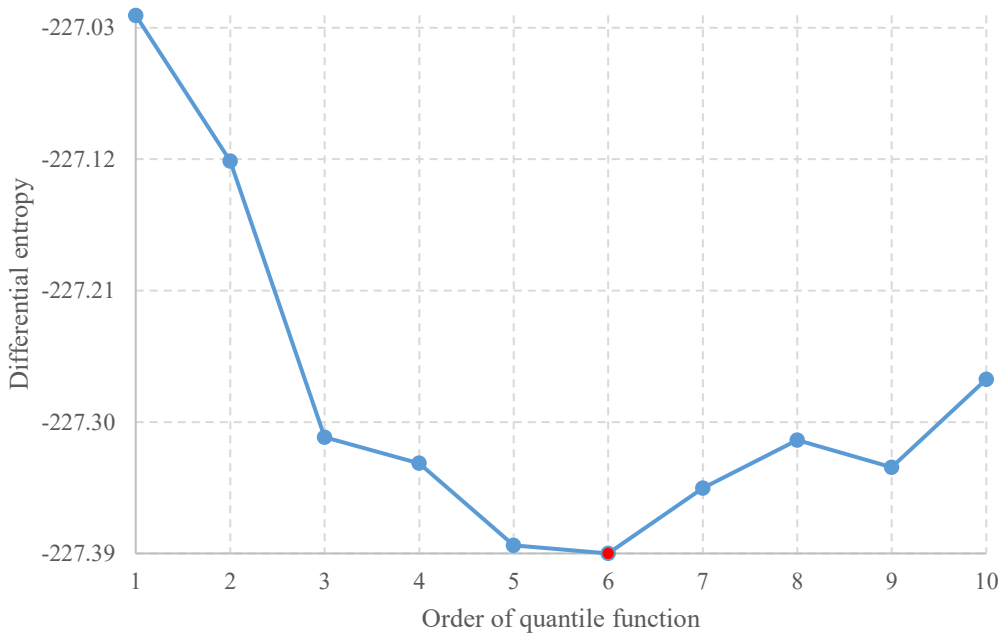

Figure C.2. Differential entropy versus order of quantile function for 6% left truncated data set (undrained shear strength of upper silty sand layer from Nipigon River Landslide)

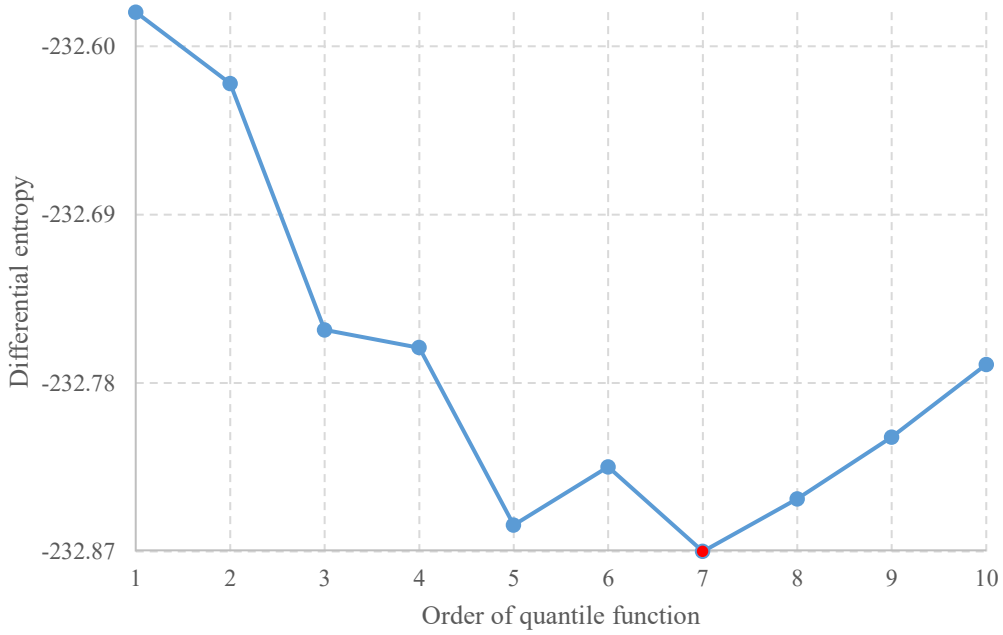

Figure C.3. Differential entropy versus order of quantile function for 8.5% left truncated data set (undrained shear strength of upper silty sand layer from Nipigon River Landslide)

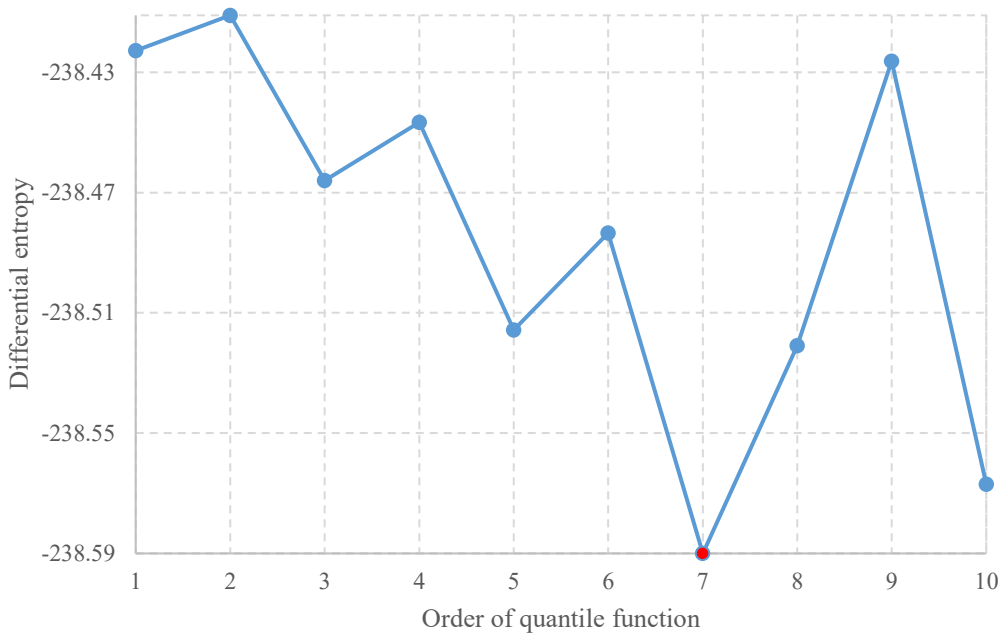

Figure C.4. Differential entropy versus order of quantile function for 11.5% left truncated data set (undrained shear strength of upper silty sand layer from Nipigon River Landslide)

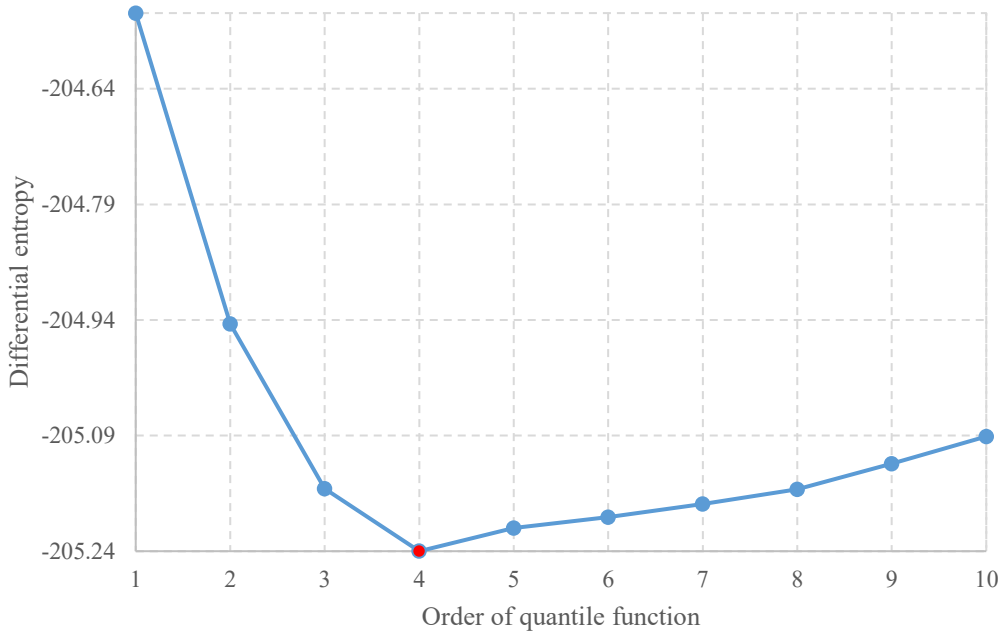

Figure C.5. Differential entropy versus order of quantile function for 6% right truncated data set (undrained shear strength of upper silty sand layer from Nipigon River Landslide)

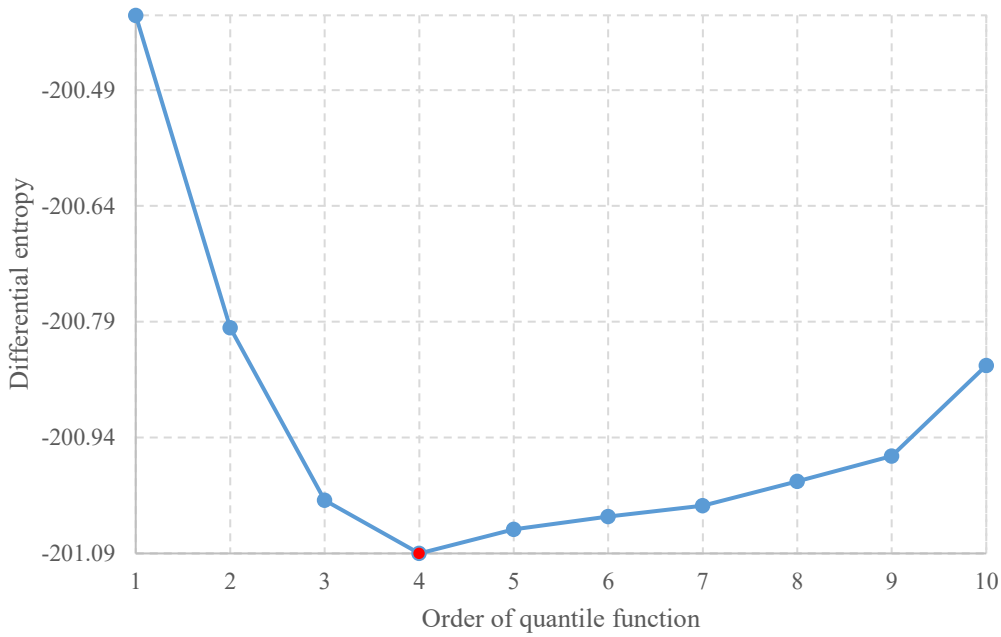

Figure C.6. Differential entropy versus order of quantile function for 8.5% right truncated data set (undrained shear strength of upper silty sand layer from Nipigon River Landslide)

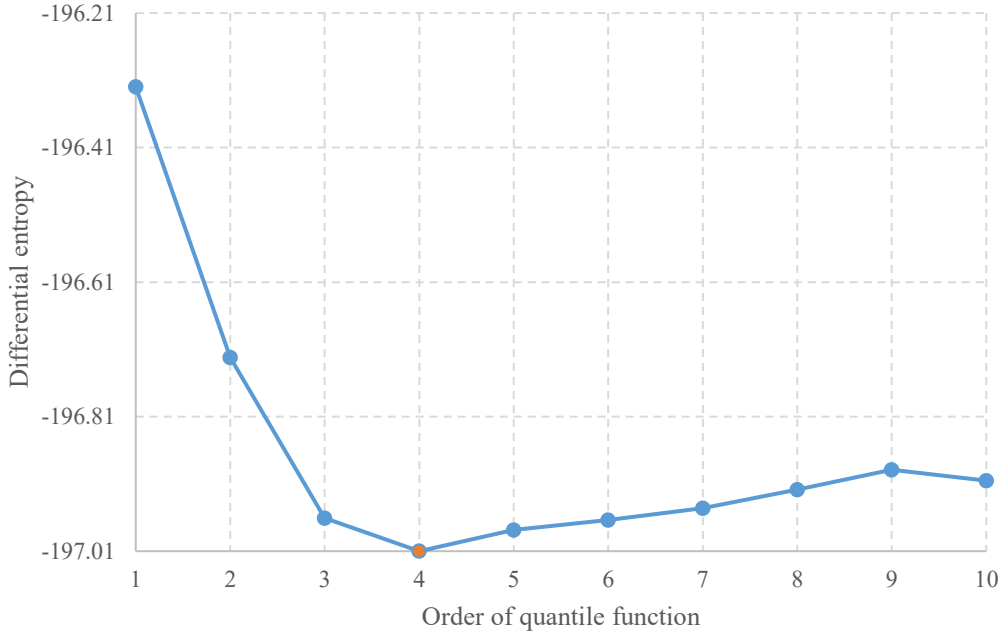

Figure C.7. Differential entropy versus order of quantile function for 11.5% right truncated data (undrained shear strength of upper silty sand layer from Nipigon River Landslide)

Appendix D Estimation Function $\lambda\ (h, \alpha)$

α \ h	.01	.02	.03	.04	.05	.06	.07	.08	.09	.10	.15
.00	.01010	.02040	.03090	.04161	.05251	.06363	.07495	.08649	.09824	.11020	.17342
.01	.01020	.02059	.03118	.04197	.05297	.06417	.07557	.08719	.09902	.11106	.17465
.02	.01029	.02077	.03145	.04233	.05341	.06469	.07618	.08787	.09978	.11190	.17586
.03	.01038	.02095	.03172	.04268	.05384	.06520	.07677	.08854	.10052	.11272	.17704
.04	.01047	.02113	.03197	.04302	.05426	.06570	.07734	.08919	.10125	.11352	.17821
.05	.01055	.02129	.03223	.04335	.05467	.06619	.07791	.08983	.10197	.11431	.17935
.06	.01064	.02146	.03247	.04367	.05507	.06667	.07846	.09046	.10267	.11508	.18047
.07	.01072	.02162	.03271	.04399	.05546	.06713	.07900	.09107	.10335	.11584	.18157
.08	.01080	.02178	.03294	.04430	.05585	.06759	.07953	.09168	.10403	.11659	.18266
.09	.01087	.02193	.03317	.04460	.05623	.06804	.08006	.09227	.10469	.11732	.18373
.10	.01095	.02208	.03340	.04490	.05660	.06848	.08057	.09285	.10534	.11804	.18479
.11	.01102	.02223	.03362	.04519	.05696	.06892	.08107	.09343	.10598	.11875	.18583
.12	.01110	.02238	.03384	.04548	.05732	.06934	.08157	.09399	.10661	.11944	.18685
.13	.01117	.02252	.03405	.04577	.05767	.06976	.08205	.09454	.10723	.12013	.18786
.14	.01124	.02266	.03426	.04604	.05802	.07018	.08254	.09509	.10785	.12081	.18886
.15	.01131	.02280	.03447	.04632	.05835	.07059	.08301	.09563	.10845	.12148	.18985
.16	.01138	.02293	.03467	.04659	.05869	.07099	.08348	.09616	.10905	.12214	.19082
.17	.01145	.02307	.03487	.04685	.05902	.07138	.08394	.09668	.10963	.12279	.19178
.18	.01151	.02320	.03507	.04712	.05935	.07177	.08439	.09720	.11021	.12343	.19273
.19	.01158	.02333	.03526	.04737	.05967	.07216	.08484	.09771	.11079	.12407	.19367
.20	.01164	.02346	.03545	.04763	.05999	.07254	.08528	.09822	.11135	.12469	.19460
.21	.01171	.02359	.03564	.04788	.06030	.07291	.08572	.09871	.11191	.12531	.19552
.22	.01177	.02371	.03583	.04813	.06061	.07329	.08615	.09921	.11246	.12592	.19643
.23	.01183	.02383	.03601	.04838	.06092	.07365	.08657	.09969	.11301	.12653	.19733
.24	.01189	.02396	.03620	.04862	.06122	.07401	.08700	.10017	.11355	.12713	.19822
.25	.01195	.02408	.03638	.04886	.06152	.07437	.08741	.10065	.11408	.12772	.19910
.26	.01201	.02420	.03656	.04909	.06182	.07473	.08783	.10112	.11461	.12831	.19997
.27	.01207	.02431	.03673	.04933	.06211	.07508	.08823	.10158	.11513	.12889	.20083
.28	.01213	.02443	.03691	.04956	.06240	.07542	.08864	.10205	.11565	.12946	.20169
.29	.01219	.02454	.03708	.04979	.06269	.07577	.08904	.10250	.11616	.13003	.20254
.30	.01224	.02466	.03725	.05002	.06297	.07611	.08943	.10295	.11667	.13059	.20338
.31	.01230	.02477	.03742	.05024	.06325	.07644	.08982	.10340	.11717	.13115	.20421
.32	.01236	.02488	.03758	.05047	.06353	.07678	.09021	.10384	.11767	.13170	.20503
.33	.01241	.02499	.03775	.05069	.06380	.07711	.09060	.10428	.11816	.13225	.20585
.34	.01247	.02510	.03791	.05090	.06408	.07743	.09098	.10472	.11865	.13279	.20666
.35	.01252	.02521	.03808	.05112	.06435	.07776	.09136	.10515	.11914	.13333	.20747
.36	.01257	.02532	.03824	.05133	.06461	.07808	.09173	.10557	.11962	.13386	.20826
.37	.01263	.02542	.03840	.05155	.06488	.07839	.09210	.10600	.12009	.13439	.20906
.38	.01268	.02553	.03855	.05176	.06514	.07871	.09247	.10642	.12057	.13491	.20984
.39	.01273	.02563	.03871	.05197	.06540	.07902	.09283	.10683	.12103	.13543	.21062
.40	.01278	.02574	.03887	.05217	.06566	.07933	.09319	.10725	.12150	.13595	.21139
.41	.01284	.02584	.03902	.05238	.06592	.07964	.09355	.10766	.12196	.13646	.21216
.42	.01289	.02594	.03917	.05258	.06617	.07994	.09391	.10806	.12242	.13697	.21292
.43	.01294	.02604	.03932	.05278	.06642	.08025	.09426	.10847	.12287	.13747	.21368
.44	.01299	.02614	.03947	.05298	.06667	.08055	.09461	.10887	.12332	.13797	.21443

References

Abdulai, M., & Sharifzadeh, M. (2019). Uncertainty and reliability analysis of open pit rock slopes: a critical review of methods of analysis. *Geotechnical and Geological Engineering*, 37, 1223-1247.

Alfredo, H. S. A., & Wilson, H. (1975). *Probability concepts in engineering planning and design*. John Wily & Sons.

Akaike, H. (1973). Information theory and an extension of the maximum likelihood principle. In B. N. P. F. Csaki (Ed.), In *Second international symposium on information theory* (pp. 267–281). Budapest: Akadémiai Kiado.

Ang, A. H. S., & Tang, W. H. (1984). *Probability concepts in engineering planning and design, vol. 2: Decision, risk, and reliability*. John Wily & Sons.

Archdeacon, T. J. (1994). *Correlation and regression analysis: a historian's guide*. University of Wisconsin Press.

Baecher, G. B., & Christian, J. T. (2005). *Reliability and statistics in geotechnical engineering*. John Wiley & Sons.

Barros, M., Mistry, K., Plummer, J., & Pyykkonen. C. (2023). *Nipigon River landslide – a case study comprehensive slope analysis and design of a cantilever retaining wall*, Lakehead University.

Bishop, A. W. (1955). The use of the slip circle in the stability analysis of slopes. *Geotechnique*, 5(1), 7-17.

Burnham, K. P., & Anderson, D. R. (2002). *Model selection and multi-model inference* (2nd ed.). Springer-Verlag.

Chen, X., & Dai, W. (2011). Maximum entropy principle for uncertain variables. *International Journal of Fuzzy Systems*, 13(3), 232-236.

Chiu, C. F., Yan, W. M., & Yuen, K. V. (2012). Reliability analysis of soil–water characteristics curve and its application to slope stability analysis. *Engineering Geology*, 135, 83-91.

Christian, J. T., Ladd, C. C., & Baecher, G. B. (1994). Reliability applied to slope stability analysis. *Journal of Geotechnical Engineering*, 120(12), 2180-2207.

Cohen, A. C. (1959). Simplified estimators for the normal distribution when samples are singly censored or truncated. *Technometrics*, 1(3), 217-237.

Cohen, A. C. (1991). *Truncated and censored samples: theory and applications*. CRC press.

Couture, R., Blais-Stevens, A., Bobrowsky, P., Wang, B., & VanDine, D. (2013). Canadian technical guidelines and best practices related to landslides: a national initiative for loss reduction. *Landslides: Global Risk Preparedness*, 315-322.

Cui, J., Jiang, Q., Li, S., Feng, X., Zhang, M., & Yang, B. (2017). Estimation of the number of specimens required for acquiring reliable rock mechanical parameters in laboratory uniaxial compression tests. *Engineering Geology*, 222, 186-200.

Das, B. M. (2002). *Principles of Geotechnical Engineering*, Pacific Grove, California, CA, USA.

Del Gaudio, V., Pierri, P., & Wasowski, J. (2003). An approach to time-probabilistic evaluation of seismically induced landslide hazard. *Bulletin of the Seismological Society of America*, 93(2), 557-569.

Deng, J., & Pandey, M. D. (2008). Estimation of the maximum entropy quantile function using fractional probability weighted moments. *Structural Safety*, 30(4), 307-319.

Deng, J., & Pandey, M. D. (2009). Using PPWMs and partial maximum entropy to estimate quantiles from censored samples. *Probabilistic Engineering Mechanics*, 24(3), 407-417.

Deng, J., Pandey, M. D., & Xie, W. C. (2012). Maximum entropy principle and partial probability weighed moments. In *Aip conference proceedings 31st* (Vol. 1443, No. 1, pp. 190-197). American Institute of Physics.

Deng, J. (2022). Direct Quantile Function Estimation Using Information Principles and Its Applications in Reliability Analysis. *International Journal of Reliability, Risk and Safety: Theory and Application*, 5(2), 63-77.

Deng, J. (2022). Probabilistic characterization of soil properties based on the maximum entropy method from fractional moments: Model development, case study, and application. *Reliability Engineering & System Safety*, 219, 108218.

Deng, J., & Pandey, M. (2023). Optimal maximum entropy quantile function for fractional probability weighted moments and its applications in reliability analysis. *Applied Mathematical Modelling*, 114, 230-251.

DeWolfe, G. F., Griffiths, D. V., & Huang, J. (2011). Probabilistic and deterministic slope stability analysis by random finite elements. In *GeoTrends: the progress of geological and geotechnical engineering in Colorado at the Cusp of a New Decade* (pp. 91-111).

Dodds, R. B., Burak, J. P., & Eigenbrod, K. D. (1993). Nipigon river landslide. *International Conference on Case Histories in Geotechnical Engineering*. St. Louis, USA.

Du, X., & Hu, Z. (2012). First order reliability method with truncated random variables. *Journal of Mechanical Design*, 134, 091005.1-9.

Fellenius, W. (1927). *Erdstatische Berechnungen*, revised edition, W. Ernst u. Sons, Berlin.

Greene, W. H. (2008). Limited dependent variables—truncation, censoring and sample selection. *Econometric analysis*, 833-902.

Greenwood, J. A., Landwehr, J. M., Matalas, N. C., & Wallis, J. R. (1979). Probability weighted moments: definition and relation to parameters of several distributions expressable in inverse form. *Water resources research*, 15(5), 1049-1054.

Guo, X., Dias, D., Carvajal, C., Peyras, L., & Breul, P. (2018). Reliability analysis of embankment dam sliding stability using the sparse polynomial chaos expansion. *Engineering Structures*, 174, 295-307.

Haldar, A., & Mahadevan, S. (2000). *Probability, reliability, and statistical methods in engineering design*. John Wily & Sons.

Highland, L. M., & Bobrowsky, P. (2008). *The landslide handbook-A guide to understanding landslides* (No. 1325). US Geological Survey.

Hoek, E., & Bray, J. D. (1974). *Rock slope engineering*. CRC press.

Hoek, E. (2006). *Practical rock engineering. Chapter 7: A slope stability problem in Hong Kong; and Chapter 8: Factor or safety and probability of failure*. Rocscience, Canada.

Hosking, J. R. M., & Wallis, J. R. (1997). *Regional frequency analysis: An Approach Based On L-Moments*. Cambridge University Press.

Huber, M. (2013). *Soil variability and its consequences in geotechnical engineering*, PhD dissertation, Institut für Geotechnik der Universität Stuttgart.

Hunger, O. (2004). Landslide Hazards in BC-Achieving Balance in Risk Assessment. *Innovation*, 2004, 12-15.

Jahanfar, M. A. (2014). *Landfill slope stability risk assessment*, Master thesis, University of Guelph.

Janbu, N. (1955). Application of composite slip surfaces for stability analysis. *European Conference on Stability of Earth Slopes*, 1955, 3, 43-49.

Jaynes, E. T. (1957). Information theory and statistical mechanics. *Physical review*, 106(4), 620.

Jaynes, E. T. (2003). *Probability Theory: The Logic of Science*. Cambridge University Press.

Jiang, S. H., Li, D. Q., Cao, Z. J., Zhou, C. B., & Phoon, K. K. (2015). Efficient system reliability analysis of slope stability in spatially variable soils using Monte Carlo simulation. *Journal of Geotechnical and Geoenvironmental Engineering*, 141(2), 04014096.

Johnson, N. L., Kotz, S., & Balakrishnan, N. (1995). *Continuous univariate distributions*. John wiley & sons.

Johari, A., Fazeli, A., & Javadi, A. A. (2013). An investigation into the application of jointly distributed random variables method in reliability assessment of rock slope stability. *Computers and Geotechnics*, 47, 42-47.

Kar, S. S., & Roy, L. B. (2022). Probabilistic based reliability slope stability analysis using FOSM, FORM, and MCS. *Engineering, Technology & Applied Science Research*, 12(2), 8236-8240.

Kamien, D. J. (1997). *Engineering and design: Introduction to probability and reliability methods for use in geotechnical engineering*. Corps of Engineers, Washington DC, USA.

Kazmi, D., Qasim, S., Harahap, I. S. H., Baharom, S., Mehmood, M., Siddiqui, F. I., & Imran, M. (2017). Slope remediation techniques and overview of landslide risk management. *Civil engineering journal*, 3(3), 180-189.

Kendall, M., & Stuart, A. (1977). *The advanced theory of statistics*. *Vol. 1: Distribution theory*. London: Griffin.

Kesavan, H. K., & Kapur, J. N. (1989). The generalized maximum entropy principle. *IEEE Transactions on systems, Man, and Cybernetics*, 19(5), 1042-1052.

Koppula, S. D. (1984). On stability of slopes in clays with linearly increasing strength. *Canadian geotechnical journal*, 21(3), 577-581.

Lee, T. E., & Lee, Y. D. (2002). An extended maximum entropy method for estimation of rare event probabilities. *European transactions on telecommunications*, 13(4), 399-407.

Liang, R. Y., Nusier, B. O., & Malkawi, A. H. (1999). A reliability-based approach for evaluating the slope stability of embankment dams. *Engineering geology*, 54(3-4), 271-285.

Low, B. K. (1989). Stability analysis of embankments on soft ground. *Journal of Geotechnical Engineering*, 115(2), 211-227.

Low, B. K. (2007). Reliability analysis of rock slopes involving correlated nonnormals. *International Journal of Rock Mechanics and Mining Sciences*, 44(6), 922-935.

Malkawi, A. I. H., Hassan, W. F., & Abdulla, F. A. (2000). Uncertainty and reliability analysis applied to slope stability. *Structural safety*, 22(2), 161-187.

Matsui, T., & San, K. C. (1992). Finite element slope stability analysis by shear strength reduction technique. *Soils and foundations*, 32(1), 59-70.

Melchers, R. E., Ahammed, M., & Middleton, C. (2003). FORM for discontinuous and truncated probability density functions. *Structural Safety*, 25(3), 305-313.

Michalowski, R. L. (2002). Stability charts for uniform slopes. *Journal of Geotechnical and Geoenvironmental Engineering*, 128(4), 351-355.

Munir, R., Saleem, M., Aslam, M., & Ali, S. (2013). Comparison of different methods of parameters estimation for Pareto Model. *Caspian Journal of Applied Sciences Research*, 2(1), 121-130.

Natural Resources Canada. (2019). *https://www.nrcan.gc.ca/hazards/landslides*.

Nair, N. U., Sankaran, P. G., & Balakrishnan, N. (2013). *Quantile-based reliability analysis*. Basel: Birkhäuser, 17 (3), 105-110.

Kapur, J. N., & Kesavan, H. K. (1992). Entropy optimization principles and their applications. In *Entropy and energy dissipation in water resources*. Dordrecht: Springer Netherlands.

Nelson, W. B. (2009). *Accelerated testing: statistical models, test plans, and data analysis*. John Wily & Sons.

Paloheimo, E., & Hannus, M. (1974). Structural design based on weighted fractiles. *Journal of the Structural Division*, *100*(7), 1367-1378.

Pandey, M. D. (2000). Direct estimation of quantile functions using the maximum entropy principle. *Structural safety*, 22(1), 61-79.

Porter, M., Van Hove, J., Barlow, P., Froese, C., Bunce, C., Skirrow, R., Skirrow, D., Lewycky, & P., Bobrowsky, P. (2019). The estimated economic impacts of prairie landslides in western Canada. In *Proceedings of the 72nd Canadian Geotechnical Conference*, St. John's, NL, Canada.

Pourkhosravani, A., & Kalantari, B. (2011). A review of current methods for slope stability evaluation. *Electronic Journal of Geotechnical Engineering*, 16, 1245-1254.

Reale, C., Xue, J., Pan, Z., & Gavin, K. (2015). Deterministic and probabilistic multi-modal analysis of slope stability. *Computers and Geotechnics*, 66, 172-179.

Rao, A., & Hsieh, C. H. (1987). Maximum entropy probability distributions for flood frequency analysis. *Civil Engineering Systems*, 4(2), 67-76.

Robert, C. P & Casella, G. (1999). *Monte Carlo statistical methods* (Vol. 2). New York: Springer.

Shore, J., & Johnson, R. (1980). Axiomatic derivation of the principle of maximum entropy and the principle of minimum cross-entropy. *IEEE Transactions on information theory*, 26(1), 26-37.

Spencer, E. (1967). A method of analysis of the stability of embankments assuming parallel inter-slice forces. *Geotechnique*, 17(1), 11-26.

Strouth, A., & McDougall, S. (2021). Historical landslide fatalities in British Columbia, Canada: trends and implications for risk management. *Frontiers in Earth Science*, 9, 606854.

Taylor, D. W. (1937). Stability of earth slopes. *J. Boston Soc. Civil Engineers*, 24(3), 197-247.

Wang, Q. J. (1990). Unbiased estimation of probability weighted moments and partial probability weighted moments from systematic and historical flood information and their application to estimating the GEV distribution. *Journal of hydrology*, 120(1-4), 115-124.

Wang, Y., Cao, Z., & Au, S. K. (2011). Practical reliability analysis of slope stability by advanced Monte Carlo simulations in a spreadsheet. *Canadian Geotechnical Journal*, 48(1), 162-172.

Wang, L., Hwang, J. H., Juang, C. H., & Atamturktur, S. (2013). Reliability-based design of rock slopes—a new perspective on design robustness. *Engineering Geology*, 154, 56-63.

Winterstein, S. R. (1988). Nonlinear vibration models for extremes and fatigue. *Journal of Engineering Mechanics*, 114(10), 1772-1790.

Wong, F. S. (1985). Slope reliability and response surface method. *Journal of geotechnical Engineering*, 111(1), 32-53.

Zhang, T., & Xie, M. (2011). On the upper truncated Weibull distribution and its reliability implications. *Reliability Engineering & System Safety*, 96(1), 194-200.